Technical University of Denmark

Rune Yding Brogaard

Control of Multi Rotor Helicopter

Master's Thesis, March 2012

DTU Electrical Engineering
Department of Electrical Engineering

Rune Yding Brogaard

Control of Multi Rotor Helicopter

Master's Thesis, March 2012

Supervisors:
Jens Christian Andersen, DTU Electrical Engineering
Nils Axel Andersen, DTU Electrical Engineering
Hans Henrik Niemann, DTU Electrical Engineering

DTU - Technical University of Denmark, Kgs. Lyngby - 2011

Control of Multi Rotor Helicopter
Styring af multirotor helikopter

This report was prepared by:
Rune Yding Brogaard

Advisors:
Jens Christian Andersen, DTU Electrical Engineering
Nils Axel Andersen, DTU Electrical Engineering
Hans Henrik Niemann, DTU Electrical Engineering

DTU Electrical Engineering
Automation and Control
Technical University of Denmark
Elektrovej, Building 326
2800 Kgs. Lyngby
Denmark
Tel: +45 4525 3576
Fax: +45 4588 1295

studieadministration@elektro.dtu.dk

Project period:	12. September 2011 - 12. March 2012
ECTS:	30
Education:	Master of Science
Field:	Electrical Engineering
Class:	Public
Remarks:	This report is submitted as partial fulfillment of the requirements for graduation in the above education at the Technical University of Denmark.

Preface

The helicopter approaches closer than any other [vehicle] to fulfillment of mankind's ancient dreams of the flying horse and the magic carpet.
- Igor Sikorsky

This thesis has been submitted to the Technical University of Denmark, as a partial fulfillment of the requirements to obtain the master degree. The work presented here was carried out at the Department of Electrical Engineering during September 12, 2011 to March 12, 2012 under the joint supervision of Jens Christian Andersen, Nils Axel Andersen and Hans Henrik Niemann.

Acknowledgments

During my project I have encountered interesting and challenging tasks. Thanks to an educational collaboration with my supervisors, I have been able to gain experiences in both theoretical and experimental directions. I am sincerely grateful to Nils, Jens Christian and Hans for their commitment and support throughout the project. A special thanks to Nils and Jens Christian for raising the opportunity to cooperate with Papagaio Film which has lead to valuable practical experience with multi rotor helicopters. I would therefore also like to thank the owner at Parpagaio Film, Nikolaj Vesselbo and his associate Anders Lilkær.

Throughout the project a series of rather noisy experiments have been performed and I would like to thank my colleagues at the office for their patience and motivation. Last, but certainly not least, I would like to thank Elbert Hendricks for kindly sharing his experiences and giving great advice on the theory of helicopters.

Rune Yding Brogaad
March 12, 2012

Abstract

The interest in multi rotor helicopters has increased rapidly during the last few years and different prototypes are occurring on the market.

The aim of this study is to increase the understanding of the physical principles of multi rotor helicopters and the influence of an increasing number of rotors. A mathematical dynamic nonlinear model of a multi rotor helicopter with n rotors has been derived. In addition to the dynamics, the rotor torque and power have been included in the model and a change in count and configuration of the rotors can be easily implemented. Based on prior work which showed good results with *Single Input Single Output* (SISO) controllers, a series of SISO controllers have successfully been designed to control the helicopter.

The model and controllers have been verified with recorded data from a four rotor helicopter produced by the leading multi rotor company Mikrokopter. The control parameters, based on the multi rotor model, are successfully implemented on the helicopter without re-tuning. Each controller was tested separately and in combination to investigate their influences on each other. The controllers designed in this study were compared to the commercial controllers designed by Mikrokopter. The controllers designed in this study proved to perform significantly better on both stability and rise time than controllers from Mikrokopter.

Contents

List of Illustrations

Figures

Tables

Nomenclature

Latin Letters

A	Rotor disc area	m^2
a	Lift slope	-
A_b	Rotor blade area	m^2
B_{Wh}	Battery watt hours	Wh
C_d	Drag constant of the propeller	-
C_Q	Torque constant	rad^{-2}
C_{pwm}	Rotor control signal to rotor speed	-
C_{QT}	Thrust to torque constant	m
C_T	Thrust constant	rad^{-2}
f_t	Rotor speed to thrust factor	m
g	gravity	m/s^2
$I_{x,y,z}$	Inertia of the helicopter around the x, y or z-axis	$kg \cdot m^2$
J_r	Propeller inertia	$kg \cdot m^2$
l	length of helicopter rod	m
m	mass of the helicopter	m/s^2
M_{tf}	Motor transfer function	-
n	Number of rotors	-
P	Power	W
P_M	Mechanical Power	W
P_H	Required power to maintain hover	W
P_E	Electrical Power	W

Q	Torque		Nm
Q_r	Vector of torques	$[Q_1 \dots Q_n]^T$	Nm
R_r	Rotor radius		m
$\mathbf{T}_r$	Vector containing the thrust of n rotors	$[T_1 \dots T_n]^T$	N
T	Thrust		N
$\mathbf{u}$	Vector containing the rotors control signal	$[u_1 \dots u_n]^T$	-
$\mathrm{U}_{\mathrm{pitch}}$	Pitch control signal		-
$\mathrm{U}_{\mathrm{roll}}$	Roll control signal		-
$\mathrm{U}_{\mathrm{thrust}}$	Thrust control signal		-
$\mathrm{U}_{\mathrm{yaw}}$	Yaw control signal		-
v_i	induced velocity		m/s
X, Y, Z	x, y, z position in the earth fix frame		m
$\dot{X}, \dot{X}, \dot{Z}$	x, y, z velocity in the earth fix frame		m/s
$\ddot{X}, \ddot{Y}, \ddot{Z}$	x, y, z acceleration in the earth fix frame		m/s^2
x, y, z	x, y, z position in the helicopter fix frame		m
$\dot{x}, \dot{y}, \dot{z}$	x, y, z velocity in the helicopter fix frame		m/s
$\ddot{x}, \ddot{y}, \ddot{z}$	x, y, z acceleration in the helicopter fix frame		m/s^2

Greek Letters

ϕ	Roll angle		rad
$\dot{\phi}$	Roll angle velocity		rad/s
$\ddot{\phi}$	Roll angle acceleration		rad/s^2
θ	Pitch angle		rad
$\dot{\theta}$	Pitch angle velocity		rad/s
$\ddot{\theta}$	Pitch angle acceleration		rad/s^2
ψ	Yaw angle		rad
$\dot{\psi}$	Yaw angle velocity		rad/s
$\ddot{\psi}$	Yaw angle acceleration		rad/s^2
$\hat{\phi}$	Estimated roll angle		rad
Θ	Vector containing the helicopter angles	$[\phi\ \theta\ \psi]^T$	rad

$\dot{\Theta}$	Vector containing the helicopter angle velocities	$[\dot{\phi}\ \dot{\theta}\ \dot{\psi}]^T$	rad/s
$\hat{\theta}$	Estimated pitch angle		rad
θ_{Acc}	Approximated angle from the accelerometer		rad
$\ddot{\Theta}$	Vector containing the helicopter angle accelerations	$[\ddot{\phi}\ \ddot{\theta}\ \ddot{\psi}]^T$	rad/s^2
Ξ	Vector containing the helicopter position	$[X\ Y\ Z]^T$	m
$\dot{\Xi}$	Vector containing the helicopter position velocities	$[\dot{X}\ \dot{Y}\ \dot{Z}]^T$	m/s
$\ddot{\Xi}$	Vector containing the helicopter position accelerations	$[\ddot{X}\ \ddot{Y}\ \ddot{Z}]^T$	m/s^2
Ω_i	Angular velocity of the i'th rotor		rad/s
Ω_r	Summed angular velocity of the rotors		rad/s
ρ	Air density		kg/m^3
σ	Solidity ratio		$-$
τ	Rotor time constant		s
θ_t	Blade angle at rotor tip		rad
$\tau_{x,y}$	Gyroscopic effect of the rotors acting on the roll and pitch axis		-
τ_z	The yaw acceleration resulting from the change in angular velocity of the rotors		m/s^2

Subscripts

h	In hover	-
i	The i'th rotor of n rotors	-
n	The n'th rotor of n rotors	-

Acronyms

HF *Helicopter-fixed frame*

EF *Earth-fixed frame*

RC *Radio Control*

FT *Flight Time*

ADC *Analog to Digital Converter*

FCB *Flight Control Board*

PID *Proportional Integral Derivative*

PD *Proportional Derivative*

PI *Proportional Integral*

LQR *Linear-Quadratic Regulator*

SISO *Single Input Single Output*

MIMO *Multiple Input Multiple Output*

FM *Figure of Merit*

PL *Power Loading*

Chapter 1

Introduction

In the last decade multi rotor helicopters have become more and more popular due to their simple mechanics. Most multi rotor helicopters consist of four rotors but in the last few years six and eight rotor helicopters have occurred on the market. The helicopters are primarily used for civil and military surveillance, but have also great potential for environmental use. Figure 1.1 shows three different multi rotor setups.

Figure 1.1: *Example of three different multi rotor helicopters*

The four rotor helicopter to the left is an example of a light and highly maneuverable multi rotor helicopter. The six rotor helicopter in the center of the figure is slightly heavier than the four rotor helicopter but can carry a higher payload. The cost of this increased payload is reduced agility. The largest multi rotor helicopter in figure 1.1, is a custom build eight rotor helicopter. It is build at the Technical University of Denmark by the author and is kindly borrowed from Papagaio Film. The primary function of the rather large multi rotor helicopters are to provide stable platforms for lifting heavy camera equipment.

The multi rotor helicopter is an unstable system and it is therefore of great interest to create a controller for multi rotor helicopters with a different number of rotors.

1.1 Prior work and litterature review

The control of four rotor helicopters has been widely investigated, where a few of the publications used in this project are [Bouabdallah and Siegwart(2007)] and [Pounds(2010)]. [Bouabdallah and Siegwart(2007)] has implemented a series of controllers such as *Proportional Integral Derivative* (PID) and *Linear-Quadratic Regulator* (LQR), from which it showed that the PID controller performed better than the LQR controller. The result from [Bouabdallah and Siegwart(2007)] are one of the reason for implementing the simple SISO controllers in chapter 7.

The projects by [Bertelsen and Magnsson(2004)] and [Pedersen(2006)] done at The Technical University of Denmark has covered LQR control of a four rotor helicopter and modeling of small rotors. Based on the prior work of the four rotor helicopters, multi rotor helicopters with n rotors are examined.

1.2 Objective

Previous research have focused on modelling and control of four rotor helicopters but do not cover the modeling and control of multi rotor helicopters with more than four rotors. The purpose of the thesis is to give insight into the modeling and control of a multi rotor helicopter with n rotors. The thesis has the following objectives:

- Construction of a mathematical dynamic nonlinear model of a multi rotor helicopter with n rotors.
- Construction of a mathematical model of the rotors, based on experimental data.
- Derivation of control algorithm to distribute the roll, pitch and yaw signals to the rotors.
- Design of SISO controllers to control the roll and pitch angle along with yaw velocity of the multi rotor helicopter.
- Implementation of the controllers on a multi rotor helicopter.

1.3 Outline

The thesis is organized as follows. First, an introduction of the basic principles of a multi rotor helicopter are explained based on a four rotor configuration in chapter 2. The four rotor configuration is chosen as this is the most simple multi rotor helicopter and this is used in the experimental part of this project. The helicopter used in the experiments is described in chapter 3 and is known as the quadrocopter.

Chapter 4 covers the dynamics of the propeller, motor and rotor. In chapter 5 the efficiency of the rotors are explained along with the propeller and motor efficiency, where the efficiency of the rotor is defined as the amount of thrust generated at a given power.

Chapter 6 covers the modelling of any multi rotor helicopter given the design requirements described in the first section of the chapter. The control of the model is described in chapter 7, where the purpose of each controller is explained in separate sections in the chapter.

Chapter 8, named Model and control verification examines the agreement between the model and the experimental data collected from the quadrocopter. In chapter 9, the controllers developed in chapter 7 is compared with the controllers from the manufacturer of the quadrocopter.

The flight time of a multi rotor helicopter and the quadrocopter is explained in chapter 10. Finally, conclusions are drawn and suggestions for model improvements and further research is given.

Chapter 2

Basic principles

The most simple type of multi rotor helicopter is the four rotor helicopter. Based on this type the general definitions will be explained. Figure 2.1 illustrates a four rotor helicopter located in the *Earth-fixed frame* (EF). The helicopter has its own coordinate system, namely the *Helicopter-fixed frame* (HF). On the x and y axis in the HF four rotors are mounted, with the rotor thrusts shown as T_1 to T_4. The thrust vectors $T_1 \dots T_n$ represents forces and are perpendicular to the HF z-axis.

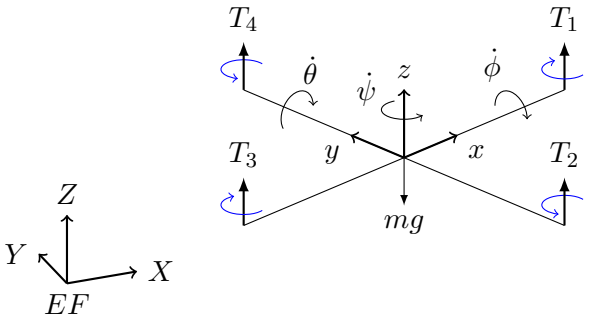

Figure 2.1: *Drawing of a four rotor helicopter with its* Helicopter-fixed frame *(HF) coordinate system. Its located in the* Earth-fixed frame *(EF). The thrust of the rotors are indicated by T_n and the rotation are shown as blue arrows around the thrust vector.*

The blue arrows show the rotation direction of each rotor, where rotors one and three are rotating clock wise and rotor two and four are rotating counter clock wise. When all rotors are rotating at the same speed, and the total thrust of all rotors is equal to the gravitational force acting on the helicopter, the helicopter will be in the stationary state called hover. In this state all accelerations in the HF and EF are equal to zero.

To decrease the pitch angle velocity, $\dot{\theta}$, of the helicopter the thrust T_1 is decreased and the thrust T_3 is increased. This change in thrust will result in the angular acceleration, $\ddot{\theta}$. The roll angle velocity can be changed using the same method but with rotors three and four instead. The rotation around the z-axis, ψ is called the yaw angle.

Chapter 3

Mikrokopter

Mikrokopter[1] is a German company producing radio controlled multi rotor helicopters, which has achieved great success within their area. Mikrokopters hardware is widely used by *Radio Control* (RC) aerial enthusiast and in the recent years also by professional aerial photographers around the world.

The control software made by Mikrokopter are in the RC community generally believed to be very stable, with a good overall performance. The helicopter used in experimental part of this project is therefore chosen to be Mikrokopters four rotor radio controlled L4-ME-model, also known as the quadrocopter, shown in figure 3.1[2].

Figure 3.1: *L4-ME Quadrocopter from Mikrokopter*

[1] http://mikrokopter.de
[2] Photo by Katja Lund-Rasmussen

3.1 Hardware

The quadrocopter is built with four 30 cm square aluminum rods formed as an "**X**". On the tip of each rod is placed a brushless motor with a EPP1045 10 inch propeller mounted on top. The motor is distributed by Mikrokopter and is of type BL-2827-35. It is controlled by the brushless motor controller "BL-controller v.1.2" designed by Mikrokopter. In the center of the helicopter, Mikrokopters Flight Control Board ME v.2.1 shown in figure 3.2[3], is placed along with the motor controllers.

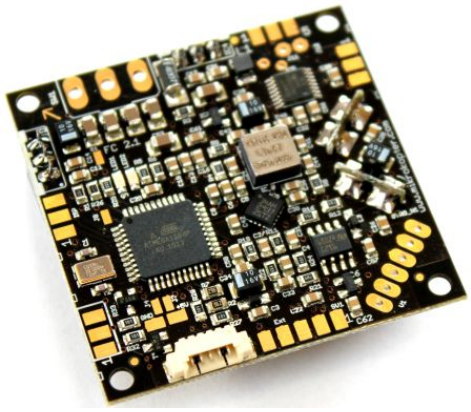

Figure 3.2: *Mikrokopters Flight Control Board ME v.2.1*

This board is used to control the helicopter and is equipped with a 3 axis $\pm$ 2g accelerometer and three $\pm 300°/s$ gyros representing the rotational velocity along three perpendicular axes. To control the helicopter the board processes the signals from the sensors with an *ATMEGA 1284P* 20 MHz processor. A more detailed description of the hardware and the sensors can be found in appendix E.

3.2 Radio control

The *Flight Control Board* (FCB) is connected to a Spektrum Satellite Receiver which receives up to seven control signals from a Spektrum DX7 radio controller. This receiver is most often used to control single rotor helicopters and is a very common radio controller. The report will therefore not cover the interface between the radio controller and the FCB.

3.3 Software

The flight control board is shipped with preconfigured open source software. This code consist of *Proportional Integral Derivative* (PID) controllers to control the attitude of the helicopter, but more important it also has of the capability to read sensor values, radio control inputs, and send control signals to the motor controllers. The code thereby gives a good starting point for the experimental part of this project. The motor controllers are also shipped with open source software, which furthermore enables some change of the motor controller.

[3]Photo by Mikrokopter

Chapter 4

Rotors

This chapter will present the rotor setup and the simplified rotor dynamics. A rotor is in this project defined as the motor and the propeller as a whole. The first section will give an overview of the physical rotor setup in the shape of the interaction and test setup of the rotor. The following sections will present physical expression for the thrust, torque, and power. Lastly the response of the rotor is examined in section 4.8.

To simplify the detailed aerodynamics of the rotor, the blades of the propeller are amused to be rigid, hence there is no blade flapping or coning. The vortex generated at the tip of the blade, also called the tip loss, is neglected in the thrust equations, but included in the power equations.

4.1 Rotor description

The rotors are, as previously mentioned, a combination of the motor and the propeller. The standard setup from Mikrokopter is a direct mount of the propeller on the motor shafts. One revolution of the rotor therefore corresponds to one revolution of the motor. The motors used in this project are Mikrokopters BL-2827-35 which are brushless 14 pole motors with 3 phases.

The motor is controlled using Mikrokopters BL-Ctrl v.1.2 which is a brushless motor controller. It receives an I^2C signal which is a 8 bit data signal which controls the current to the motor. To get one revolution with this type of motor, the phases have to shift 42 times, which corresponds to 42 positions pr. revolution. The time it takes the motor to move from one position to the next position, can then be used to estimate the angular velocity Ω_i of the rotor in rad/s. This can be expressed by equation 4.1, where t is the time between the phase shifts in seconds.

$$\Omega_i = \frac{2\pi}{42t} \tag{4.1}$$

By use of this equation the angular velocity and thereby also the rotor speed are measured and calculated. The experimental measurements of the rotor speed, thrust, torque, and electrical power of the rotor are conducted on the test bench shown in figure 4.1.

The rotor is mounted on a strain gauge, capable of measuring thrust and torque. The strain gauge is mounted on a vertical rod with a height of 1 meter to minimize the ground effect. The ground effect is an increase of thrust when the rotors are operating close to the ground. The ground effect depends on the rotor radius and the distance to the ground. According to [Leishman(2006), p. 260] the ground effect can be neglected at a distance of 3 times the rotor radius.

The rotor is set to spin at different velocities and the thrust, T_i and the torque, Q_i are measured. All measurements of the rotor are done with a constant voltage of 13.5 volt, which is estimated to be the average battery voltage during flight in hover. The measurements are done on one rotor and it is therefore assumed that the all rotors have the measured characteristics.

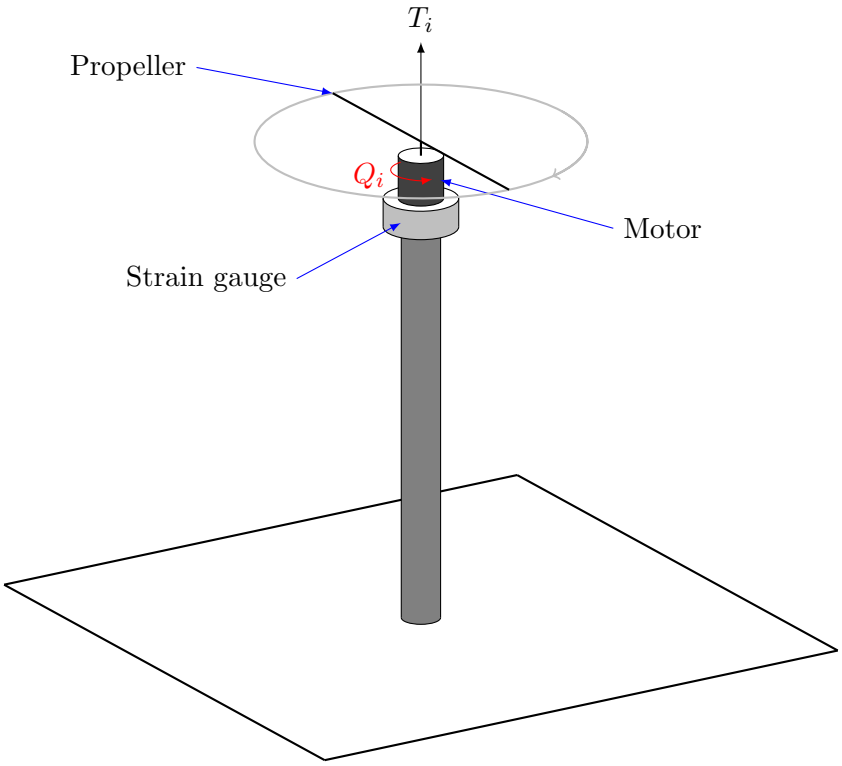

Figure 4.1: *The rotor test bench used to measure the thrust, torque and power of a rotor.*

4.2 Correlation between control signal and rotor speed

The correlation between the control signal and the rotor speed are an important factor, since it will be shown in the next sections that the thrust, torque and power depend on the rotor speed. The rotor is, as described in the previous section, controlled by an I^2C-signal, which control the current to the rotor. The signal is an 8 bit signal, and the correlation between the signal and the rotor speed are shown in figure 4.2,

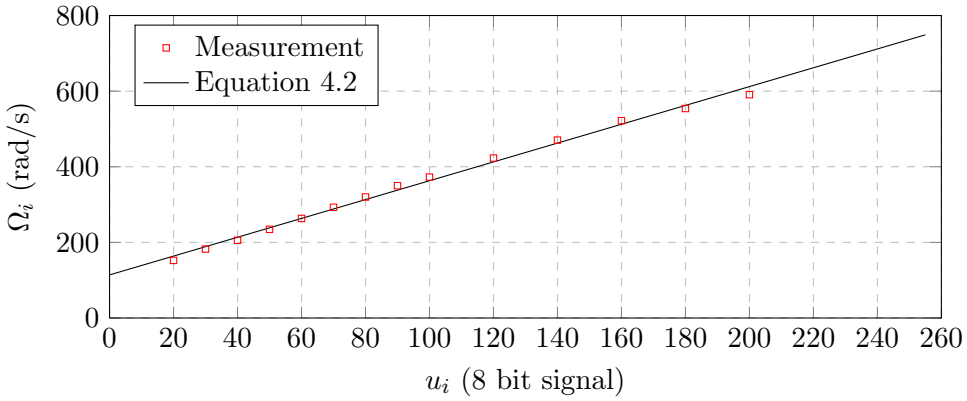

Figure 4.2: *Correlation between control signal and rotor speed.*

where the red points are the measured rotor speed and the black line is a fitted function represented by equation 4.2,

$$\Omega_i = 2.49u_i + 114 \tag{4.2}$$

where u_i is the the control signal. The fitted line in 4.2 is only well represented for control signals between 20 and 200, and all measurements in the following sections are made within this interval.

4.3 Thrust

The vertical thrust, T_i, of one rotor along the z axis can according to [Leishman(2006), p. 67] be expressed by equation 4.3,

$$T_i = C_T \rho A (\Omega_i R_r)^2 \tag{4.3}$$

where C_T is the thrust constant, A the rotor disc area, R_r the rotor radius and ρ the density of air. The angle of the blade, also called the pitch of blade, has a great influence on the thrust. The pitch of the blade is stated as; the distance the propeller would ideally move upwards in a solid material within one revolution.

Since the tip of the blade is traveling a larger distance than a section close to the center, the angle of the blade has to increase as the radius decreases. The change in angle compared to the radius is called the blade twist. If an ideal blade twist is assumed, the thrust constant, C_T can be determined by equation 4.4,

$$C_T = \frac{a\sigma}{4}\left(\theta_t - \frac{\dot{z} + v_i}{\Omega_i R_r}\right) \tag{4.4}$$

where a is the lift slope of the blade, θ_t is the angle of the propeller at the tip and σ is the solidity ratio defined by equation 4.5.

$$\sigma = \frac{A_b}{A} \tag{4.5}$$

A_b is the blade area. $\dot{z}$ in equation 4.4 is the velocity of the rotor in the z direction of the helicopter-fixed frame and v_i, described by equation 4.6,

$$v_i = \sqrt{\frac{T_h}{2\rho A}} \tag{4.6}$$

is the required velocity of air flowing through the disc area to maintain hover. v_i is often called the induced velocity. T_h is the thrust required to hover and can be expressed as equation 4.7,

$$T_h = \frac{mg}{n}. \tag{4.7}$$

where m is the total mass of the helicopter, g the gravity and n the number of rotors on the multi rotor helicopter.

4.3.1 Determination of the thrust constant

Due to lack of documentation of the dynamics of the propellers the thrust constant, C_T needs to be determined experimentally. The rotor is set to spin at different angular velocities and the thrust is measured[1] using the test setup in figure 4.1.

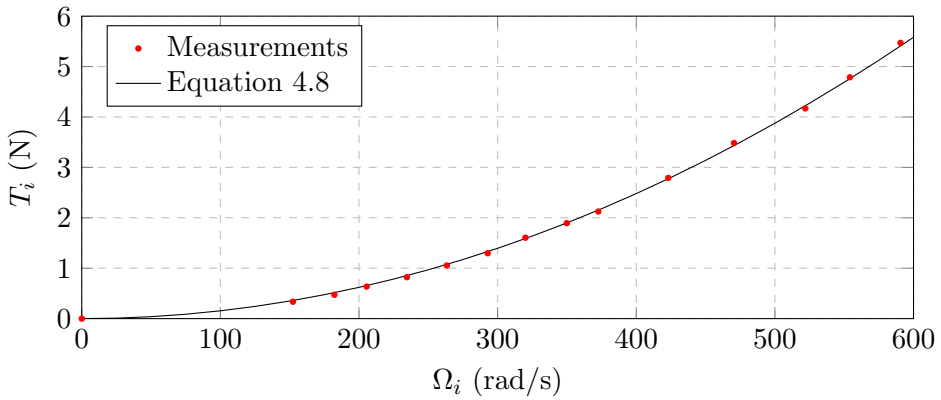

Figure 4.3: *Correlation between angular velocity and thrust.*

Figure 4.3 depicts these measurements where the black curve represents equation 4.8 which shows the correlation between the angular velocity, Ω_i and the generated thrust.

$$T_i = 1.55 \cdot 10^{-5} \Omega_i^2 \tag{4.8}$$

If equation 4.8 is compared to 4.3 it is seen that $1.55 \cdot 10^{-5}$ equals $C_T \rho A R_r^2$ and it is therefore possible to determine the thrust constant:

$$C_T = \frac{1.55 \cdot 10^{-5}}{\rho A R_r^2} = 0.0158\,\text{rad}^{-2} \tag{4.9}$$

[1] See appendix B.1 for test description and appendix B.2 for data points.

4.4 Torque

The torque, Q_i, of one rotor in the helicopter x, y plane can according to [Leishman(2006), p. 67] be described by equation 4.10

$$Q_i = C_Q \rho A (\Omega_i R_r)^2 R_r \tag{4.10}$$

where C_Q is the torque constant. If constant weight and therefore constant induced velocity(v_i) are assumed, the torque constant, C_Q can according to [Bramwell(2001), p. 50] be determined by equation 4.11,

$$C_Q = \frac{C_d}{8} + \frac{C_T}{\sigma} \frac{\dot{z} + v_i}{\Omega_i R_r} \tag{4.11}$$

where C_d is the drag constant for the propeller blade.

4.4.1 Determination of the torque constant

Due to lack of documentation of the dynamics of the propellers, the torque constant, C_Q is determined experimentally. The rotor is, as with the thrust measurements, set to spin at different angular velocities and the torque is measured using a strain gauge.

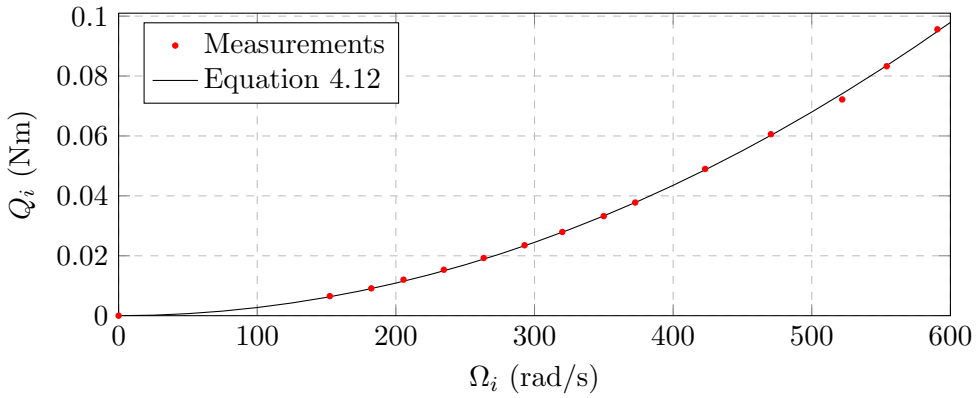

Figure 4.4: *Correlation between angular velocity and torque.*

Figure 4.4 depicts these measurements, where the black curve represent equation 4.12 which shows the correlation between the angular velocity, Ω_i and the generated torque.

$$Q_i = 2.72 \cdot 10^{-7} \Omega_i^2 \tag{4.12}$$

By applying equation 4.12 to 4.10, the drag constant, C_Q is calculated in equation 4.13.

$$C_Q = \frac{2.72 \cdot 10^{-7}}{\rho A R_r^3} = 0.0023\,\mathrm{rad}^{-2} \tag{4.13}$$

4.5 Correlation between thrust and torque

The correlation between thrust and torque can be expressed by equation 4.14 and calculated using equation 4.3 and 4.10.

$$C_{QT} = \frac{Q_i}{T_i} = \frac{C_Q R_r}{C_T} \tag{4.14}$$

If the experimentally determined values for the thrust and torque constants from equations 4.13 and 4.9, are inserted into equation 4.14 the result is represented by the constant C_{QT} in equation 4.15.

$$C_{QT} = \frac{0.0023\,\mathrm{rad}^{-2} 0.126\mathrm{m}}{0.0158\,\mathrm{rad}^{-2}} = 0.0176\mathrm{m} \tag{4.15}$$

The experimental correlation for the torque related to the thrust is expressed by equation 4.16, which fits nicely with the measurements shown in figure 4.5.

$$Q_i = 0.0176 T_i \tag{4.16}$$

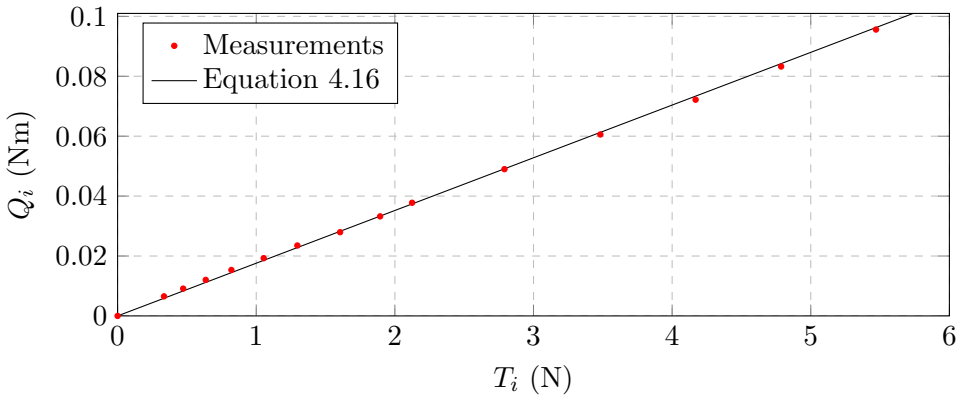

Figure 4.5: *Correlation between thrust and torque.*

4.6 Power

The power required to produce the thrust T_i can according to [Leishman(2006), p. 67] be expressed by equation 4.17,

$$P = C_P \rho A (\Omega R_r)^3 \tag{4.17}$$

where C_p is the power coefficient, and P, the power in watts. It should be noticed that equation 4.17 is very similar to the earlier described torque in equation 4.10. The relation between the two equations can be expressed as:

$$\frac{Q_i \Omega}{C_Q} = \frac{P}{C_P} \tag{4.18}$$

Since mechanical power is related to torque by $P = \Omega Q_i$, then numerically $C_P = C_Q$. In section 4.4, C_Q was determined to 0.0023 and C_P is therefore known to be 0.0023. The power coefficient can be split into two contributions. The first contribution is the required power to move the air through the disk area A. The second contribution is the required power to suppress the drag of the propeller. These two contributions can be expressed by equation 4.19,

$$C_P = C_{Pi} + C_{P0} \tag{4.19}$$

where C_{Pi}, expressed by equation 4.20,

$$C_{Pi} = \frac{kC_T^{(3/2)}}{\sqrt{2}} = 0.0015 \tag{4.20}$$

is the power required to produce the thrust with propeller drag neglected. The induced power correction factor k, is an expression of non ideal physical effects acting on the propeller such as tip loss, nonuniform inflow and so on. It is derived from the rotor measurements where the derivation is shown in appendix A. C_{P0} is the power required to exceed the drag of the propeller, and can be expressed by equation 4.21,

$$C_{P0} = \frac{\sigma C_d}{8} \tag{4.21}$$

where C_d is the drag coefficient of the propeller. Since C_P is equal to C_Q, and C_{Pi} is calculated based on the induced power correction factor from appendix A, C_{P0} can be derived from equation 4.19, and be expressed as:

$$C_{P0} = C_P - \frac{kC_T^{(3/2)}\sqrt{2}}{2} = 0.0008 \tag{4.22}$$

Figure 4.6 shows equation 4.17 where C_P is found as C_{P0}, C_{Pi} and the total mechanical power consumption, C_P.

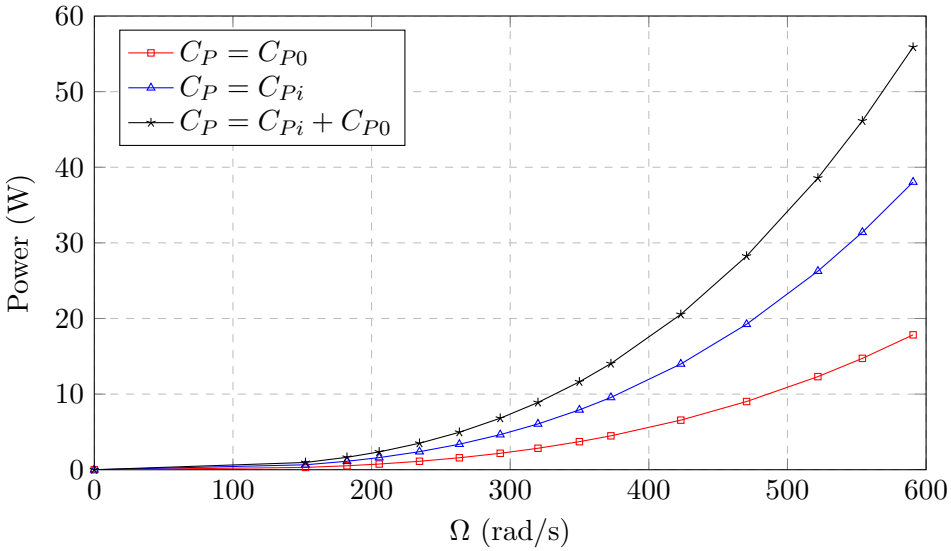

Figure 4.6: *Plot of equation 4.17, with C_P represented as C_{P0}, C_{Pi} and $C_{Pi} + C_{P0}$.*

It is clear from the figure that the power increases rapidly with the rotor speed. If equation 4.3 is compared to 4.17 it is seen that the mechanical power related to the rotor speed is $P \propto (\Omega R_r)^3$ whereas the thrust is related to the rotor speed as $T \propto (\Omega R_r)^2$.

From this it can be concluded that to produce a given thrust, with minimum amount of power, a large rotor radius is desired to keep the angular velocity at a minimum. This conclusion is built on the earlier described assumptions like rigid blades and zero coning. A low power consumption is often wanted and the correlation between number of rotors and power consumption is examined in the next section.

4.7 Correlation between number of rotors and power consumption

The correlation between the number of rotors and the maximal flight time is an expression of the helicopter mass and the total mechanical power consumed by n rotors at hover. To gain a long flight time it is therefore important to have a low power consumption. As previously mentioned the mechanical power is defined as:

$$P = \Omega Q \tag{4.23}$$

In section 4.5 it was shown that the correlation between thrust and torque of one rotor could be expressed by equation 4.14. Using this equation, the power of one rotor can be expressed by equation 4.24.

$$P = \Omega_i \frac{C_Q R_r T_i}{C_T} \tag{4.24}$$

Ω_i depends on the thrust, T_i, and can therefore be derived from equation 4.3 which results in equation 4.25.

$$\Omega_i = \frac{\sqrt{C_T \rho A T_i}}{C_T \rho A R_r} \tag{4.25}$$

Inserting the new expression for Ω_i into equation 4.24 results in the power equation 4.26.

$$P = \frac{C_Q T_i \sqrt{C_T \rho A T_i}}{C_T^2 \rho A} \tag{4.26}$$

The thrust required from each rotor to lift the helicopter is expressed by equation 4.27,

$$T_i = \frac{mg}{n} \tag{4.27}$$

where m is the total mass of the helicopter. Substituting T_i in equation 4.26 with the definition from equation 4.27 results in equation 4.28.

$$P = \Omega Q = \sqrt{\frac{m^3 g^3 C_Q^2}{C_T^3 \rho A n}} \tag{4.28}$$

Figure 4.7 shows the correlation between the total mass of the helicopter and the required power to maintain hover for n rotors, where the power is calculated from equation 4.28. It can be seen from the figure that at a given weight the mechanical power decreases with the number of rotors.

Figure 4.7 assumes that the total mass of the helicopter can be kept constant despite of adding an extra rotor. This is in reality not a very good assumption since adding an extra rotor will at least increase the total mass of the helicopter by the mass of the rotor. The total mass of the helicopter depending on the number of rotors, can be described by equation 4.29,

$$m_h = m_{FCB} + n(l \cdot m_{rod} + m_{Rotor}) + m_{Payload} \tag{4.29}$$

where m_h is the total mass of the helicopter, m_{FCB} is the mass of the Flight Control Board and the basic construction. m_{rod} is the mass of the rod pr. meter, m_{Rotor} is the mass of the rotor and $m_{Payload}$ is the mass of the payload and the battery.

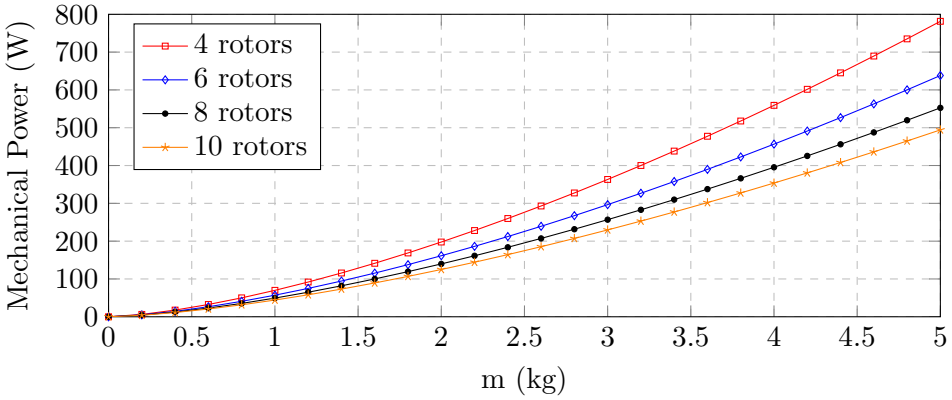

Figure 4.7: *Plot of equation 4.28 for different mass of the helicopter.*

It is important to notice, from equation 4.29, that the total mass of the helicopter is increasing with the number of rotors. The mass m_h can be calculated for different payloads and different number of rotors, based on the mass specifications of the quadrocopter, in appendix E.3.

A plot of equation 4.28 for different payloads is shown in figure 4.8, where m is now the mass m_h specified by equation 4.29.

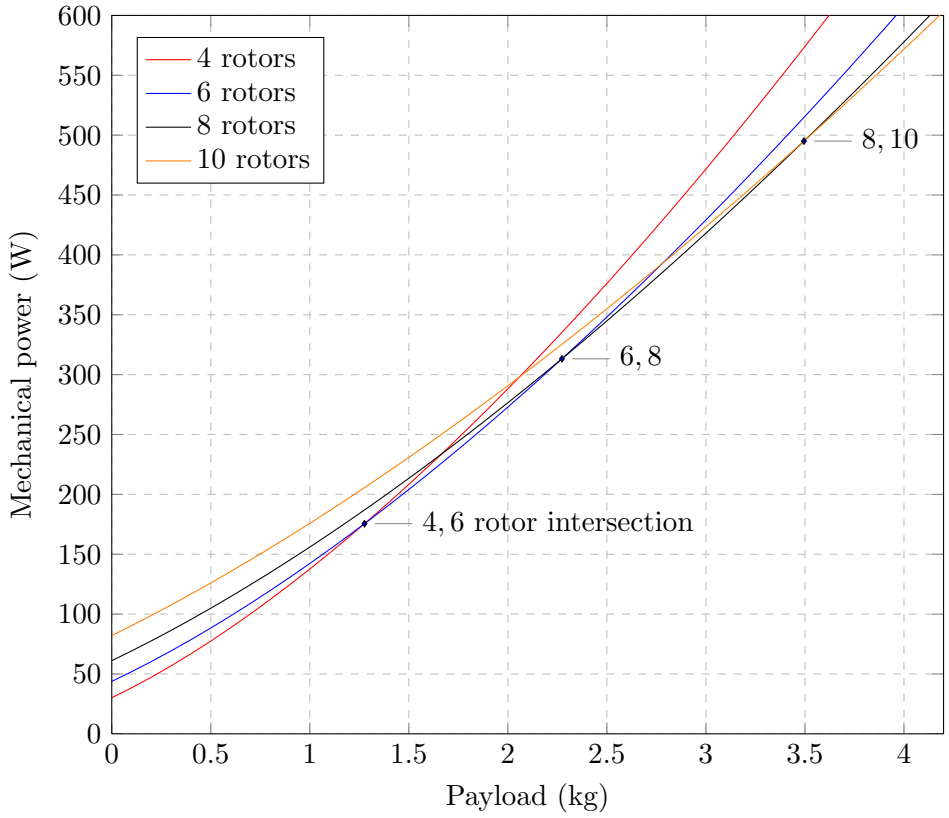

Figure 4.8: *Plot of equation 4.28 with the mass specified by equation 4.29 for varying payloads with n equal to 4, 6, 8 and 10 rotors.*

The figure shows the *total* mechanical power consumption at various payloads for a configuration of 4, 6, 8 and 10 rotors, where the four lines represent each number of rotors. It is seen that at small payloads the lowest power consumption is achieved from the 4 rotor helicopter, while at high payloads the best performance is achieved with 10 rotors. This correlation between rotors and payload will continue but it is up to the helicopter designer to estimate the benefits of an increased number of rotors instead of larger more powerful rotors.

From this observation it is clear that the optimal number of rotors depends on the payload. The point where the optimal number of rotors changes is marked as black dots in the figure. The first dot from the left is the "4,6 rotor intersection" which represents the point where the optimal number of rotors changes from four to six. Likewise the point "6,8" is the point where the optimal rotor number changes from six to eight rotors. From this figure it is concluded that the optimal number of rotors depends on the payload of the helicopter.

4.8 Rotor response

To model the response of the rotor a step is applied the rotor. Figure 4.9 illustrates such a step, where the rotor is given a control signal corresponding to a rotation of 185 rad/s and is then applied a new control signal corresponding to a step to 267 rad/s.

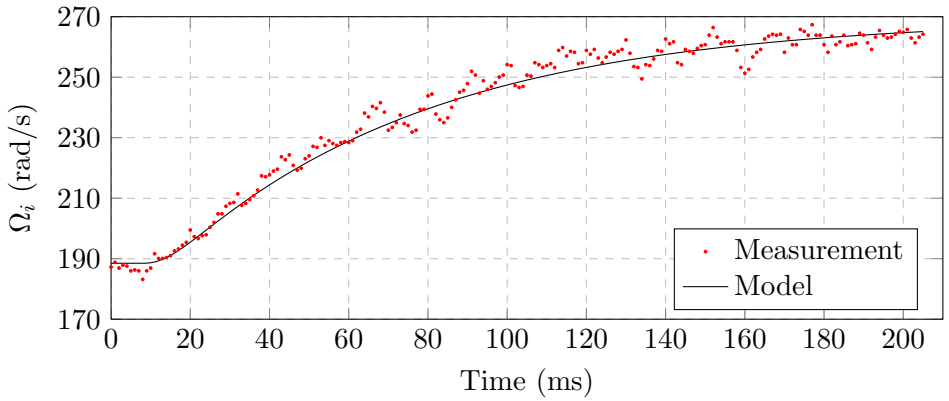

Figure 4.9: *Step response of a single rotor. Step from 185 to 267 rad/s at 10ms.*

The measured speed is passed through a low pass filter. The step response is assumed to be a response of a second order system. This assumption is based on the horizontal asymptote at the point when the step is applied. Since the low pass filter adds an order to the system, it is assumed that the rotor can be modeled as the first order transfer function shown in equation 4.30,

$$M_{tf} = \frac{1}{\tau s + 1} \tag{4.30}$$

where τ for these rotors are 0.067 s. The first order transfer function is a rather crude simplification of the rotor response but proved to be accurate to reproduce the experimental data.

The standard motor controllers from Mikrokopter are not configured to use feedback from the angular velocity of the rotor. Since it is only the current which is controlled by the motor controller, the angular velocity of the rotor decreases when the battery voltage decreases. From equation 4.3 it can be seen that this furthermore leads to a decrease in the thrust of the rotor. To avoid this decrease in angular velocity a *Proportional Integral* (PI) controller can be implemented to maintain the desired rotor speed. A PI controller will also be able to increase the response time of the rotor, and thereby decreasing the value of τ. However due to lack of memory on the motor control board it has not been possible to implement both the angular velocity counter and a fixed point PI controller.

To prove the idea of an actual controller on the motor control board, it has been possible to implement a simple P-controller. The step response of the controller with different P-gains are shown in figure 4.10.

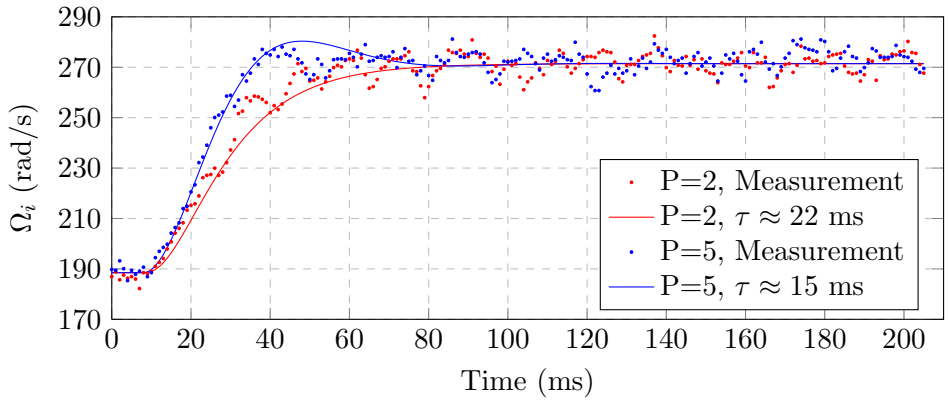

Figure 4.10: *Step response of a single rotor with a P controller with gains of 2 and 5. Step from 185 to 271 rad/s at 10ms.*

It can be seen that the response time has decreased by a factor of three for a p gain of two. During the implementation of a P-controller some of the error handling on the motor control board had been removed to free up space for the P-controller. This has unfortunately lead to an unstable motor control board, and the standard software, without an controller, is therefore used throughout the project.

4.9 Summary

This chapter presented the rotor dynamics and described the expressions for the rotor thrust, torque and power based on the assumption that the rotor was rigid, hence there were no blade flapping or coning. The correlation between thrust and torque was found to be linear, and was described by the constant C_{QT}. Measurements of the rotor used in the experimental part of the thesis were conducted and provided accurate results compared to the theoretical equations.

Based on the experimental data of the rotor, the constants for the rotors were calculated. Furthermore the response of the rotor was examined and it was seen that the rotor could modelled as an first order transfer function.

Chapter 5

Rotor efficiency

The efficiency of an rotor can generally be seen as an ratio of the thrust generated at a given power consumption. The efficiency of the rotor is therefore a combination of the efficiency of the propeller and the efficiency of the motor. The first section in this chapter will give insight into two ways of calculating the propeller efficiency and show the results with the propellers used by the quadrocopter from Mikrokopter. The second section will present the calculations of the motor efficiency and show the efficiency of the motors used by the quadrocopter. The last section present the combination of the quadrocopters propeller and the motor efficiencies. By this combination the overall rotor efficiency is calculated.

5.1 Propeller efficiency

The propeller efficiency can, according to [Leishman(2006)] be expressed by two equations. The first equation is the so called *Figure of Merit* (FM) which is used to compare two or more propellers with the same disk loading, where the disk loading is expressed as T_i/A. FM of the propeller can be calculated by equation 5.1

$$\text{FM} = \frac{C_T^{3/2}}{C_P\sqrt{2}} \tag{5.1}$$

The FM of the propellers used on the quadrocopter are calculated to be 0.60, where a good FM in most cases are between 0.7 and 0.8 according to [Leishman(2006)]. The second way of determining the efficiency, is by the *Power Loading* (PL), which is expressed by equation 5.2,

$$\text{PL} = \frac{T_i}{P} = \frac{C_T}{(\Omega R_r)C_P} \tag{5.2}$$

The PL of the propeller, as a function of the rotor speed, is shown in figure 5.1. From the figure it can be seen that the efficiency decreases with the rotor speed. It is therefore also seen by the figure and by equation 4.17 that a good efficiency of the propeller is achieved at low rotor speeds. This is due to the fact that the mechanical power related to the rotor speed are $P \propto (\Omega R_r)^3$ whereas the thrust is expressed as $T \propto (\Omega R_r)^2$.

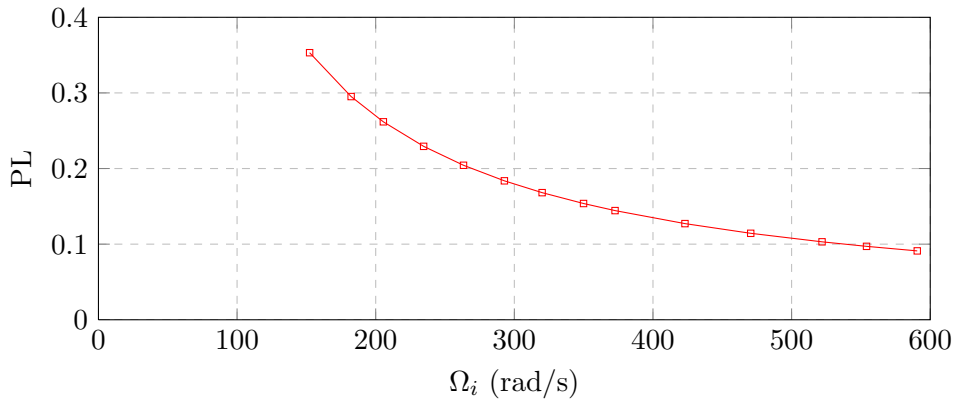

Figure 5.1: *Propeller efficiency depicted as the power loading with respect to* Ω_i.

5.2 Motor efficiency

The propeller is, as previously mentioned, mounted directly on the shaft of the motor. Due to friction in the motor and resistance in the motor control board, the motor efficiency will be below 100%. Furthermore electrical motors often have an operating range where the efficiency is optimal. The efficiency of the *rotor* is therefore a combination of the propeller and motor efficiency. The efficiency of the motor can be calculated as the ratio between the electrical power consumed by the motor and the mechanical power consumed by the propeller, as shown in equation 5.3,

$$\text{Efficiency} = \frac{P_M}{P_E} \tag{5.3}$$

where P_M and P_E are respectively the mechanical and electrical power. During the measurement of the thrust and torque of the rotor, the current used by the motor control board and the motor was measured. From this the electrical power was calculated and can be seen in appendix B.2.

Figure 5.2 shows the electrical and mechanical power used by the rotor, and depicts the motor efficiency as a function of the rotor speed. Based on the high electrical efficiency at high rotor speeds one might be tempted to pursue a higher angular velocity of the rotor. The result from section 5 should be kept in mind which states that the efficiency of the propeller is decreased at higher rotor speeds. It is therefore often unfortunate to pursue high rotor speeds.

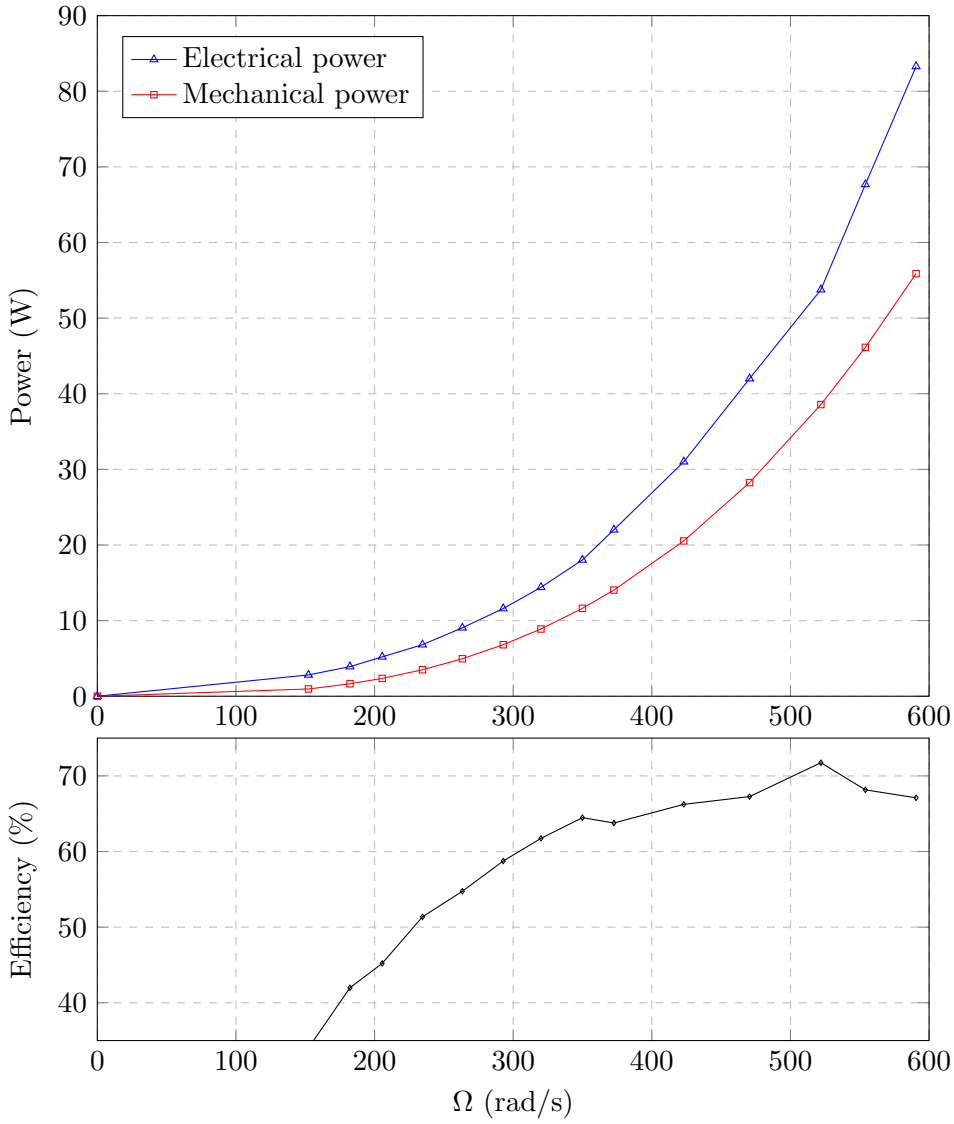

Figure 5.2: *Plot of equation 4.17, with P representing the mechanical or the electrical power used by the rotor. The efficiency of the rotor, in percent, is presented below the power plot.*

5.3 Combining propeller and motor

Since a propeller is no good without an motor, and vice versa, the efficiency of the combination is examined. The efficiency is found using the power loading equation in section 5.1, where P now represents the electric power. The power for the rotor can therefore be expressed by equation 5.4,

$$\mathrm{PL} = \frac{T_i}{P_E} \tag{5.4}$$

where P_E is the electrical power used by the rotor. The power loading is calculated based on the electrical power consumed by the rotor at the thrust T_i. A plot of the power loading for the whole rotor is shown in figure 5.3.

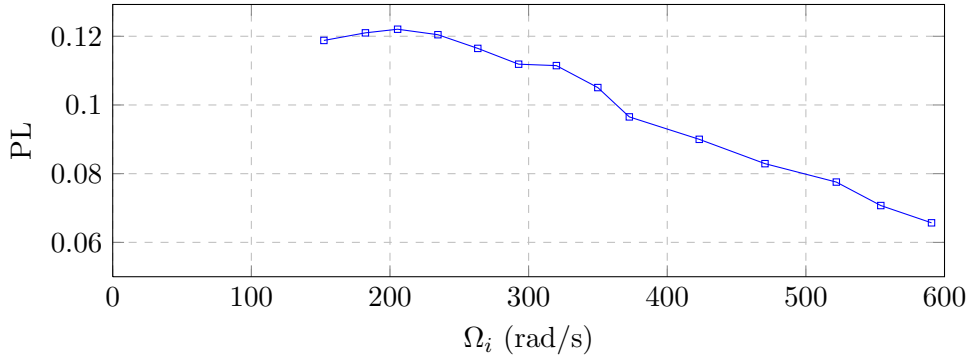

Figure 5.3: *Power loading efficiency plot of the rotor with respect to Ω_i.*

The plot shows a small maximum at 205 rad/s, at which the rotor is most effective. The corresponding thrust, is found from the table in appendix B.2, and is at this point 0.64N. The thrust required by each rotor to make the quadrocopter hover is 1.97N, corresponding to 360rad/s.

It can therefore be concluded that the maximum of the power plot is located 155 radians below the optimum for the case of the quadrocopter. The correlation between the mechanical power loading of the propeller and the electrical efficiency described by equation 5.4, is shown in figure 5.4.

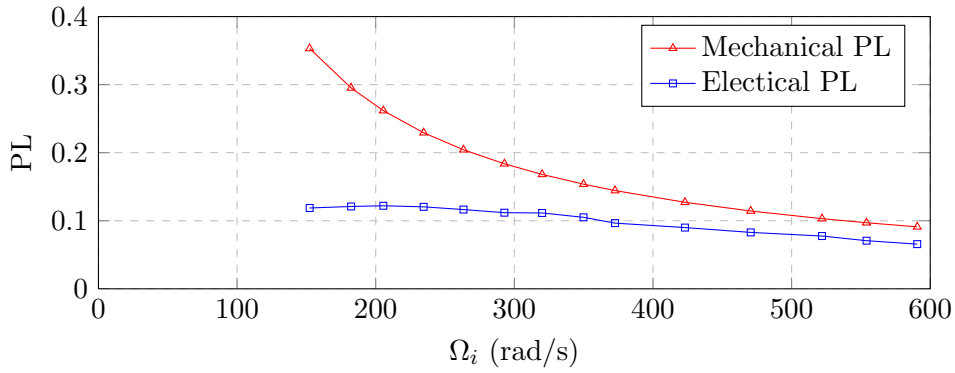

Figure 5.4: *Mechanical propeller efficiency and electrical rotor efficiency depicted as the power loading with respect to Ω_i.*

The low electrical rotor efficiency at low rotor speeds is due to the low efficiency of the brushless motor at low speeds. It can be seen that the efficiency of the electrical rotor is almost linear compared to the propeller efficiency, and at low speeds there is great room for improvement of the electrical efficiency. The thrust of the rotor compared to the electric power consumption is shown in figure 5.5.

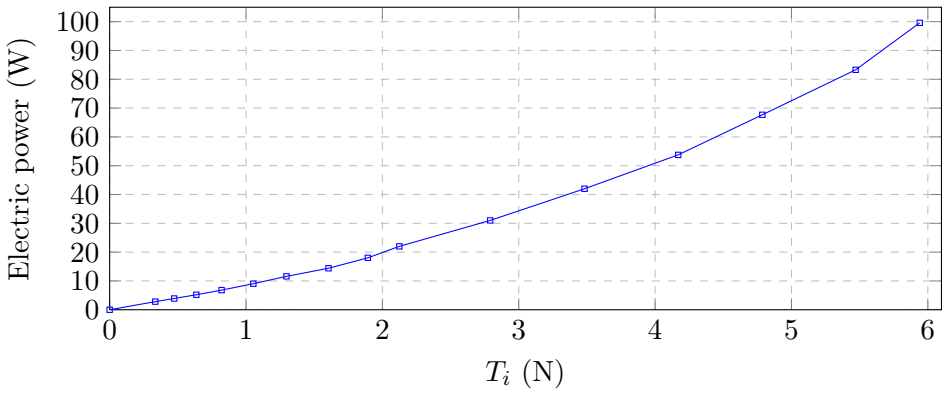

Figure 5.5: *Electric power consumption with respect to thrust.*

As can be seen from the figure, the slope of the graph increased with the thrust, hence the required power increases with the thrust. Even though the increased power consumption might look insignificant with these measurements, this is worth noting, since the power has influence on the overall flight time.

5.4 Summary

In this chapter the efficiency of the rotor was divided into a propeller efficiency, a motor efficiency and the total rotor efficiency. The efficiency of the propeller was presented by two equations in this chapter. The first was a constant expression named *Figure of Merit* (FM) which were used to determine if the propeller was well designed. The FM were found to be 0.6 which was below the definition of a good performing propeller with a FM of 0.7 to 0.8. The second, and more dynamic, way of determining the efficiency of the propeller were found by the *Power Loading* (PL). The PL depended on the rotor speed and it was seen that the efficiency decreased with the rotor speed.

The electrical efficiency of the motor was also determined and it was seen that the best efficiency was achieved at high angular velocities. The total rotor efficiency was furthermore depicted and the most efficient rotor speed was determined.

Chapter 6

Modelling

A multi rotor helicopter can have various designs, and the model must therefore have the following requirements for the physical design:

- The number of rotors, n, are even numbers of $4, 6, 8, 10, ...$ and always above 4.
- Rotor one is always located on the x axis and is rotating clockwise.
- All rotors are located in a circle in the xy-plane with radius $\geq l$.
- The angle between each rod is $\frac{2\pi}{n}$ rad.
- The structure is assumed rigid.
- The center of gravity and the helicopter-fixed frame origin are assumed to coincide.
- Thrust and torque are proportional.

An example of a six and eight rotor helicopter which fulfill the assumptions above are shown in figure 6.1.

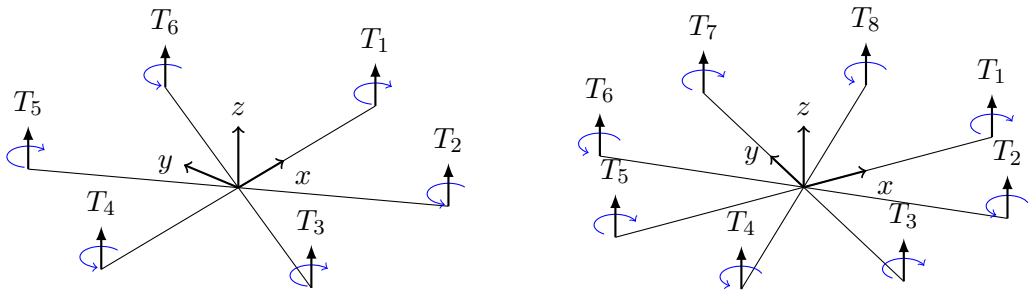

Figure 6.1: *Example of a six and a eight rotor helicopter*

To avoid the propellers colliding while rotating in the x, y plane in the HF, the minimum length, l, of each helicopter rod can be determined by equation 6.1,

$$l \geq \frac{R_r}{\sin\frac{\pi}{n}} \tag{6.1}$$

where R_r is the radius of the rotor. The rotors of the helicopter are located in the same plane to minimize the aerodynamic interaction between the rotors. The model of a multi rotor helicopter can be divided into four blocks as illustrated in figure 6.2, where each block and signal is described in the following sections. The matlab simulink model of the system is depicted in appendix F.

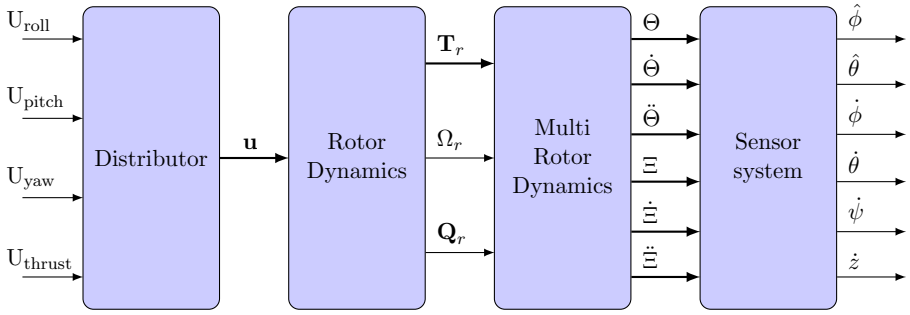

Figure 6.2: *Block diagram of the multi rotor helicopter model*

6.1 Distributor

The distributor receives the control signals for roll, pitch, yaw and thrust and distributes these signals to the correct rotors. The basic idea of the distributor was previously explained in chapter 2, where it was seen that for a four rotor helicopter a positive roll movement was achieved by increasing the thrust of rotor four and decreasing the thrust of rotor two.

The distributor thereby creates the rotor control signals to provide the roll acceleration. For a multi rotor helicopter there are many different thrust combinations which result in for instance a roll acceleration. In this report the distributor for an n rotor helicopter is created as expressed by equation 6.2, where the signal to the the i'th rotor is described by u_i.

$$\begin{aligned}
\mathrm{u_1} &= \mathrm{U_{thrust}} + \mathrm{U_{pitch}} \cdot \cos\frac{0}{\mathrm{n}} + \mathrm{U_{roll}} \cdot \sin\frac{0}{\mathrm{n}} - \mathrm{U_{yaw}} \\
\mathrm{u_2} &= \mathrm{U_{thrust}} + \mathrm{U_{pitch}} \cdot \cos\frac{2\pi}{\mathrm{n}} + \mathrm{U_{roll}} \cdot \sin\frac{2\pi}{\mathrm{n}} + \mathrm{U_{yaw}} \\
\mathrm{u_i} &= \mathrm{U_{thrust}} + \mathrm{U_{pitch}} \cdot \cos\frac{2\pi(\mathrm{i}-1)}{\mathrm{n}} + \mathrm{U_{roll}} \cdot \sin\frac{2\pi(\mathrm{i}-1)}{\mathrm{n}} + (-1)^i \cdot \mathrm{U_{yaw}} \\
&\vdots \\
\mathrm{u_n} &= \mathrm{U_{thrust}} + \mathrm{U_{pitch}} \cdot \cos\frac{2\pi(\mathrm{n}-1)}{\mathrm{n}} + \mathrm{U_{roll}} \cdot \sin\frac{2\pi(\mathrm{n}-1)}{\mathrm{n}} + (-1)^n \cdot \mathrm{U_{yaw}}
\end{aligned} \tag{6.2}$$

If an n equal to 4 rotor helicopter, previously shown in figure 2.1, is considered, it is seen from equation 6.2, that rotor one(u_1) is only affected by thrust, pitch and yaw signals, and not by the roll signal. This is because rotor one is located directly on the x axis in the HF. It can also be seen from the figure, that rotor two is located exactly on the y-axis and therefore is only affected by thrust, roll and yaw signals. For a n equal to 6 rotor helicopter, shown to the left in figure 6.1, rotor two will still be affected by thrust and yaw signals but also by both roll and pitch signals.

From equation 6.2 it can be seen that a pitch signal on rotor two will affect it by $cos\frac{2\pi}{6}$ or 50 percent of the pitch signal. Since rotor two is closer to the y axis, and therefore has greater influence on roll maneuvers, it is affected by $sin\frac{2\pi}{6}$ or 87 percent of the roll signal. With the distributor it is possible to design a *Single Input Single Output* (SISO) controller on each axis. If a *Multiple Input Multiple Output* (MIMO) control approach is considered the distributor can be left out.

6.2 Rotor dynamics

The Rotor dynamic block describes the motors and propellers combined dynamics and is based on the results from chapter 4. The block receives the rotor control signals and turns them into the rotor speeds, force and torque generated by the rotors. The correlations between the control signal and the generated rotor speeds, thrust and torque were determined in chapter 4. Based on this chapter the model for the rotors can be expressed as shown in figure 6.3.

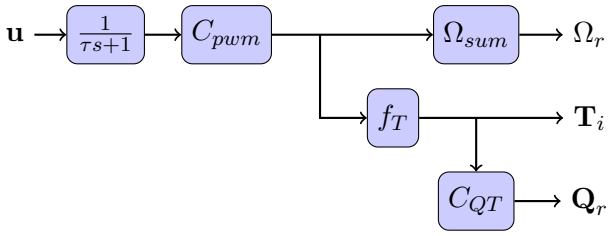

Figure 6.3: *Rotor dynamics*

All the signals in the figure, except Ω_r, are vectors consisting of n elements. $\mathbf{u}$ is the vector containing the control signals to the rotors. From the step response in chapter 4 it was seen that an approximation of the rotor response could be modeled as a first order transfer function.

The first block from the left in the figure describes this first order transfer function for the rotor, with τ as the time constant. C_{pwm} represents the correlation between the control signal and the rotor speeds as shown in equation 4.2. The output of C_{pwm} is therefore the rotor speeds. The correlation between the rotor speeds and the force are represented by the f_T-block, which represent equation 4.3. Likewise the correlation between the thrust and torque are shown as C_{QT}. The block Ω_{sum} receives a vector containing the rotor speeds of all rotors and adds them together with the use of equation 6.3 to get Ω_r,

$$\Omega_r = (-1)^i \sum_{i=1}^{n} \Omega_i \tag{6.3}$$

where Ω_i is the angular velocity of rotor i, and is always positive, independent of the rotation direction. By use of equation 6.3 it is possible to determine if the clockwise rotating propellers are rotating faster than the counter clockwise and vice versa. This information is used in next section.

6.3 Multi rotor dynamics

This part of the model describes the helicopter dynamics in form of the orientation and position in the *Earth-fixed frame* (EF). It can be divided into a system describing the orientation/attitude of the helicopter and a system describing the position of the helicopter in the EF. The systems are based on the equations of a four rotor helicopter from [Bouabdallah and Siegwart(2007)].

6.3.1 Orientation

The orientational subsystems consist of the roll, pitch and yaw movements of the helicopter. The roll and pitch are very much alike and consists of three contributions. The first contribution acting on the helicopter is the one caused by the thrust of the rotors. When the total thrust on one side of an axis is greater than the total thrust of the other side, the helicopter starts to accelerate around that axis. This angular acceleration can be described by equation 6.4 for the roll axis and by equation 6.5 for the pitch axis,

$$\ddot{\phi} = \frac{l}{I_x} \sum_{i=1}^{n} T_i \sin \frac{2\pi(i-1)}{n} \tag{6.4}$$

$$\ddot{\theta} = \frac{l}{I_y} \sum_{i=1}^{n} T_i \cos \frac{2\pi(i-1)}{n} \tag{6.5}$$

where l is the length of the rod from the rotor to the center of the helicopter. The second effect acting on the helicopter is the inertial effect during roll and pitch velocities. This effect can be described by equation 6.6 for the roll axis and by equation 6.7 for the pitch axis,

$$\ddot{\phi} = \frac{\dot{\theta}\dot{\psi}(I_y - I_z)}{I_x} \tag{6.6}$$

$$\ddot{\theta} = \frac{\dot{\phi}\dot{\psi}(I_z - I_x)}{I_y} \tag{6.7}$$

where I_x, I_y and I_z is the inertia of the helicopter on the x-, y- and z-axis. The last part of the modeled physical effects acting on the roll and pitch axis of the helicopter is the gyroscopic effect of the rotors, which is described by equation 6.8 and 6.9,

$$\tau_x = \frac{J_r \dot{\theta} \Omega_r}{I_x} \tag{6.8}$$

$$\tau_y = \frac{J_r \dot{\phi} \Omega_r}{I_y} \tag{6.9}$$

where J_r is the inertia of the rotor including the rotating part of the motor. Ω_r is the resulting angular velocity as described by equation 6.3.
When the above equations are combined the total roll and pitch acceleration of the helicopter in the HF can be determined respectively from equations 6.10 and 6.11.

$$\ddot{\phi} = \frac{\dot{\theta}\dot{\psi}(I_y - I_z) + J_r \dot{\theta} \Omega_r + l \sum_{i=1}^{n} T_i \sin \frac{2\pi(i-1)}{n}}{I_x} \tag{6.10}$$

$$\ddot{\theta} = \frac{\dot{\phi}\dot{\psi}(I_z - I_x) - J_r\dot{\phi}\Omega_r + l\sum_{i=1}^{n} T_i \cos\frac{2\pi(i-1)}{n}}{I_y} \tag{6.11}$$

Beside the roll and pitch orientation, there is an angular orientation around the z-axis called yaw. The yaw acceleration can, like the roll and pitch accelerations, be divided into three contributions. The first contribution is the torque caused by the rotors cutting through the air and thereby creating drag.

As shown in section 4.5 the ratio between torque and thrust of a rotor can be considered proportional, and is described by the factor C_{QT}. The total torque caused by the rotors can therefore be calculated by use of equation 6.12.

$$\tau_{\mathrm{r}} = \frac{C_{QT} l (-1)^i \sum_{i=1}^{n} T_i}{I_z} \tag{6.12}$$

When a rotor changes its angular velocity this leads to an angular acceleration which acts as an torque, τ_z, around the z-axis in the HF. This torque can be expressed by equation 6.13, where J_r is the rotor inertia including the inertia of the rotating motor component.

$$\tau_z = \frac{J_r\dot{\Omega}_r}{I_z} \tag{6.13}$$

The last component acting on the yaw acceleration is the inertia of the helicopter which for the yaw-axis can be described by equation 6.14.

$$\ddot{\psi} = \frac{\dot{\theta}\dot{\phi}(I_x - I_y)}{I_z} \tag{6.14}$$

The resulting yaw acceleration is then expressed by equation 6.15.

$$\ddot{\psi} = \frac{\dot{\theta}\dot{\phi}(I_x - I_y) + J_r\dot{\Omega}_r + \tau_r}{I_z} \tag{6.15}$$

6.3.2 Position

The position of the helicopter in the earth-fixed frame can be expressed by the EF horizontal and vertical accelerations, $\ddot{X}$, $\ddot{Y}$ and $\ddot{Z}$, in equation 6.16, 6.17 and 6.18,

$$\ddot{X} = \sum_{i=1}^{n} T_i \frac{\sin\psi\sin\phi + \cos\psi\sin\theta\cos\phi}{m} \tag{6.16}$$

$$\ddot{Y} = \sum_{i=1}^{n} T_i \frac{-\cos\psi\sin\phi + \sin\psi\sin\theta\cos\phi}{m} \tag{6.17}$$

$$\ddot{Z} = \frac{\sum_{i=1}^{n} T_i \cos\psi\cos\phi}{m} - g \tag{6.18}$$

where m is the total mass of the helicopter. An integration of these accelerations will result in the velocity, and a further integration will result in the position of the helicopter.

6.4 Sensors

For the helicopter to be able to measure its angles and angle velocities it is, as earlier mentioned, equipped with an accelerometer and a $\pm 300°/s$ gyro which also have to be considered in the model. The combination and dynamics of these sensors are described in the sensor block in the model shown in figure 6.2.

6.4.1 Angle estimation

The pitch and roll angle of the helicopter in the EF is determined using the accelerometer and the gyro. The combination of these measurements gives a good roll and pitch angle estimation, despite of disturbances on the x, y, z, ϕ and θ axis. The gyro is used to avoid large angle errors due to sudden acceleration disturbances on the x, y and z axis. Likewise the accelerometer is used to compensate for small drift errors in the gyro.

In the stationary state, where the velocities along the X,Y and Z-axis in the EF are constant, the roll and pitch angle of the helicopter can be calculated using equation 6.19, where $\ddot{x}$, $\ddot{y}$ and $\ddot{z}$ are respectively the measured accelerations in the x, y and z direction in the HF.

$$\theta = \arctan \frac{\ddot{x}}{\ddot{z}} \quad , \quad \phi = \arctan \frac{\ddot{y}}{\ddot{z}} \tag{6.19}$$

The arctangent function is implemented on the flight control board as as the approximation shown in appendix H.1. In the dynamic case, where the helicopter velocities along the X, Y and Z-axes in the EF are not constant, the angular velocities are integrated to get the angles:

$$\theta = \int \dot{\theta} \, \mathrm{d}t \quad , \quad \phi = \int \dot{\phi} \, \mathrm{d}t \tag{6.20}$$

The signal from the gyro is therefore passed through a high pass filter and the angle from the accelerometers is passed through a low pass filter. The gyro and accelerometer angle measurements are combined as shown in figure 6.4.

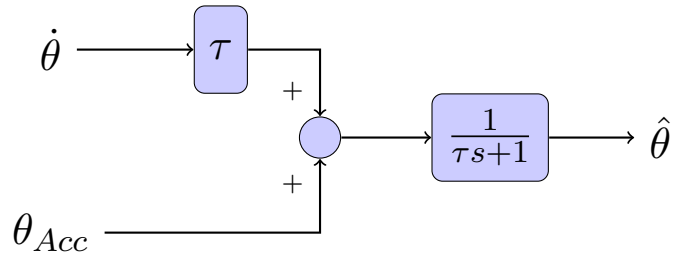

Figure 6.4: *Angle estimation*

The derivation of the angle estimate shown in figure 6.4 can be seen in appendix D. $\dot{\theta}$ represents the angular velocity measured by the gyro and θ_{Acc} represents the approximated angle from the accelerometer values. This combination of measurements results in the angle estimation $\hat{\theta}$.

The sensors on the quadrocopter used in the experiments are not located directly in center of rotation of the quadrocopter. The accelerometer is located 3.2

cm above the center of rotation on the x and y axis. This leads to an angular acceleration during changes in the roll and pitch angles. A matlab simulink model has been created to simulate the accelerometer and its displacement, and can be seen in figure F.9 in appendix F.

The model also includes the simulation of the gyro and the angle estimation algorithm, and is based on the sensor specifications of the quadrocopter. The time constant, τ is set to 2.2s, which is experimental determined to be the best value. A step response of the pitch angle is shown in figure 6.5.

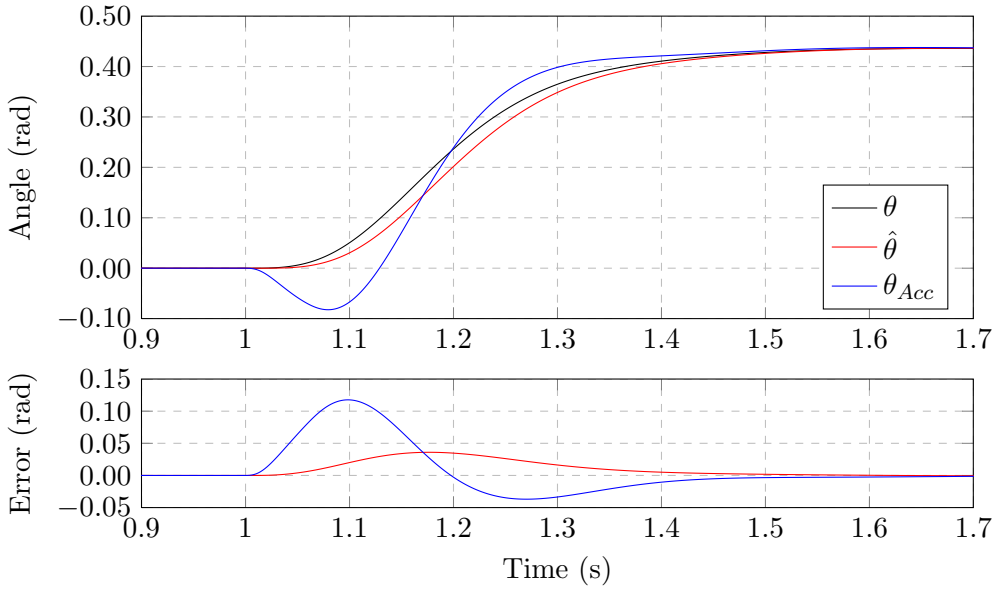

Figure 6.5: *Real and estimated angle plotted at a step response.*

The true angle is depicted as the black line, and the estimated angle is depicted as the red line. The blue line represents the angle generated by the accelerometer based on equation 6.19. It can be seen from the figure that the estimated angle lags a little bit behind the true angle which is due to the large negative angle generated by the accelerometer. This is only a minor error compared to the fact that the angular acceleration affecting the angle generated from the accelerometer, θ_{Acc}, is suppressed.

6.5 Summary

This chapter presented the dynamic nonlinear model of a multi rotor helicopter with n rotors. The model was divided into four parts. The first part described the distribution of the roll, pitch, yaw and thrust signals to rotors.

The second part described the rotor dynamics based on the results form chapter 4. The third part described the dynamics of the multi rotor helicopter by both the orientation and position in the *Earth-fixed frame* (EF). The last part described the dynamics of the sensors and an angle estimation algorithm was derived.

Chapter 7

Control

This chapter will present the layout and combination of the controllers used to control the multi rotor model from chapter 6. To keep the orientation of the helicopter stable a series of controllers are implemented. The controllers are divided into three parts:

- The roll and pitch angles are controlled by PID controllers.
- The roll and pitch angle velocities are controlled by *Proportional Derivative* (PD) controllers.
- The yaw angle velocity is controlled by a PID controller.

The above controllers are chosen based on [Bouabdallah and Siegwart(2007)] results which showed that the simple SISO controllers performed just as well as the *Linear-Quadratic Regulator* (LQR). To create the SISO controllers the model is linearized around hover, i.e. the roll, pitch and yaw angles are equal to zero. The linearization around hover is chosen based on the assumption that during normal flight the helicopter will most likely be operating around hover, with only small angles and velocities in the earth-fixed frame.

The first section will present the layout of the angle velocity controller. The second section explains the angle controllers combined with the angle velocity controllers. Since the model from chapter 6 is a general model for an n rotor helicopter, the specific values for the controllers are only calculated for the quadrocopter. The last section in this chapter will therefore describe the controllers used on the quadrocopter.

7.1 Angle velocity control

The angular velocity control of the helicopter has been designed based on the previously mentioned linearization of the model from chapter 6. The linearized angle velocities, in the Laplace domain, can therefore be expressed by equation 7.1, 7.2 and 7.3,

$$\dot{\phi}(s) = \frac{1}{s} \frac{l \sum_{i=1}^{n} T_i \sin \frac{2\pi(i-1)}{n}}{I_x} \tag{7.1}$$

$$\dot{\theta}(s) = \frac{1}{s} \frac{l \sum_{i=1}^{n} T_i \cos \frac{2\pi(i-1)}{n}}{I_y} \tag{7.2}$$

$$\dot{\psi}(s) = \frac{1}{s}\frac{J_r\Omega_r s - \Omega_r(0) + \tau_r}{I_z} \tag{7.3}$$

where τ_r is described in equation 6.12.

7.1.1 Roll and pitch angular velocity control

The PD controller for the roll and pitch angular velocities can be designed as shown in figure 7.1,

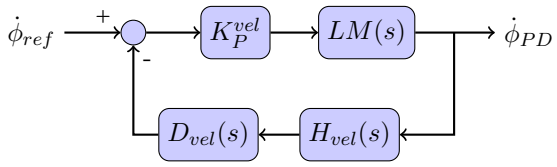

Figure 7.1: *PD controller*

where K_P^{vel} and D_{vel} are respectively the proportional and derivative gain. $LM(s)$ is the linearized model in form of the distributor, rotor dynamics and helicopter dynamics, $\dot{\phi}(s)$. H_{vel} is the transfer function for the sensor system, where the sensor system, in this case, is a low pass filter which filters the gyro signal. The derivative gain is located in the feedback loop to minimize the overshoot. The closed loop transfer function for the angular velocity PD controller can be expressed by equation 7.4.

$$G_{vel}(s) = \frac{K_P^{vel} LM(s)}{1 + K_P^{vel} LM(s) D^{vel}(s) H_{vel}(s)} \tag{7.4}$$

A PD controller has been chosen to control the roll and pitch angle velocities because of its capability of achieving high bandwidth. An integrator has not been added to the controller since it would decrease the bandwidth, and any steady state error of the angular velocity will be caught by the angle controller as explained in the next section. The design of the PD controllers for the quadrocopter is explained in appendix G.

7.1.2 Yaw angular velocity control

The model from chapter 6 only controls the yaw velocity and not the yaw angle, due to an assumed lack of a heading sensor such as an compass. A PID controller has therefore been designed to control the yaw velocity. The PID controller has been chosen to avoid steady state errors. The controller can be designed as depicted in figure 7.2,

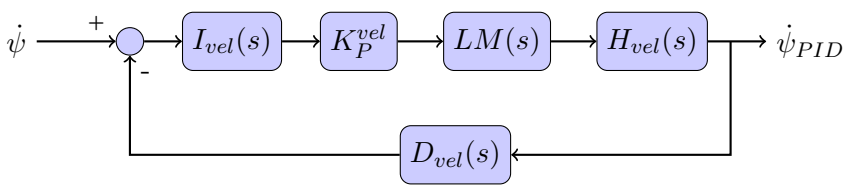

Figure 7.2: *Yaw velocity PID controller.*

where K_P^{vel}, D_{vel} and I_{vel} are respectively the proportional gain, the derivative and the integral term of the PID angle velocity controller.

7.2 Roll and Pitch angle control

The angle control of the helicopter is based on the transfer function determined in equation 7.4. The PD controlled angle velocity, G_{vel}, is integrated to get the angle of the helicopter. It should be noted that the integrated angle velocity is the calculated value and not the value from the sensor, H_{vel}. The roll angle of the helicopter can therefore be expressed by equation 7.5.

$$\phi(s) = \frac{1}{s} G_{vel}(s) \tag{7.5}$$

The PID angle controllers are designed as shown in figure 7.3,

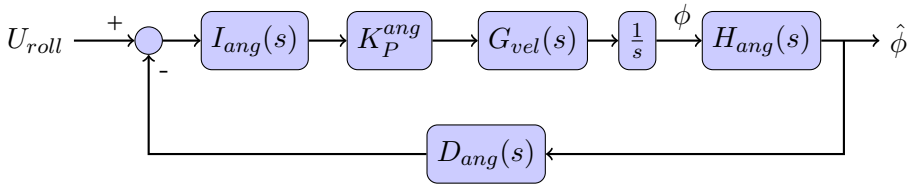

Figure 7.3: *Roll PID controller*

where K_P^{ang}, D_{ang} and I_{ang} are respectively the proportional gain, the derivative and the integral term of the PID angle controller. H_{ang} is the transfer function for the angle estimation system. The transfer function for the PID controller are expressed by equation 7.6.

$$G_{ang}(s) = \frac{\hat{\phi}}{U_{roll}} = \frac{I_{ang}(s) K_p^{ang} G_{vel}(s) \frac{1}{s} H_{ang}(s)}{1 + D_{ang}(s) I_{ang}(s) K_p^{ang} G_{vel}(s) \frac{1}{s} H_{ang}(s)} \tag{7.6}$$

7.3 Angle thrust compensation

To make it easier for the pilot to maintain the acceleration on the Z axis during roll and pitch maneuvers an angle dependent thrust compensation has been added to the controller.

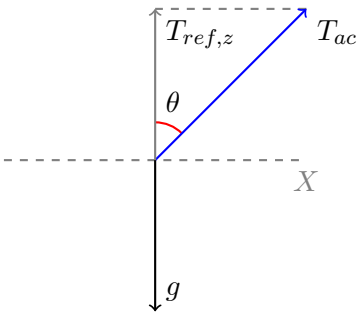

Figure 7.4: *Thrust vector, T_{ac}, depicted with respect to the pitch angle θ.*

When the helicopter is hovering the total thrust of the rotors, is equal to the gravitational force acting on the helicopter, mg. If the pilot pitches the helicopter with the angle θ, the total thrust required to maintain hover is increased. It is therefore desired to find the thrust vector, T_{ac}, which maintain the acceleration, $T_{ref,z}$, along the Z-axis, independent of the roll and pitch angles. The thrust vector, T_{ac}, for the pitch angle θ and a roll angle of 0 degrees is displayed in figure 7.4. The thrust vector T_{ac} shown in figure 7.4 can be calculated using equation 7.7.

$$T_{ac} = \frac{T_{ref,z}}{\cos\theta} \tag{7.7}$$

In the case where both the roll and pitch angle are different from zero, the size of the thrust vector can be calculated using the three dimensional Euclidean rotation matrices shown in appendix C. Based on practical experience it is assumed that the yaw angle is most often zero, and based on that assumption it is seen from the rotational matrices, that the angle between the gravitational vector and the helicopter z vector only depends on the roll(ϕ) and pitch(θ) angle of the helicopter. The angle compensated thrust vector can therefore be calculated as described by equation 7.8,

$$T_{ac} = \frac{T_{ref,z}}{\cos\theta\cos\phi} \tag{7.8}$$

where $T_{ref,z}$ is the desired Thrust which results in the desired acceleration along the z-axis, and T_{ac} is the necessary thrust to maintain the Z-acceleration $T_{ref,z}$. Equation 7.8 is illustrated in figure 7.5, where the color on the plot describe the vector T_{ac}/T_{ref}.

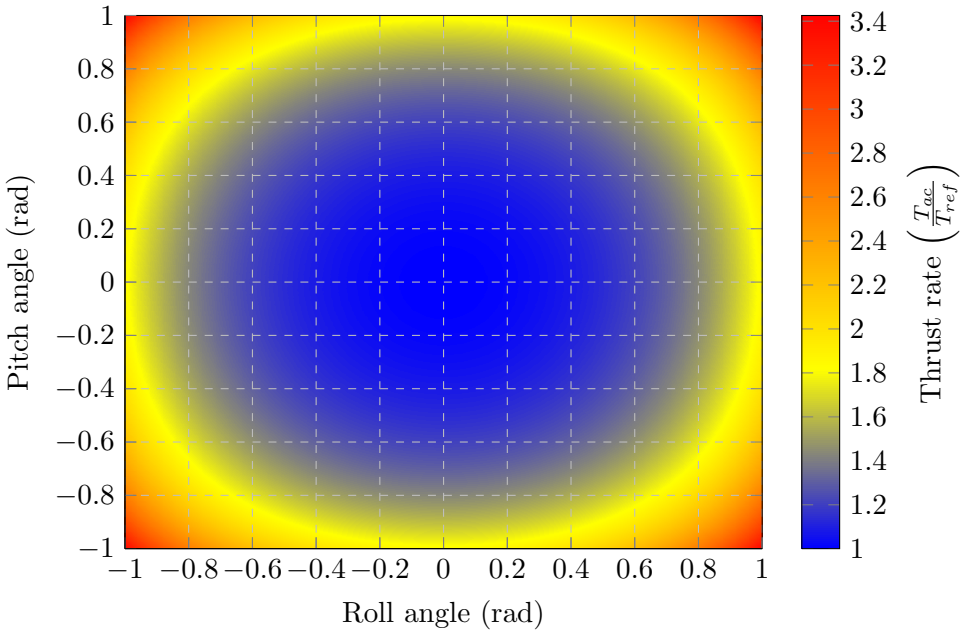

Figure 7.5: *Angle compensated thrust with respect to roll and pitch angle.*

At angles above 0.5 radians (30^o) the thrust compensation increases significantly, and at 1 radian (60^o) the thrust to maintain the z acceleration is between 2 to 3.5 times the zero angle thrust vector T_{ref}.

It should be noticed that this controller on the Z axis receives no feedback

and the output depends only on the roll and pitch angle. The cosine function is implemented on the FCB as an fourth order Taylor approximation shown in appendix H.2.

7.4 Control of the quadrocopter

The controllers described above are now designed to control a model of the quadrocopter. The model is based on the rotor measurements from chapter 4, and the specifications of the quadrocopter from appendix E.3. All controllers are designed with good stability in mind and they therefore all have phase margins larger than 60 degrees. The phase margin and bandwidth of the controllers for the model are shown in table 7.1, and a design overview, along with the bode plots of each controller are shown in appendix G.

Controller	**Phase margin**	**Gain margin**	**Bandwidth**
Roll vel.	65.4 [deg.]	17.4 [dB]	12.97 [rad/s]
Pitch vel.	65.4 [deg.]	17.4 [dB]	12.97 [rad/s]
Yaw vel.	63.7 [deg.]	11.2 [dB]	39.97 [rad/s]
Roll ang.	61.9 [deg.]	14.0 [dB]	5.42 [rad/s]
Pitch ang.	61.9 [deg.]	14.0 [dB]	5.42 [rad/s]

Table 7.1: *Phase, gain margin and bandwidth of SISO controllers*

From the table it can be seen that all controllers have a high phase margin. Some of the bandwidth has been sacrificed due to this choice of high phase margin. It should however be noticed that the yaw controller has both a high phase margin and high bandwidth. A high phase margin and therefore a highly stable system has been chosen to keep the quadrocopter stable during varying disturbances.

7.4.1 Implementation

The controllers are implemented as discrete controllers on the *Flight Control Board* (FCB) with a sample time of 1/478 s, which is the sample time used by Mikrokopter. This sample time is estimated to be sufficient, and is therefore also used for the controllers designed in this report. The angle velocity controllers are implemented as 16 bit fix point controllers to minimize calculation time. The angle controllers are implemented as floating point controllers, where the code of both angle and velocity controllers are shown in appendix H.3.5.

The measured angle is based on the angle estimation algorithm from section 6.4.1. This algorithm uses the arctangent function to estimate the angle based on the x, y and z accelerations from the accelerometer. The arctangent function is implemented as the approximation shown in equation 7.9.

$$arctan(x) \approx \frac{\pi}{4}x + 0.285x(1 - |x|) \tag{7.9}$$

The approximation is based on the work done by [Rajan(MAY 2006)] and [Shima(1999)], and has an error of maximum 0.0038 rad or 0.21 degree. The approximation is described in detail in appendix H.1 and the code is shown in appendix H.3.2. The

earlier described thrust compensation uses the cosine function to calculate the required thrust. The cosine function is likewise implemented as an approximation. The approximation is created as a fourth order Taylor polynomial and the cosine function can therefore be expressed as equation 7.10.

$$cos\theta \approx 1 - \frac{1}{2}\theta^2 + \frac{1}{24}\theta^4 \tag{7.10}$$

The derivation of the approximation can be seen in appendix H.2. Figure 7.6 shows the approximation of the cosine function and the relative error of the approximation.

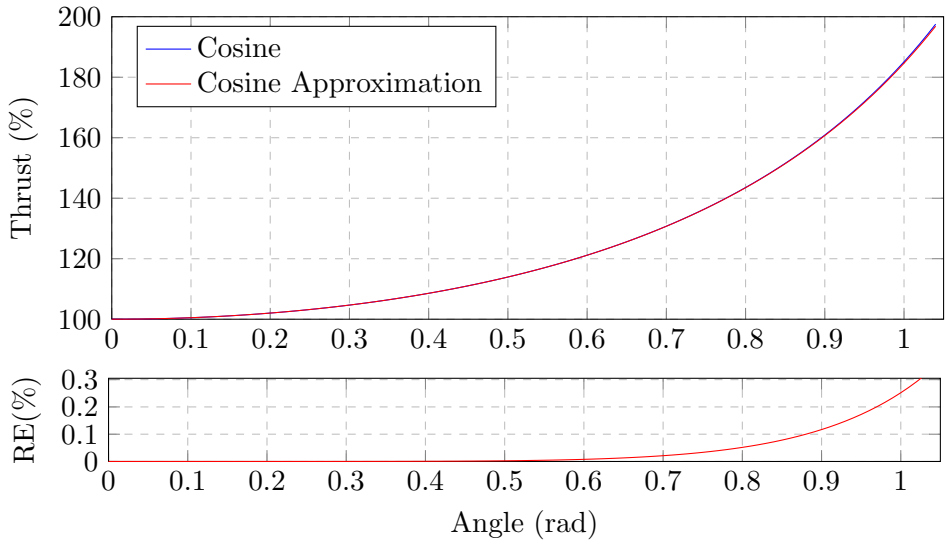

Figure 7.6: *Cosine approximation, where RE is the Relative error in percent and Thrust describe the necessary thrust to maintain the given height acceleration.*

From the figure it can be seen that the approximation fits well with the cosine function up to around 1 radian. The normal area of flight should never exceed 1 radian since this will result in horizontal accelerations above $1.8g = 17m/s^2$ due to the thrust compensation algorithm trying to maintain the height. To avoid dangerous situations the angle of the helicopter is however limited to 0.8 radians equal 45 degrees since the normal area of flight is usually located within angles of ± 0.4 radians.

7.5 Summary

The control of the multi rotor helicopter model was described in this chapter. The controllers used to stabilize the helicopter were *Single Input Single Output* (SISO). The roll and pitch angular velocities of the helicopter were controlled by PD controllers and the roll and pitch angles were controlled by PID controllers. The yaw velocity was controlled by a PID controller.

An angle dependent thrust compensation was derived to maintain a constant Z acceleration during roll and pitch maneuvers. The controllers were then implemented as discrete controllers on the flight control board of the quadrocopter.

Chapter 8

Model and control verification

To validate the model from chapter 6, the specifications of the quadrocopter described in chapter 3, are inserted into the model. The PD and PID controllers are designed based on the methods from chapter 7, where the values for each controller are given in appendix G.3.

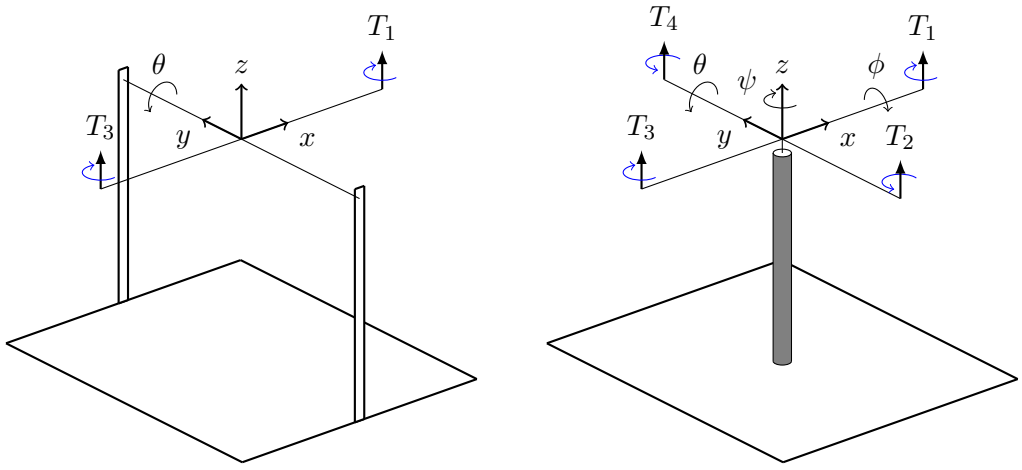

(a) *Test rig A* **(b)** *Test rig B*

Figure 8.1: *Test rigs used to validate the model and test the controllers.*

To validate the model and the controllers, the quadrocopter is attached to two different test rigs. The test rigs, shown in figure 8.1, are created to ensure a safe and consistent test environment during all test. The first test rig(A) were used to measure the angular velocity and orientation of the quadrocopter on either the pitch or roll axis. If a test of the pitch controller is performed, the quadrocopter is mounted on rig A by inserting a bolt into each rod on the y axis. The orientation of the helicopter is now restricted to rotations only around the y axis, i.e. pitch maneuvers.

Test rig B can be used to test the yaw controller and the combination of the roll, pitch and yaw controllers. It consist of a rod and a ball joint, where the quadrocopter is mounted on top of the ball joint with the quadrocopters center of rotation located 8 cm above the center of rotation point of the ball joint. This has no effect on the yaw controller but can affect the roll and pitch controllers, since the model does not include the difference from the real world and the test environment.

8.1 Angular velocity validation

The angular controllers on the roll, pitch and yaw axes are tested separately with use of the test rig in figure 8.1a. All controllers have a step of 0.4 rad/s, approximately 30 degrees/s applied and the measured step response is compared to the modeled step response.

8.1.1 Roll & Pitch

For the roll measurements the quadrocopter was mounted on the x axis on the test rig from figure 8.1a. Rotor two and four on the y axis, are set to spin at rotor speeds corresponding to $mg/4$. Rotor one and three on the x axis are disabled. When the rotors start, the controller is set to maintain zero roll angular velocity. After one second a step of 0.4 rad/s was applied. The step response was measured using the value from the gyro and compared to the theoretical response from the model, as shown in figure 8.2,

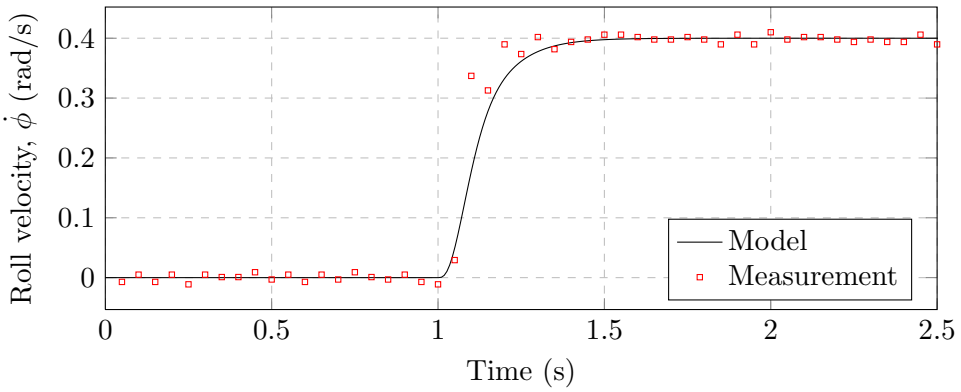

Figure 8.2: *Step response on the roll velocity with a step of 0.4 rad/s.*

where the black line is the theoretical response and the red squares are the measured values from the quadrocopter. The theoretical and experimental rise times of the step responses are shown in table 8.1, where the rise time is described as the time it takes the controller to get from 10 to 90% of the step size.

Control	Model (s)	Experiment (s)
Roll, $\dot{\phi}$	0.259	0.210
Pitch, $\dot{\theta}$	0.260	0.216
Yaw, $\dot{\psi}$	0.042	0.056

Table 8.1: *Rise time of angular velocity controllers*

The quadrocopter was then mounted on the y axis on the same test rig. The method described above was used to get the step response for the pitch axis, where rotor one and three were rotating and rotor two and four were stopped. The step response is shown in figure 8.3, and the rise time is depicted in table 8.1.

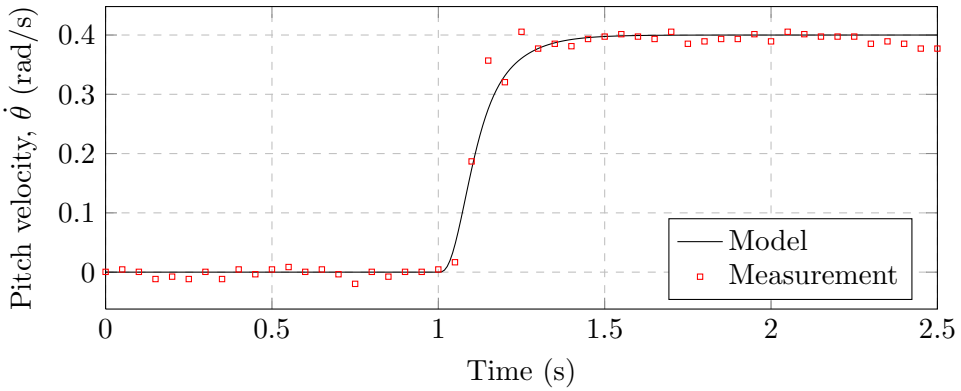

Figure 8.3: *Step response on the pitch velocity with a step of 0.4 rad/s.*

If the step response of the actual quadrocopter is compared to the model it is seen that the quadrocopter has a faster rise time than the model, but overall there is a good agreement between the model and the measurements on both the roll and pitch response.

8.1.2 Yaw

The yaw measurements of the quadrocopter were conducted on test rig B from figure 8.1, where the quadrocopter is attached so the roll and pitch angles are equal to zero and locked during the experiment. All rotors are set to spin at speeds corresponding to the hover thrust. When the rotors started the controller was set to maintain zero angular velocity on the yaw axis. After one second a step of 0.4 rad/s was applied. The step response was measured using the value from the gyro and compared to the theoretical response from the model, as shown in figure 8.4,

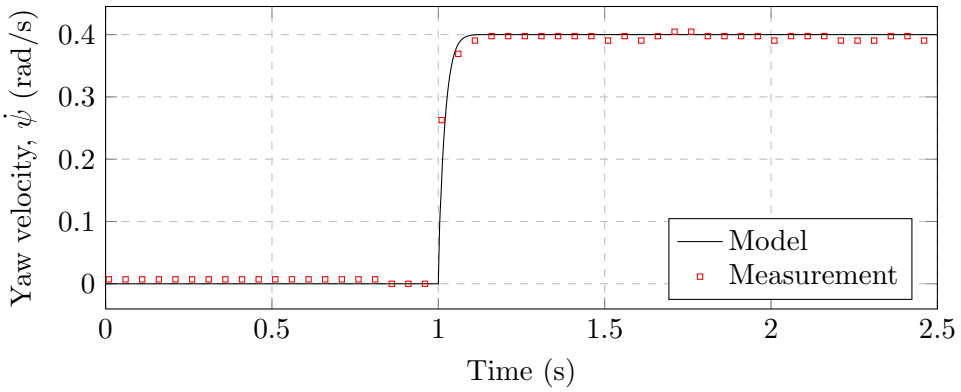

Figure 8.4: *Step response on the yaw velocity with a step of 0.4 rad/s.*

where the black line is the theoretical response and the red squares are the measured values from the quadrocopter. The theoretical and experimental rise time of the step response is shown in table 8.1.

8.2 Roll and Pitch angle validation

The roll and pitch angles are controlled using a PID controllers. The yaw angle is not controlled due to lack of an angle/heading sensor, a compass, on the quadrocopter. To test the angle controllers the quadrocopter was mounted on the rig shown in figure 8.1a. The test method from section 8.1 was used, but instead of a angular velocity step, a step on the angle was applied, and the angle was measured using the algorithm from section 6.4.1. The step, of size 0.4 rad, was applied after one second.

8.2.1 Roll & Pitch

The step response of the roll angle is shown in figure 8.5, and the step response of the pitch angle is shown in figure 8.6.

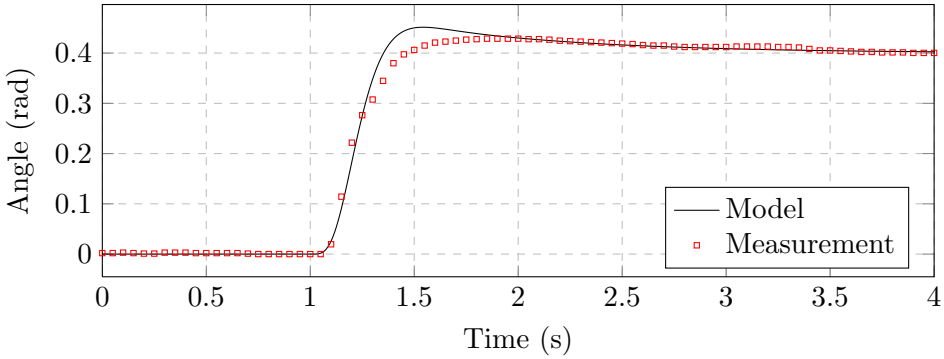

Figure 8.5: *Step response on the roll axis with a step of 0.4 radian.*

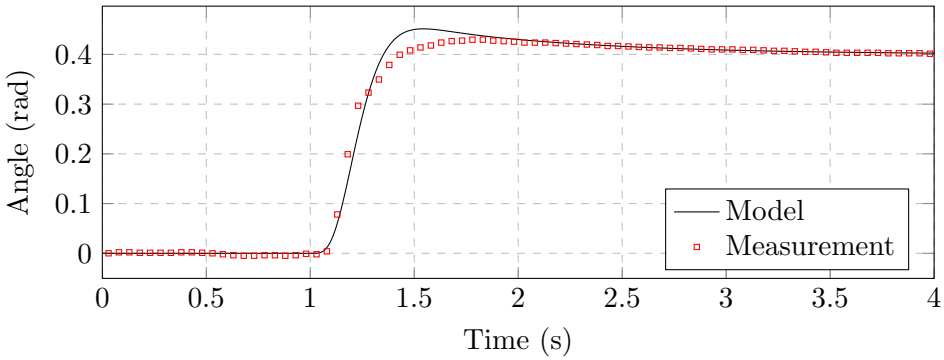

Figure 8.6: *Step response on the pitch axis with a step of 0.4 radian.*

The rise time and overshoot of the roll and pitch angle controller are shown in table 8.2, where the rise time is still described as the time it takes the controller to get from 10 to 90% of the step size.

Rise time	**Model (ms)**	**Experiment (ms)**
Roll, ϕ	0.196	0.243
Pitch, θ	0.196	0.260
Overshoot	**Model (%)**	**Experiment (%)**
Roll, ϕ	9.21	7.42
Pitch, θ	9.21	7.18

Table 8.2: *Rise time and overshoot of angle controllers*

The rise time of the roll model is 20 percent faster than the experimental results, but in return the experimental overshoot is 24 percent less than the model. This can most likely be described by some uncertainty in the model, and partly due to friction in the rotating part of the test rig.

8.3 Controller interaction

The tests in the sections above only test one controller on one axis at a time. These tests simulates each axis very well and present very accurate results for each controller. In hover the quadrocopter is however able to both pitch, roll and yaw and it is therefore necessary to test the controllers influence on each other. The quadrocopter is therefore attached to test rig B shown in figure 8.1b, where roll, pitch and yaw movements are possible at the same time. The ball joint in the test rig has a low friction but limits the roll and pitch angles to 0.5 radians. The center of rotation located in the ball joint is 8 cm from the actual center of rotation of the quadrocopter.

The quadrocopter is attached to the rig and a series of steps at different times are sent to the helicopter to test the combination of the controllers. The resulting angle and yaw velocity of the steps are depicted in figure 8.7.

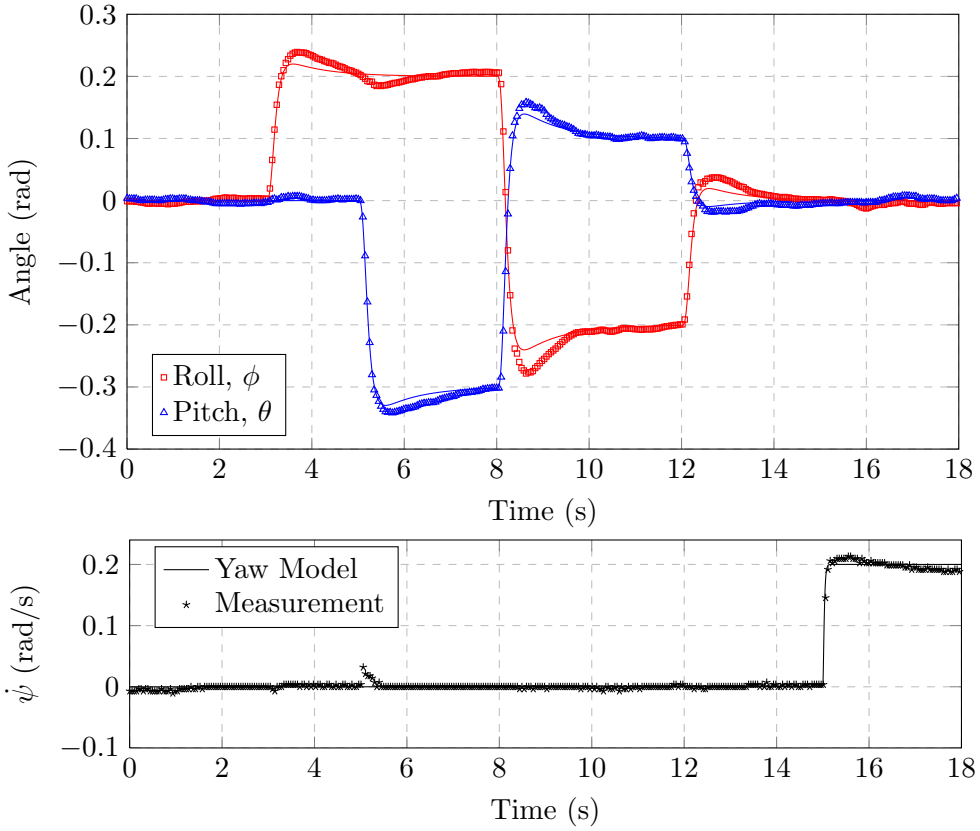

Figure 8.7: *Step responses of roll and pitch angle and yaw velocity.*

The measurement points are marked as squares and triangles for respectively the roll and pitch angle. The angles from the model from chapter 6 are marked as continuous lines. The yaw velocity measurement points are marked with stars and are shown in bottom of the figure.

The fist step is to the roll angle at three seconds and is of size 0.2 rad. From the step it can be seen that there is a bit of extra overshoot compared to the model. This is most probably caused by the earlier mentioned displacement of the center of rotation. The second step is applied to the pitch angle at five seconds and is of size -0.3 rad. This step causes a temporarily and rather insignificant increase in the yaw velocity.

The quadrocopter is now pitching -0.3 rad and rolling 0.2 rad, where hover corresponds to angles equal to zero. To see the impact of steps on both the pitch and roll angle at an orientation away from the linearization point, the roll angle is applied a step of size -0.4 rad and the pitch angle is applied a step of size 0.4 at 8 seconds. This result in the orientation of a pitch angle of 0.1 rad and a roll angle of -0.2 rad. The overshoot of the measured steps are still noticed to be larger than the steps from the model, and this is assumed to be caused by primarily the displacement of the center of rotation. At 12 seconds the roll and pitch angles receives steps of respectively 0.2 and -0.1 rad which return the helicopter to hover. A step of size 0.2 rad/s is applied the yaw angle velocity at 15 seconds, which fit nicely with the model.

8.4 Summary

In this chapter the model from chapter 6 and the controllers from chapter 7 were validated by use of two test rigs. The results showed an accurate model and stable controllers with either zero or only minor overshoot.

The combination of the controllers were examined and tested on the test rig. The results were accurate with only minor deviation from the model where the deviations were expected to be due to the test rig environment.

Chapter 9

Controller comparison

The products from Mikrokopter are widely used in the multi rotor community due to their simplicity and the open source code. Likewise a lot of upcoming aerial photographers are using their platforms to sell aerial videos. It is therefore of great interest to see how the controller designed during the project performs compared to the commercial designed controller by Mikrokopter. The most important controllers are the angle controllers since they keep the helicopter steady at hover. Small angle errors will result in rather large velocities in the XY-plane after a few seconds.

9.1 Roll and pitch angle control

To be able to compare the controllers the quadrocopter was placed in test rig B depicted in figure 8.1. The overall thrust of the helicopter was set to hover thrust, and the remote controls were set to maintain roll and pitch angles equal to zero. The test was performed with the controller designed in this report and with the built-in controller from Mikrokopter, where the results are shown in figure 9.1.
The thin blue line represent the resulting angle when using the controller developed by Mikrokopter and the red line represents the resulting angle achieved using the controller developed by the author. The controller used by Mikrokopter will be named MK and the controller developed by the author will be named RB. The control parameters for the RB controller can be found in appendix G.3. The dashed lines in the figure depicts the boundaries of a 95 pct. confidence interval, corresponding to two standard deviations, for each controller. The standard deviation of both controllers can be seen in table 9.1.

Axis	**MK (rad)**	**RB (rad)**
Roll, ϕ	0.0067	0.0025
Pitch, θ	0.0076	0.0033

Table 9.1: *Standard deviation of roll and pitch angle controller*

It is seen from the table and figure 9.1 that the the standard deviation of the RB angle controllers are more than twice as accurate as the MK angle controllers. This accuracy is highly prioritized by aerial photographers to maintain a steady picture during video recordings. For an aerobatic pilot the hover point is not as important as the response time of the system.

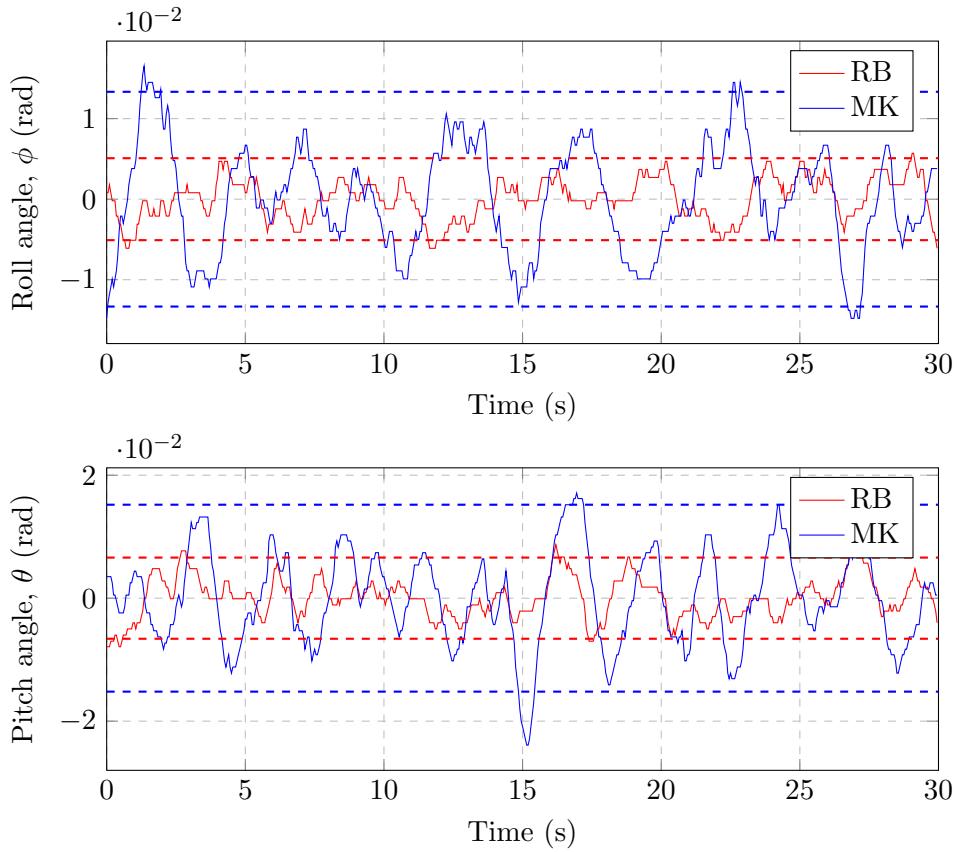

Figure 9.1: *Roll and pitch angle of the helicopter during hover on the test rig from figure 8.1b. The dashed lines depicts the boundaries of a 95% confidence interval of the angle signals.*

It is therefore also valuable to take a look at the step response of the angle controllers to get an idea of the rise time and overshoot of the controllers. The quadrocopter was attached to the test rig shown in figure 8.1a, and a step of 0.4 rad was applied to the controller delivered by Mikrokopter. The step response of the Mikrokopter controller, MK, is plotted with the step response from section 8.2 and are depicted in figure 9.2.
It can be seen from figure 9.2 that the lowest rise time on the roll and pitch angle is achieved from the RB controller. The rise time along with the overshoot are tabulated in table 9.2.

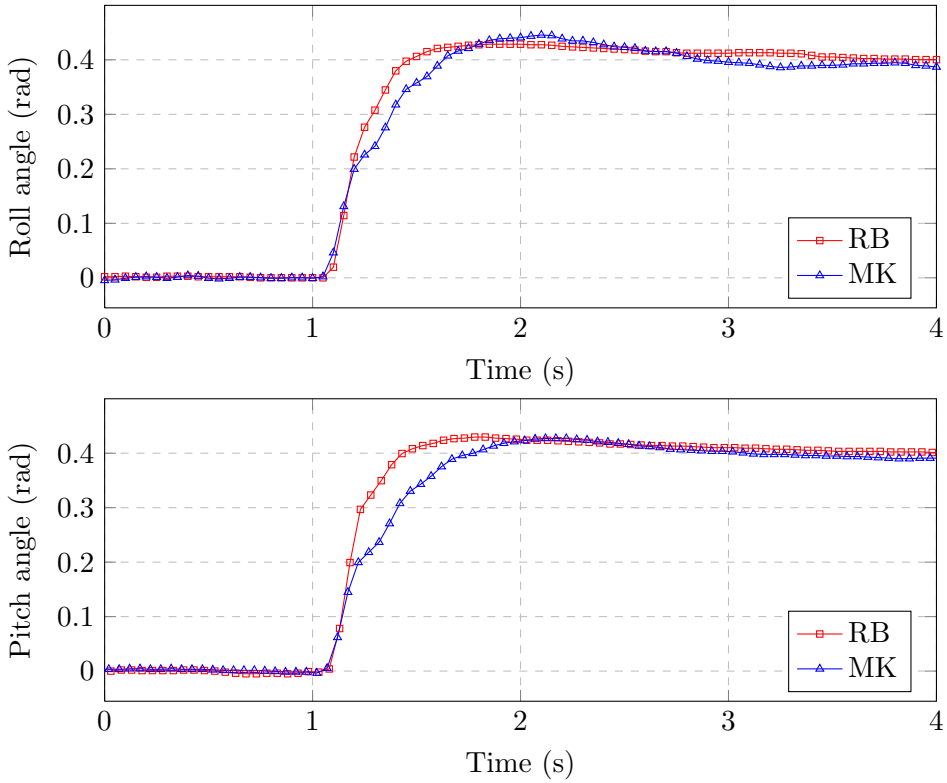

Figure 9.2: *Step response of the angle controllers designed by Mikrokopter, MK, and the ones designed in this project, RB.*

Rise time	**RB (s)**	**MK (s)**
Roll angle	0.243	0.475
Pitch angle	0.260	0.417
Overshoot	**RB (%)**	**MK (%)**
Roll angle	7.18	11.39
Pitch angle	7.42	7.40

Table 9.2: *Rise time and overshoot of Mikrokopters angle controllers and the controllers designed in the report.*

9.2 Yaw velocity controller

The velocity around the z axis of the multi rotor helicopter is also important to the aerial photographers, since errors will cause undesired pan movement during video recording. To test the stability of the yaw velocity at hover the quadrocopter was attached to test rig B from figure 8.1b and the motors were set to provide a thrust equal to mg. The yaw controller from Mikrokopter was set to maintain zero angle velocity and the angle velocity was measured over a period of 30 seconds. The same test method was used to test the yaw controller designed in this project. Figure 9.3 shows the measured yaw velocity of both the MK and RB controllers during 30 seconds.

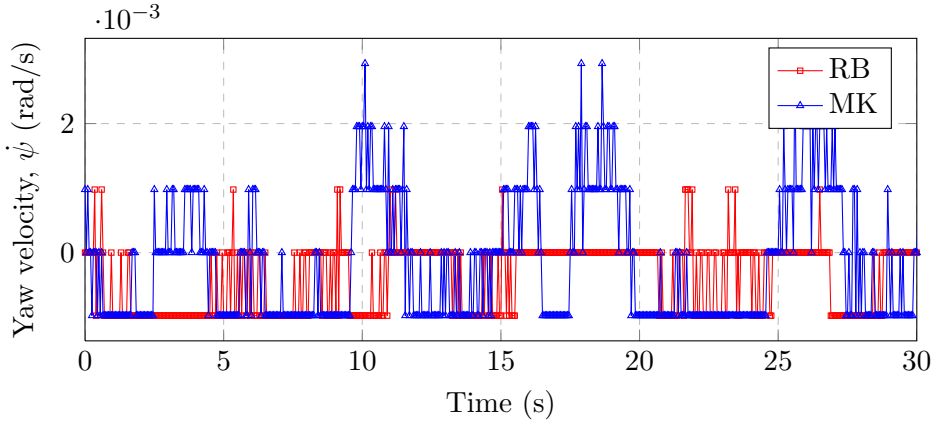

Figure 9.3: *Yaw angle velocity of the helicopter during hover on the test rig from figure 8.1b.*

It can be seen from the figure that both controllers maintain an velocity practically equal to zero. The figure shows that the stability is somewhat limited by the resolution of the *Analog to Digital Converter* (ADC). The standard deviation of the MK and RB controller are respectively $6.6 \cdot 10^{-3}$ and $5.3 \cdot 10^{-4}$ rad/s. It should be kept in mind that the yaw velocity depicted in the figure is the measured velocity. The actual velocity will differ from the measured, where the difference is caused by the drift in the gyro and the resolution in the ADC. The drift in the gyro used by the quadrocopter is by the manufacturer stated to be 0.06 rad or 3.3 degrees pr. minute at a constant operating temperature.

9.3 Summary

In this chapter the controllers designed in chapter 7 were compared to the controllers from one of the leading multi rotor manufacture Mikrokopter. The experimental data collected from both controller systems showed and increased stability of the controller designed in chapter 7. The rise times of the controllers designed in this thesis were faster than controllers from Mikrokopter.

Chapter 10

Flight Time

The *Flight Time* (FT) of the multi rotor helicopters studied in this report, depends primarily on the power consumed by the rotors, and the capacity of the battery. It is assumed that the optimal flight time of an electrical multi rotor helicopter can be calculated as: the power used by the flight control board and the total power required by the rotors to maintain hover in an disturbance free environment. The maximal FT can therefore be expressed as equation 10.1,

$$\text{FT} = \frac{B_{Wh}}{P_H} \tag{10.1}$$

where P_H is the total electrical power used by the helicopter at hover and B_{Wh} is the battery capacity in watt hours. In section 4.7 the correlation between power and number of rotors was derived and the flight time of an n rotor helicopter can therefore be expressed as equation 10.2.

$$\text{FT} = \frac{B_{Wh}}{\sqrt{\frac{m^3 g^3 C_Q^2}{C_T^3 \rho A n}}} \tag{10.2}$$

From equation 10.2 it can be seen that the flight time of electrical multi rotor helicopters depends on many variables like the number of rotors, battery capacity and the mass of the helicopter. To give insight into the flight time of an multi rotor helicopter the quadrocopter used in the experiments above is therefore used as an example in the next section.

10.1 Quadrocopter

The correlation between thrust and electrical power used by a rotor were found in section 4.6. Since the total mass of the quadrocopter is known, the power required to hover, P_H is known for different masses of the quadrocopter. This is due to the fact that the thrust required to hover is proportional to the weight with a factor of g.
The quadrocopter is equipped with a 32Wh battery and by use of equation 10.1 the flight time can be calculated. The minimum mass of the helicopter with the 32Wh battery is 0.8 kg and the theoretical maximum mass is 2.39 kg. The flight time for various payloads are shown in figure 10.1.

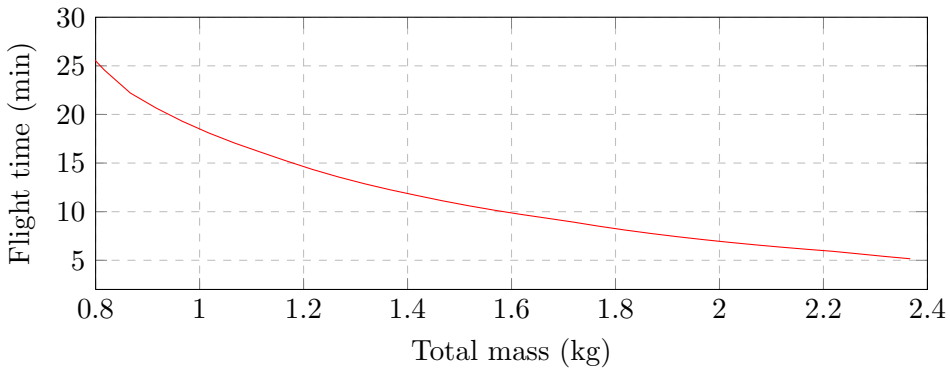

Figure 10.1: *Flight time of Mikrokopters quadrocopter with increasing total mass.*

It is assumed that the capacity of the battery is known and constant, independent of the load. This is often not the case and the announced capacity is generally decreased at large currents. For simplicity this has been assumed, but at high payloads and therefore large currents, this assumption should be kept in mind.

The flight time can be increased by using a battery with a higher capacity (Wh). If the battery capacity is increased the mass of the battery is most often also increased. The correlation between battery capacity and mass of three different manufacture's batteries are depicted in figure 10.2[1].

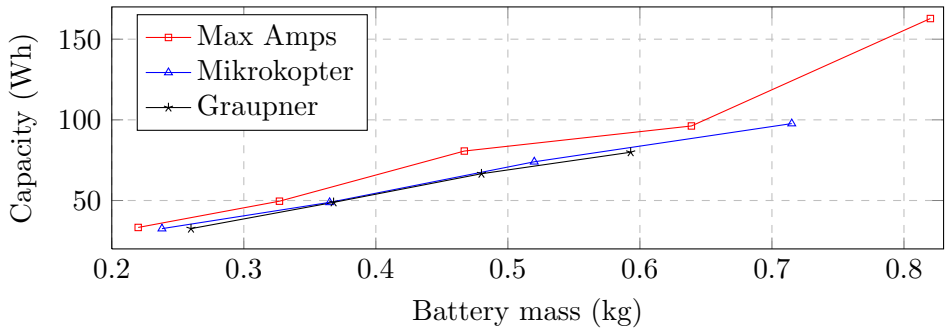

Figure 10.2: *Capacity to mass ratio of LiPo 4 cell 14.8v batteries from Max Amps, Mikrokopter and Graupner.*

[1]The battery information are shown in appendix E.4

It can be seen from the figure that the battery capacity is approximately a linear function of the mass of the battery. The influence on the flight time by use of larger batteries are shown for four different batteries in figure 10.3, where the x axis is the payload, which could be a camera or environmental sensor equipment.

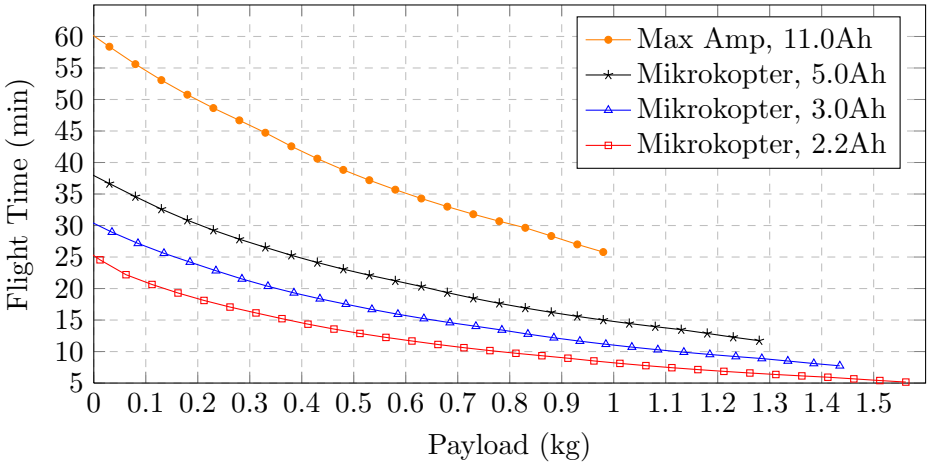

Figure 10.3: *Flight time vs. payload of the quadrocopter with four different batteries.*

It is seen from the figure that the flight time is increases but at the cost of less payload. It should be kept in mind that when the payload increases the maneuverability of the helicopter decreases. If a higher payload is required the number of rotors can be increased.

10.2 Summary

This chapter derived the flight time of multi rotor helicopters based on the power equation derived in section 4.7. The quadrocopter used in the experiments was used as an example, and it was seen that a larger battery lead to a longer flight time. The cost of a larger battery was a reduction in maximum payload.

Chapter 11

Conclusion

During this thesis a model of the rotors and a multi rotor model for n rotors have successfully been developed. The major findings of this thesis have been summarized in four sections: rotors, nonlinear model, multi rotor control and experimental results.

11.1 Rotor

The physical expression for the rotors thrust, torque and power have been modelled based on a series of experimental measurements and by using the theoretical results of [Leishman(2006)]. The efficiency of the rotor, motor and the propeller is derived. The measurements have proven to be very accurate and comply with general helicopter rotor theory.

The correlation between the power consumption and the number of rotors is furthermore derived, and the method to determine the optimal number of rotors explained. It has furthermore been concluded that to obtain the best efficiency of an electric rotor in hover, the following requirements must be satisfied:

- Large rotor radius and thereby low rotor speeds at hover.
- Large values of the thrust constant, C_T, and low values of the torque constant, C_Q, leading to an efficient propeller at hover.
- If a brushless motor is used a large number of poles are required to maintain a high electrical efficiency at low rotor speeds.

It has furthermore been concluded that the optimal number of rotors depend on the mass of the payload.

11.2 Multi rotor model

A dynamic multi rotor model, independent of the number of rotors, has been developed. The model is a general model to ensure that the model is adaptable to the most common multi rotor helicopters. The distribution of the roll, pitch and yaw signal to the rotors was furthermore derived.

An angle estimation model was developed by use of simple sensor fusion between an angle velocity sensor and an accelerometer. The multi rotor model was verified on a four rotor helicopter, which showed results in good accordance with the model derived.

11.3 Multi rotor control

A series of SISO controllers have been designed based on the multi rotor model, where all controllers has proven to be successful within the area of normal flight. Furthermore a thrust compensation has been developed to ensure height stability during rolling and pitching.
The interaction between the controllers was examined and it was seen that all controllers performed satisfactory.

11.4 Experimental results

The controllers based on the model were successfully implemented on a four rotor helicopter from Mikrokopter without re-tuning. The controllers were able to stabilize the velocities, the roll and pitch angle of the helicopter. Likewise the step response of the controllers showed good results.

The controllers were compared to the controllers developed by one of the leading multi rotor manufactures, Mikrokopter. The result showed a significantly increased performance with the controllers based on the multi rotor model developed in this thesis. The rise time of the controllers in this thesis was notable faster than the controllers from Mikrokopter. The stability around hover was expressed by the standard deviation of the angles where the controllers in this thesis was significantly better than Mikrokopters controllers.

Chapter 12

Future research

The area of multi rotor systems with more than four rotors are a relatively new area of research. There are a lot of possible new areas of research like fault tolerant control, the aerodynamic influence of airflow between the rotors, and the optimal location of the rotors. Adding position sensors to the helicopter would furthermore give rise to position control, path planning and obstacle avoidance.

Even though the model has proven to be sufficient to control a multi rotor helicopter the model has however some room for improvement. During the experimental part of the thesis it was found that the model was highly dependent on an accurate time constant of the rotor response. A more precise model of the motor would improve the accuracy of the model. Adding an angular velocity controller to the rotor would furthermore make it possible to increase the bandwidth of the system. The model does not include the ground effect and the accuracy of the model in ground effect could be improved by taking this into account.

The bandwidth of the system could also be increased by controlling the angle of attack of the rotor blades. This might however compromise the mechanical simplicity of the multi rotor system.

Bibliography

[Andersen(2009)] N. Andersen. *Implementation of Digital Controllers*. DTU-Elektro, 2009.

[Bertelsen and Magnsson(2004)] A. Bertelsen and S. Magnsson. Modeling and control of a 4-rotor helicopter. *Technical University of Denmark, Ørsted*, 2004.

[Bouabdallah and Siegwart(2007)] S. Bouabdallah and R. Siegwart. Full control of a quadrotor. *Intelligent Robots and Systems, 2007. IROS 2007. IEEE/RSJ International Conference*, 2007.

[Bramwell(2001)] et. al. Bramwell, A. *Bramwell's Helicopter Dynamics*. Butterworth-Heinemann, second edition edition, 2001.

[Leishman(2006)] J. Gordon Leishman. *Principles of Helicopter Aerodynamics*. Cambridge University Press, second edition edition, 2006.

[Pedersen(2006)] A. Pedersen. *Test and Modelling of Four Rotor Helicopter Rotors*. Technical University of Denmark, Ørsted, 2006.

[Pounds(2010)] et. al. Pounds, P. Modelling and control of a quad-rotor robot. *Australian National University, Canberra, Australia*, 2010.

[Rajan(MAY 2006)] et. al. Rajan, S. Efficient approximations for the arctangent function. *IEEE SIGNAL PROCESSING MAGAZINE*, MAY 2006.

[Shima(1999)] Jim Shima. Fixed-point atan2 with self normalization. *http://www.dspguru.com/dsp/tricks/fixed-point-atan2-with-self-normalization*, 1999.

Appendices

Appendix A

Induced power correction factor

The ideal power, without drag considerations, tip losses and wake swirls required to produce the thrust T_i can be expressed by equation A.1.

$$C_p = \frac{C_T^{(3/2)}}{\sqrt{2}} \tag{A.1}$$

If the thrust constant, C_T found in section 4.3 is inserted, then the ideal power C_p can be calculated to:

$$C_p = \frac{0.0158^{(3/2)}}{\sqrt{2}} = 0.0014 \tag{A.2}$$

Due to a number of non ideal physical effect acting on the blade, such as wake swirl, tip losses, non uniform inflow and so on, the induced power correction factor k is added to equation A.1. The power, still without drag considerations, can be expressed by equation A.3.

$$C_{Pi} = \frac{kC_T^{(3/2)}}{\sqrt{2}} \tag{A.3}$$

The thrust measurements, T_i from appendix B.2 is used to estimate the induced power correction factor, by use of equation A.4 from [Leishman(2006)].

$$P = T_i v_i = 2\rho A v_i^3 \tag{A.4}$$

where v_i can be calculated as shown in equation A.5.

$$v_i = \sqrt{\frac{T_i}{2\rho A}} \tag{A.5}$$

The power related to the speed of the rotor can, according to [Leishman(2006)] be depicted as equation A.6.

$$C_P = \frac{P}{\rho A(\Omega R_r)^3} \tag{A.6}$$

The P from equation A.4, which was based on the measured thrust, is inserted into equation A.6 which result in a C_P of 0.0015. The induced power correction factor k can then be found using equation A.7.

$$k = \frac{C_P}{C_p} = 1.067 \tag{A.7}$$

From this result it can be seen that there is a 6.7% effect-loss in non ideal physical effects acting on the propeller. C_{Pi} are therfore equal to:

$$C_{Pi} = \frac{kC_T^{(3/2)}}{\sqrt{2}} = 0.0015 \tag{A.8}$$

Appendix B

Experimental results

B.1 Experimental Thrust and Torque

The rotor thrust and torque are measured using the Mini40 F/T Sensor by ATI industrial Automation, which is a 6 axis strain gage capable of measuring the force in three dimensions and the torque in three dimensions as well. The sensor is mounted on a vertical stick of 1 meter and the rotor is then mounted on top of the sensor as depicted in figure 4.1. The rotor is set to spin at different speeds and the thrust and torque are logged to a datafile using the Net Box by ATI industrial Automation.

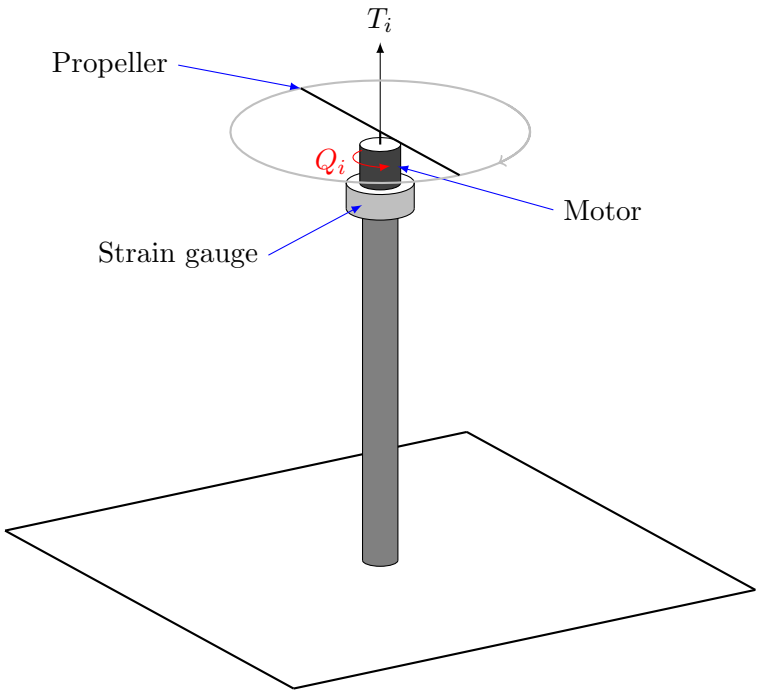

Figure B.1: *Rotor test bench*

B.2 Measured rotor data

PWM (%)	Thrust (N)	Torque (Nm)	Ω (rad/s)	Power (W)
0	0.00	0.0000	0.00	0.00
8	0.33	0.0065	152.33	2.82
12	0.47	0.0091	182.27	3.91
16	0.63	0.0120	205.52	5.21
20	0.82	0.0153	234.58	6.82
24	1.05	0.0193	263.34	9.05
27	1.30	0.0235	292.82	11.59
31	1.61	0.0280	320.04	14.40
35	1.89	0.0332	349.92	18.02
39	2.12	0.0378	372.64	22.00
47	2.79	0.0490	423.08	31.00
55	3.48	0.0606	470.50	42.00
63	4.17	0.0722	521.96	53.76
71	4.78	0.0833	554.04	67.68
78	5.47	0.0956	590.63	83.28
86	5.94	0.1036	N/A	99.60
94	6.06	0.1058	N/A	N/A

Table B.1: *Thrust, Torque, Angular velocity and power measurements at a voltage of 13.5v*

Appendix C

Angle thrust calculations

The angle compensated thrust described in equation 7.8 in section 7.3, is based on the following three rotation matrices:

$$R_x = \begin{pmatrix} 1 & 0 & 0 \\ 0 & \cos\phi & -\sin\phi \\ 0 & \sin\phi & \cos\phi \end{pmatrix} \tag{C.1}$$

$$R_y = \begin{pmatrix} \cos\theta & 0 & \sin\theta \\ 0 & 1 & 0 \\ -\sin\theta & 0 & \cos\theta \end{pmatrix} \tag{C.2}$$

$$R_z = \begin{pmatrix} \cos\psi & -\sin\psi & 0 \\ \sin\psi & \cos\psi & 0 \\ 0 & 0 & 1 \end{pmatrix} \tag{C.3}$$

where R_x,R_y and R_z is respectively the rotation about the x,y and z-axis. If the yaw angle is assumed constant and equal to zero, it is seen from the two rotational matrices, shown in equation C.4 and C.5, that the normalized vector on the z-axis is identical, namely $\cos\phi\cos\theta$.

$$R_xR_y = \begin{pmatrix} \cos\theta & 0 & \sin\theta \\ \sin\phi\sin\theta & \cos\phi & -\sin\phi\cos\theta \\ -\cos\phi\sin\theta & \sin\phi & \cos\phi\cos\theta \end{pmatrix} \tag{C.4}$$

$$R_yR_x = \begin{pmatrix} \cos\theta & \sin\phi\sin\theta & \cos\phi\sin\theta \\ 0 & \cos\phi & -\sin\phi \\ -\sin\theta & \sin\phi\cos\theta & \cos\phi\cos\theta \end{pmatrix} \tag{C.5}$$

This is furthermore illustrated in figure C.1, where θ and ϕ is respectively the roll and pitch angle of the helicopter in the earth fixed frame. The green vector, n_g is the normalized vector to g. The length of n_g can then be used to calculate the

angle compensated thrust as shown in equation C.6.

$$T_{ac} = \frac{T_{ref,z}}{\cos\theta \cos\phi} \tag{C.6}$$

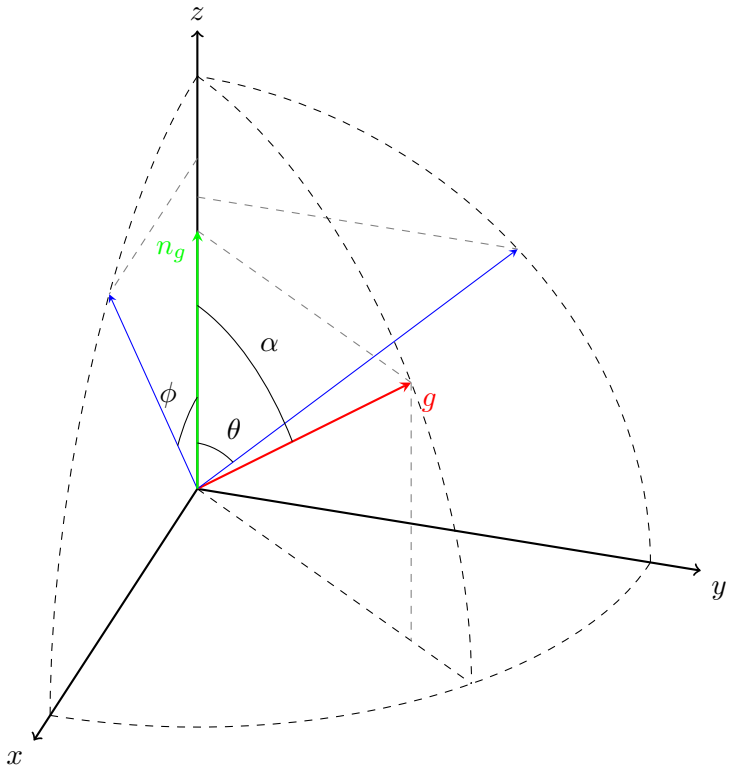

Figure C.1: *Roll and Pitch Angle thrust compensation.*

Appendix D

Angle estimation

The combination of the accelerometer and the gyro to get the angle is based on the assumption that at stationary conditions the accelerometer is most reliable sensor to estimate the angle. At dynamic conditions the gyro is the best sensor reliable sensor. This fusion of the sensors can be expressed by an high pass filter and a low pass filter.
The angle approximation from the accelerometer is passed through a low pass filter and the integrated gyro signal is passed thorough a high pass filter. This principle is shown in figure D.1, where $\dot{\theta}$ represent the angular velocity measured by the gyro and θ_{Acc} represents the approximated angle from the accelerometer values. This combination results in the angle estimation $\hat{\theta}$.

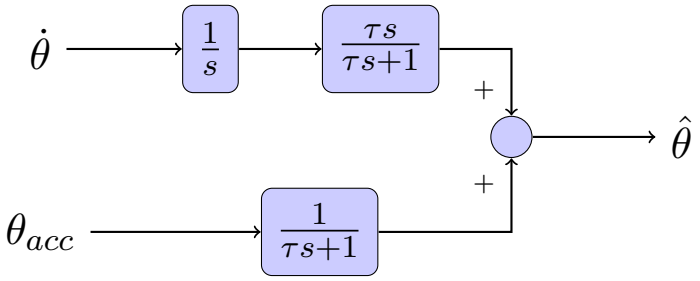

Figure D.1: *Angle estimation*

Figure D.1 can be simplified to figure D.2.

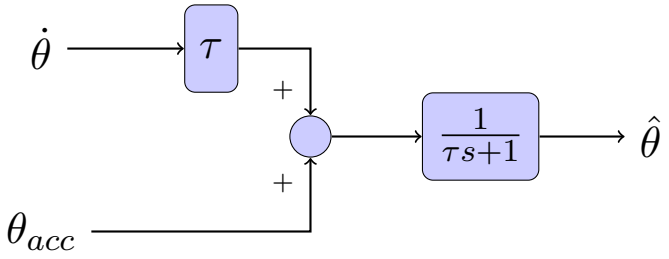

Figure D.2: *Simple angle estimation*

Appendix E

Hardware

The Flight Control Board, motor controllers and motors are described in this appendix. The diagram of the Flight Control Board is shown in appendix E.1.5.

E.1 Flight Control Board

The flight control board is the part of the helicopter which reads the on-board sensors, send the I^2C to the motor controllers and receives the signal from Spektrums RC satellite. It is equipped with an ATMEGA 1284P 20 Mhz processor which is equipped with an internal ADC which read the analog signals from the sensors and convert them to 10 bit digital signals. The following sections will present the sensors and the ADC.

E.1.1 Gyro (ADXRS610)

To measure the angular rates on the Pitch, Roll and Yaw axis, three ADXRS610 gyros from Analog Devices is used. The angular rate on each axis of the helicopter is measured with the ADXRS610 angular rate sensor from Analog Devices. The sensor is rated to ±300 degrees pr. second and the output signal is a voltage proportional to the angular rate, with 3.6mV pr. Degree pr sec. To reduce high frequency noise in the system the sensor is equipped with a hardware low pass filter (R=6.8 Kohm, C = 100nf). The cut off frequency of the output is therefore:

$$f_c = \frac{1}{2\pi \mathrm{RC}} = \frac{1}{2\pi \cdot 6.8\mathrm{K}\Omega \cdot 100\mathrm{nF}} \approx 234\mathrm{Hz} \tag{E.1}$$

The output of the gyro is measured using the 10 bit ADC described in section E.1.3. The resolution of the gyro can therefore be calculated as shown in equation E.2.

$$\text{Gyrorate} = \frac{3.6\mathrm{mV}/^\circ/\mathrm{s}}{2.93\mathrm{mV/bit}} = 0.814\frac{^\circ/\mathrm{s}}{\mathrm{bit}} = 0.0142\frac{\mathrm{rad/s}}{\mathrm{bit}} \tag{E.2}$$

E.1.2 Accelerometer (LIS344ALH)

The direction of the gravitational acceleration acting on the helicopter in the HF are measured with a 3 axis accelerometer from STMicroelectronics. The accelerometer

is not equipped with an hardware low pass filter.

$$\text{Acc} = \frac{3000\text{mV}}{5\text{g}} = 600\text{mV/g} = 61.1\text{mV/m/s}^2 = \frac{2.93mV/bit}{61.1\text{mV/m/s}^2} = 0.048\frac{\text{m/s}^2}{\text{bit}} \tag{E.3}$$

E.1.3 AD Converter (Atmega1284)

The ADC is an on-board 10 bit converter with a reference voltage of 3000mv and a conversion time of 83μ seconds.

E.1.4 Atmega1284 calculation time

During the implementation the calculation time of the different operations were examined. The measured calculation times were found by implementing a loop with 5000 multiplications or additions. Just before the microprocessor entered the loop a pin on the board was set to high. When the calculations were done the same pin was set to low. The time between high and low were then used to determine the time it took to do a multiplication or an addition of following data types: 32 bit long, 16 bit short and 32 bit float. The result is shown in table E.1.

	Floating point	long(32bit)	short(16bit)
One addition:	0.0102 ms	0.00164 ms	0.00108 ms
One multiplication:	0.00672 ms	0.00432 ms	0.00148 ms

Table E.1: *Atmega 1284p Calculations*

E.1.5 Diagram of Flight Control Board

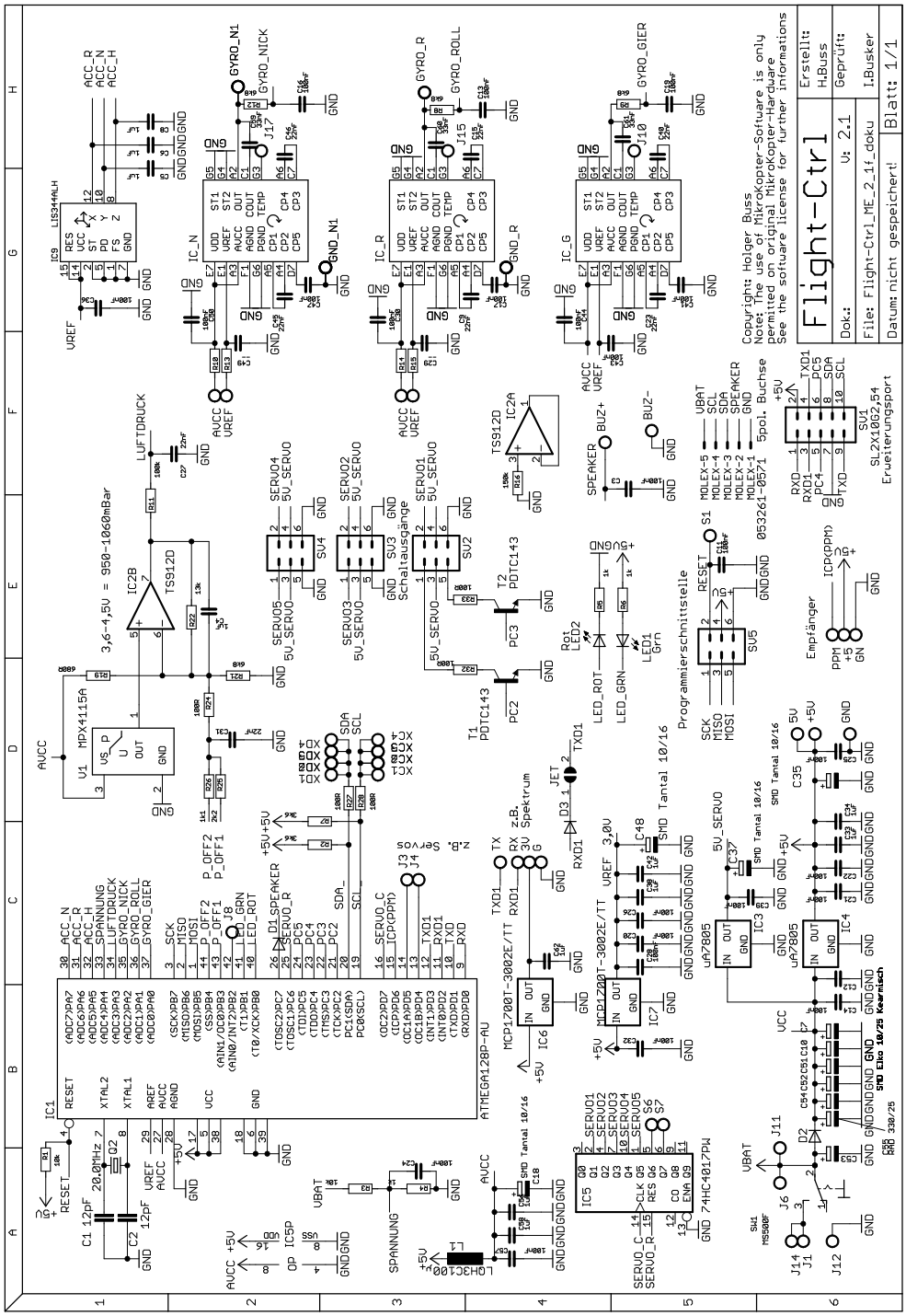

Figure E.1: *Mikrokopters diagram of the Flight Control Board ME v.2.1*

E.2 Propeller

The propellers used in this project are the ones delivered with the quadrocopter from Mikrokopter. It has not been possible to get all of the desired information, such as blade twist and solidity ratio. However the radius and the advance distance of the propeller is printed on the blades as 10x4.5 which corresponds to a diameter of 10 inches, and an advance distance of 4.5 inches. The advance distance is expressed as the optimal distance the propeller will travel within one revolution.

Radius, R_r	0.126 m
Disk Area, A	0.049 m^2
C_T	0.0158 rad^{-2}
C_Q	0.0022 rad^{-2}
FM	0.6

Table E.2: *Propeller specifications*

E.3 Quadrocopter Specifications

Mass specifications	
Type	**Mass**
FCB	0.169 [kg]
Bat.	0.238 [kg]
Motor	0.069 [kg]
Prop.	0.008 [kg]
Rod	0.143 [kg/m]

Table E.3: *Quadrocopter mass specifications.*

E.4 Batteries

Max Amp		*Mikrokopter*		*Graupner*	
Ah	**Mass (g)**	**Ah**	**Mass (g)**	**Ah**	**Mass (g)**
2.25	220	2.20	238	2.20	260
3.25	327	3.30	365	3.30	368
5.45	467	5.00	520	4.50	480
6.50	639	6.60	715	5.40	593
11.00	820				

Table E.4: *Overview of the 4s 14.8v LiPo batteries used in figure 10.2.*

Appendix F

Simulink model

In this appendix the equations from chapter 6 will be shown as Matlab Simulink diagrams. Figure F.2 shows the total multi rotor model, including the block *Controllers* which implements the controllers from chapter 7.
The model is divided into the five blocks: Controllers, Distributor, Rotor Dynamics, Dynamicss and Sensors. Each subsystem is shown in the following figures.
The simulink models uses Matlab functions to calculate the different variables. The Matlab functions are presented in section F.1.

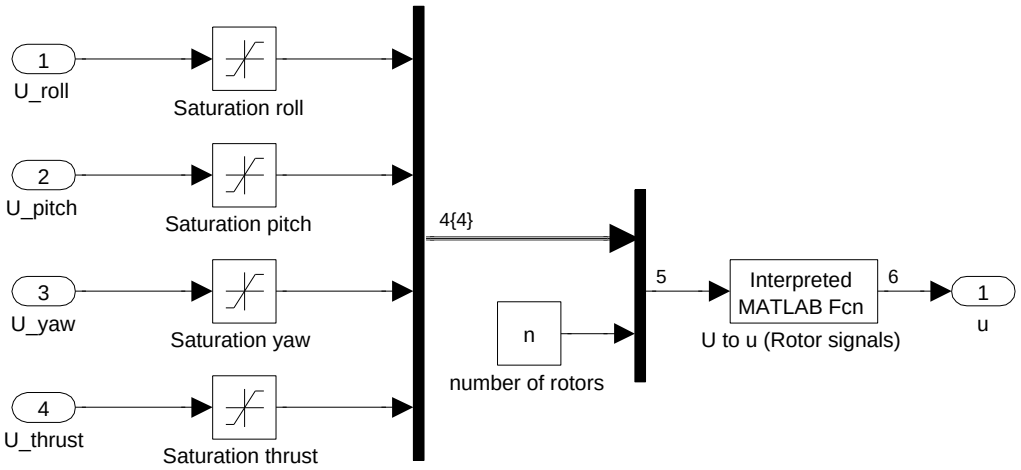

Figure F.1: *Simulink model of the distributor*

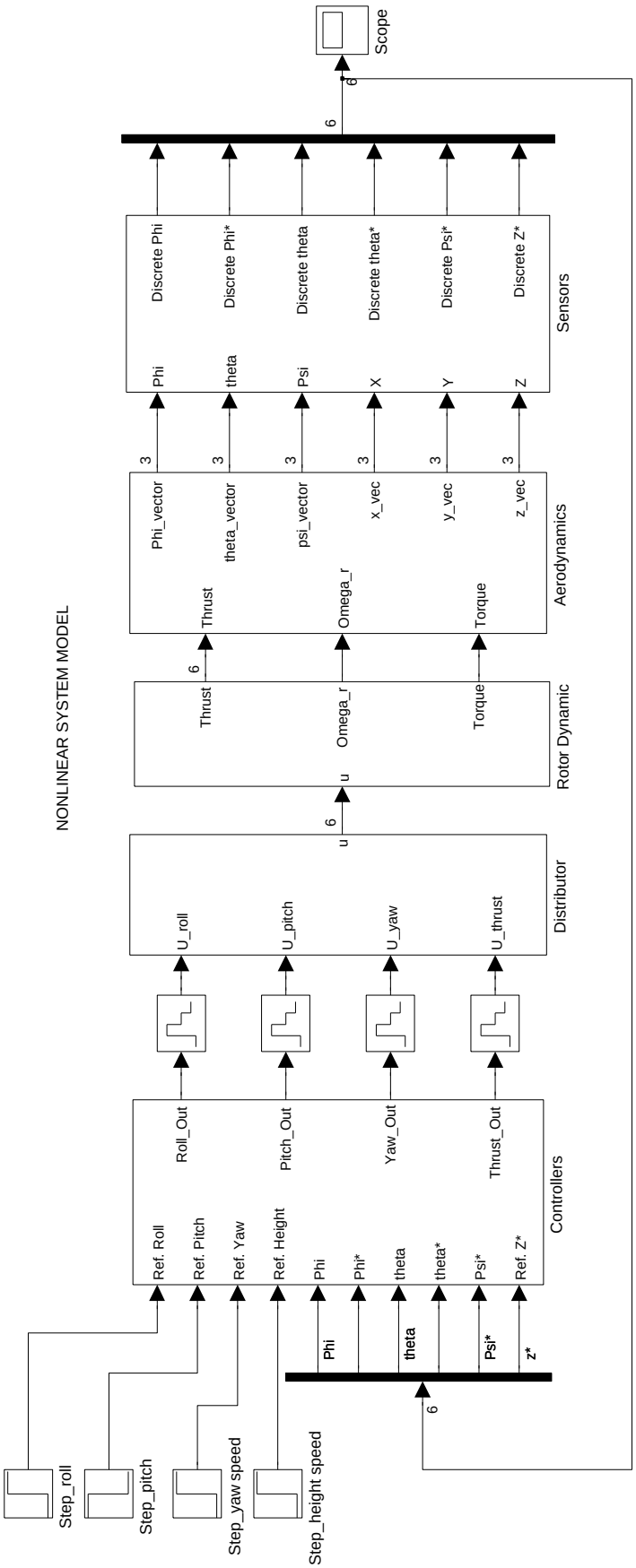

Figure F.2: *Simulink model of a multi rotor helicopter*

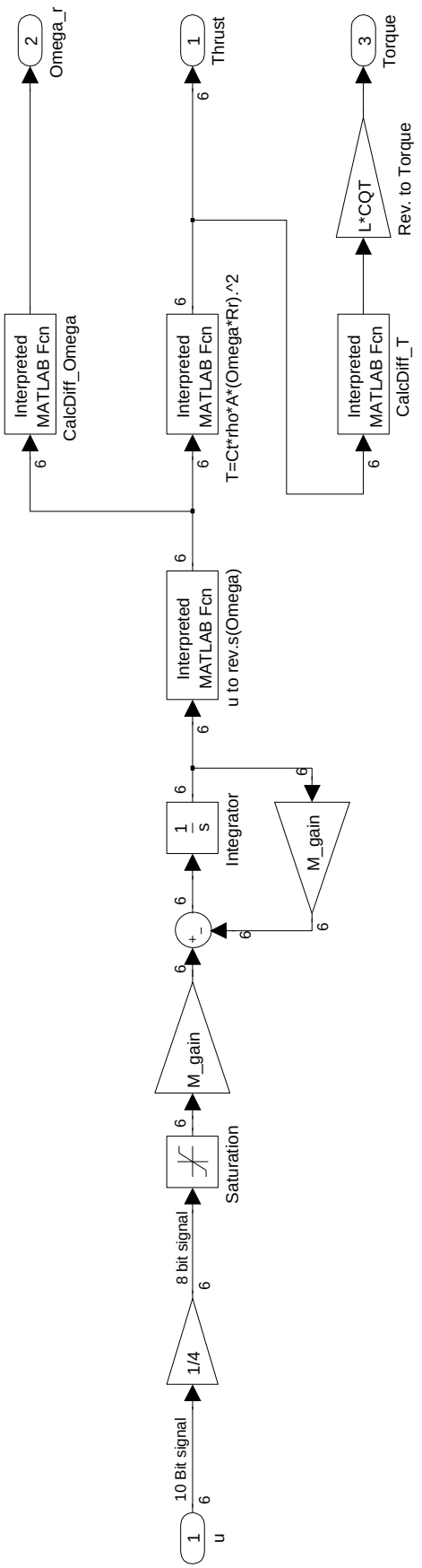

Figure F.3: *Simulink model of the rotor dynamics*

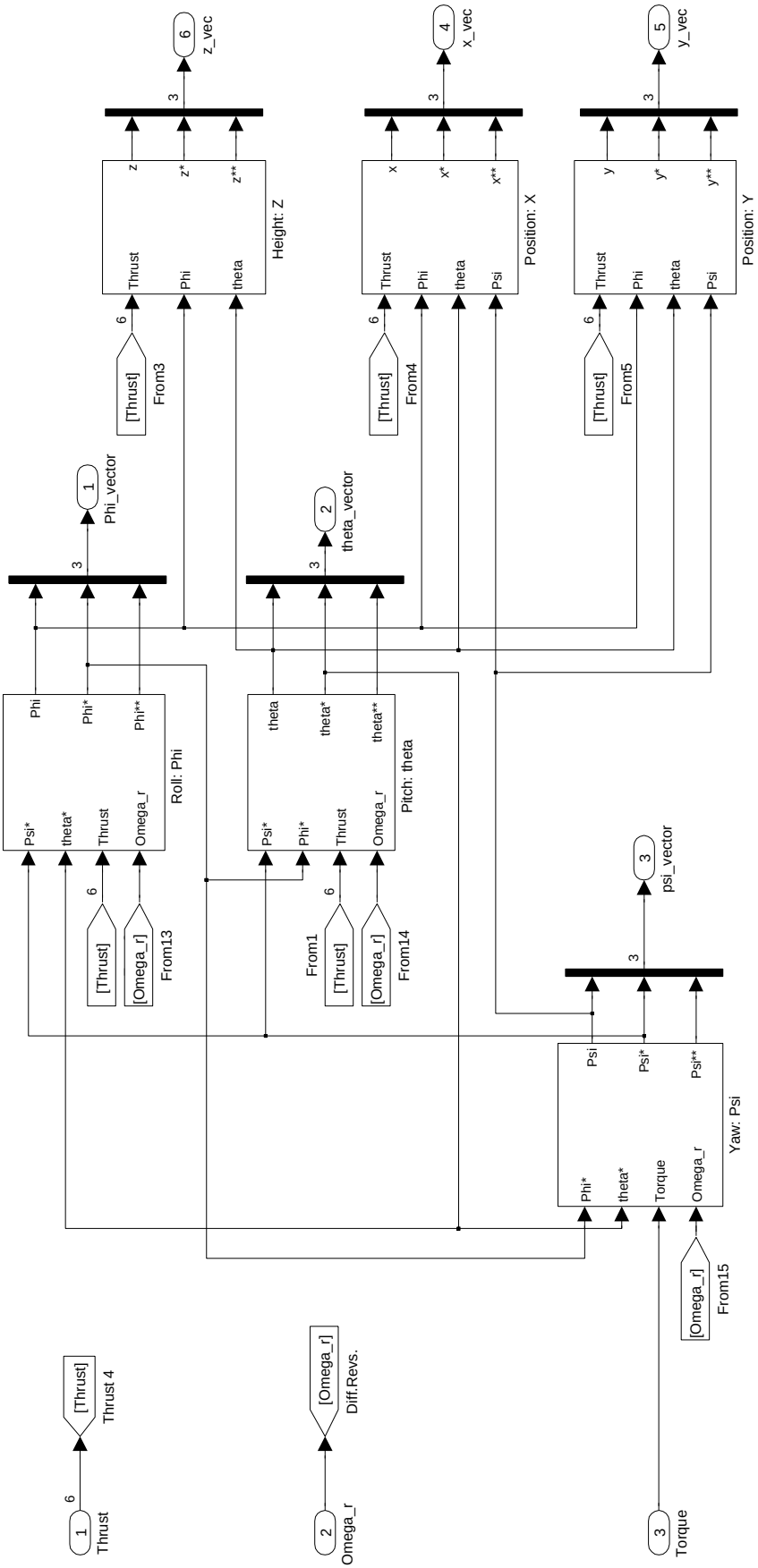

Figure F.4: *Simulink model of the helicopter dynamics*

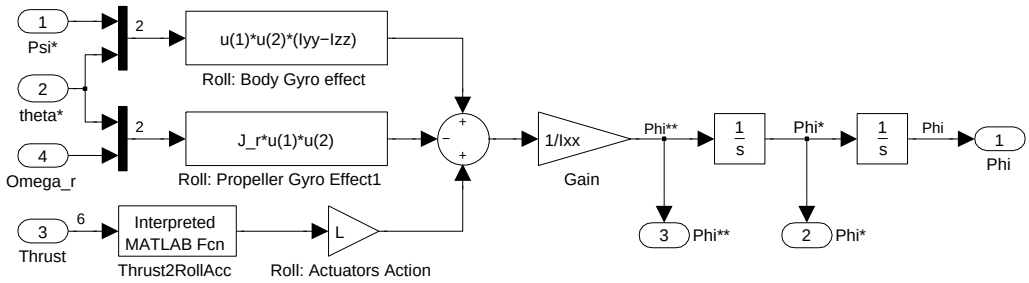

Figure F.5: *Simulink model of the roll dynamics*

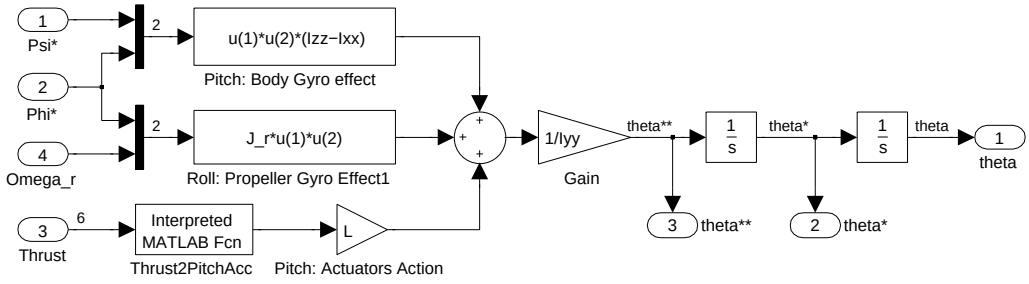

Figure F.6: *Simulink model of the pitch dynamics*

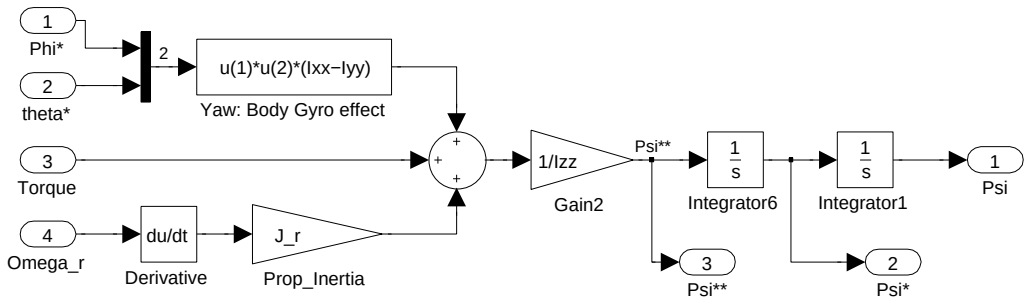

Figure F.7: *Simulink model of the yaw dynamics*

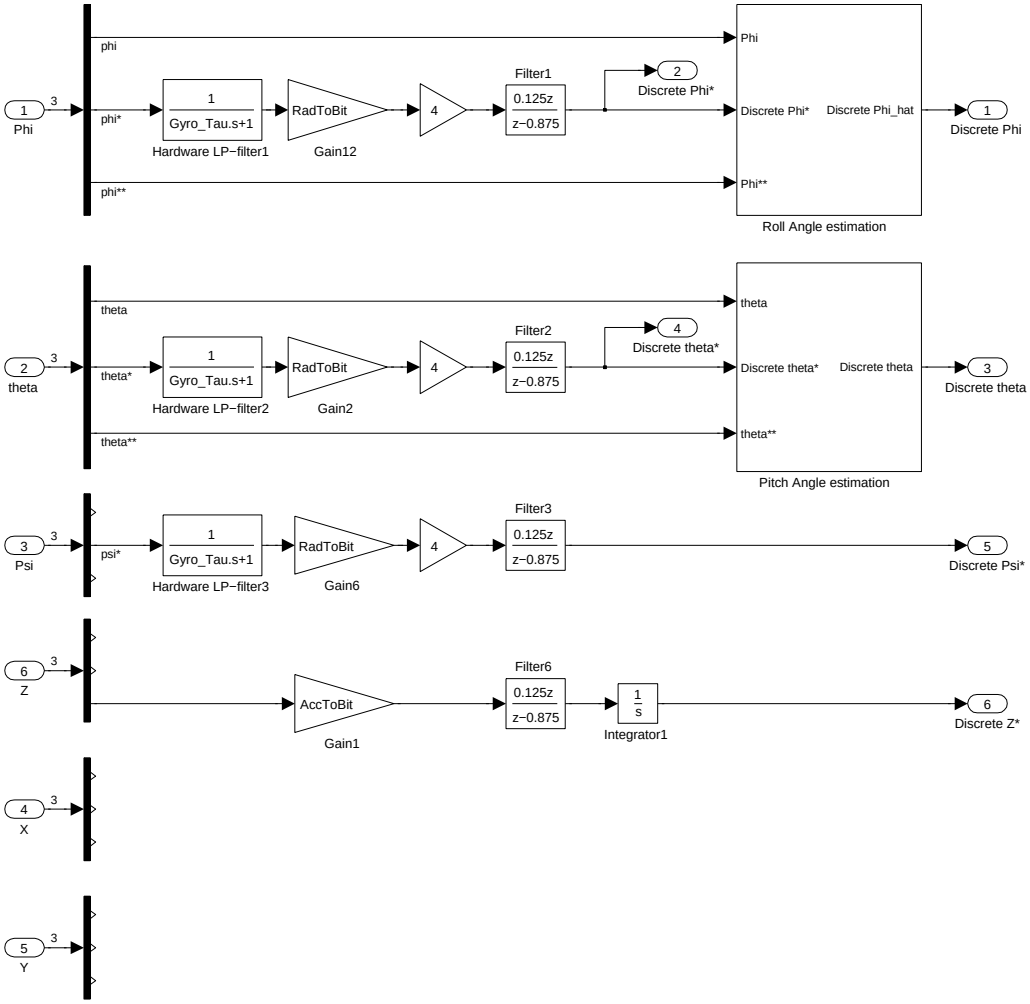

Figure F.8: *Simulink model of the sensor system*

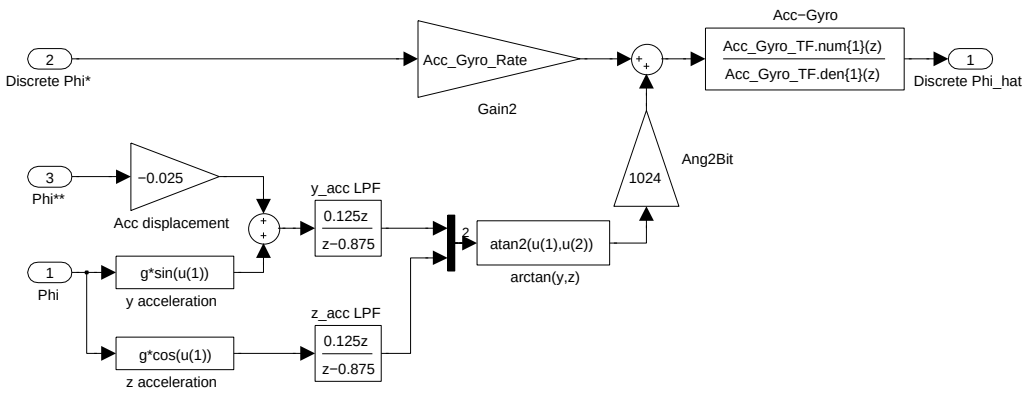

Figure F.9: *Simulink model of the roll angle estimator*

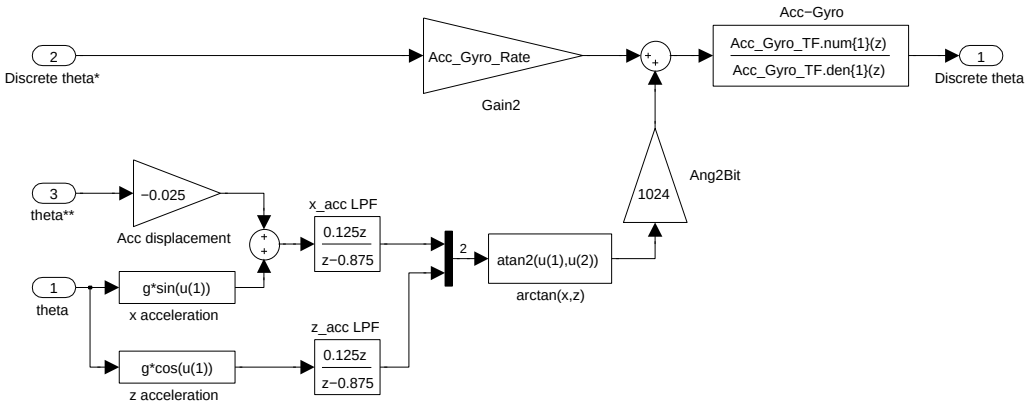

Figure F.10: *Simulink model of the pitch angle estimator*

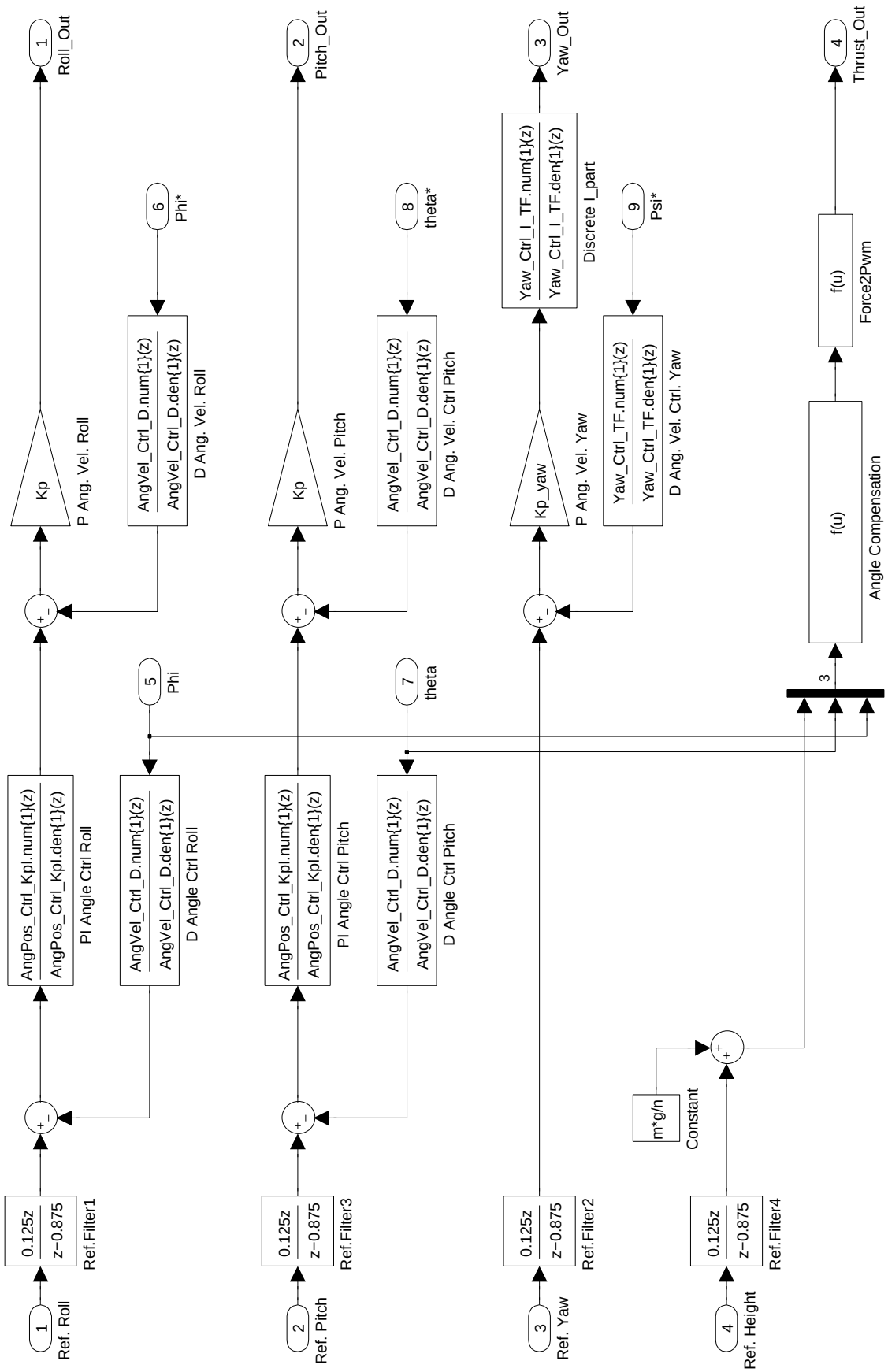

Figure F.11: *Simulink model of the SISO controllers*

F.1 Matlab functions

The following Matlab functions are used in the simulink models previously shown.

F.1.1 DistributorCalc

Calculates the rotor control signals based on equation 6.2.

```
function u = DistributorCalc(Roll,Pitch,Yaw,Thrust,n)
%DISTRIBUTORCALC:
%Takes the roll, pitch, yaw and thrust control signals followed by ...
    the number of rotors as arguments.
%The output is a vector containing the rotor control signals.
u = zeros(1,n);
    for q=1:1:n
        angle = (2*pi*(q-1))/n;
        u(q) = Thrust + Pitch*cos(angle) + Roll*sin(angle) + Yaw...
            *((-1)^(-q));
    end
end
```

F.1.2 CalcDiff

Calculates the difference in rotor speed of the right and left rotating propellers, by use of equation 6.3.

```
function Diff = CalcDiff(u)
%Takes and vector of rotor signals and substract element 2 from ...
    element 1: u(1)-u(2)+u(3)-u(4)+u(5)-u(6)..-u(n).
    w=0;
    Diff=0;
    for q=1:1:size(u)
        if (w==0)
         Diff = Diff - u(q);
         w=1;
        else
         Diff = Diff + u(q);
         w=0;
        end
    end
end
```

F.1.3 Thrust2Roll

Calculate the roll acceleration shown in equation 6.4.

```
function RollAcc = Thrust2Roll(Thrust)
%Calculate the roll acceleration based on the thrust of each ...
    propeller
    NumberOfRotors = max(size(Thrust));
    RollAcc = zeros(1,NumberOfRotors);
    for q=1:1:NumberOfRotors
        RollAcc(q) = Thrust(q)*sin((2*pi*(q-1))/NumberOfRotors);
    end
    RollAcc = sum(RollAcc);
end
```

F.1.4 Thrust2Pitch

Calculate the pitch acceleration shown in equation 6.5.

```
function PitchAcc = Thrust2Pitch(Thrust)
%Calculate the pitch acceleration based on the thrust of each ...
    propeller
    NumberOfRotors = max(size(Thrust));
    PitchAcc = zeros(1,NumberOfRotors);
    for q=1:1:NumberOfRotors
        PitchAcc(q) = Thrust(q)*cos((2*pi*(q-1))/NumberOfRotors);
    end
    PitchAcc = sum(PitchAcc);
end
```

Appendix G

Control design

The design of the controllers described in chapter 7 is quite simple and will only quickly be presented in this appendix. The open and closed loop bode plot of each controller is presented in the following sections. All controllers are discrete and designed with a sample time of (1/487)s. The sample time is the same as the one used by Mikrokopter.

G.1 Angular velocity control

G.1.1 Roll PD control

The angular velocity controller on the roll axis is a PD controller. A PD is chosen due to its capability of a high bandwidth. An integrating part of the controller is not desired since it will slow down the response of the system and any stationary errors are caught in the angle controller. The bode plot of the open loop P-controller, shown in figure G.1, with the proportional gain K_p^{vel} equal to $10^{-18/20}$=0.126, are shown in figure G.2. It can be seen from the figure that the phase margin is 65.3.

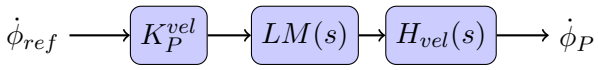

Figure G.1: *PD controller*

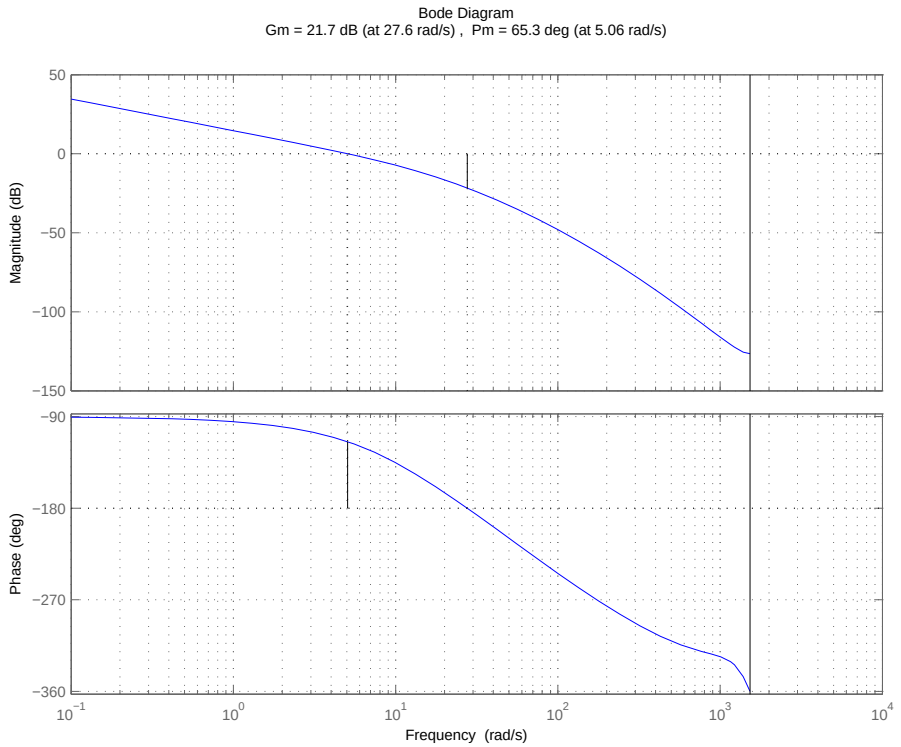

Figure G.2: *Bode plot of the open loop roll angular velocity P-controller as shown in figure G.1*

The bandwidth of the closed loop P-controller is 8.32 rad/s. To increase the bandwidth of the close loop system a Derivative is designed, where the derivative is placed based on equation G.1,

$$\omega_t = \frac{1}{\tau_D \sqrt{0.1}} \tag{G.1}$$

where τ_D is equal to 5.06 rad/s which is the frequency corresponding to the phase margin of 65.3 deg. The D-part can be expressed by equation G.2.

$$D_{vel} = \frac{\tau_D s + 1}{0.1\tau_D s + 1} \tag{G.2}$$

The PD controller is setup with the D-part in the feedback to reduce the overshoot and is shown in figure G.3. The bode plot of the open loop PD controller, with the new $K_p^{vel} = 10^{-7/20} = 0.45$, is shown in figure G.4.

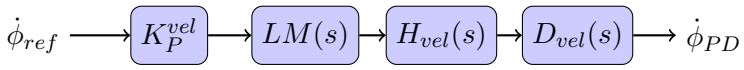

Figure G.3: *PD controller*

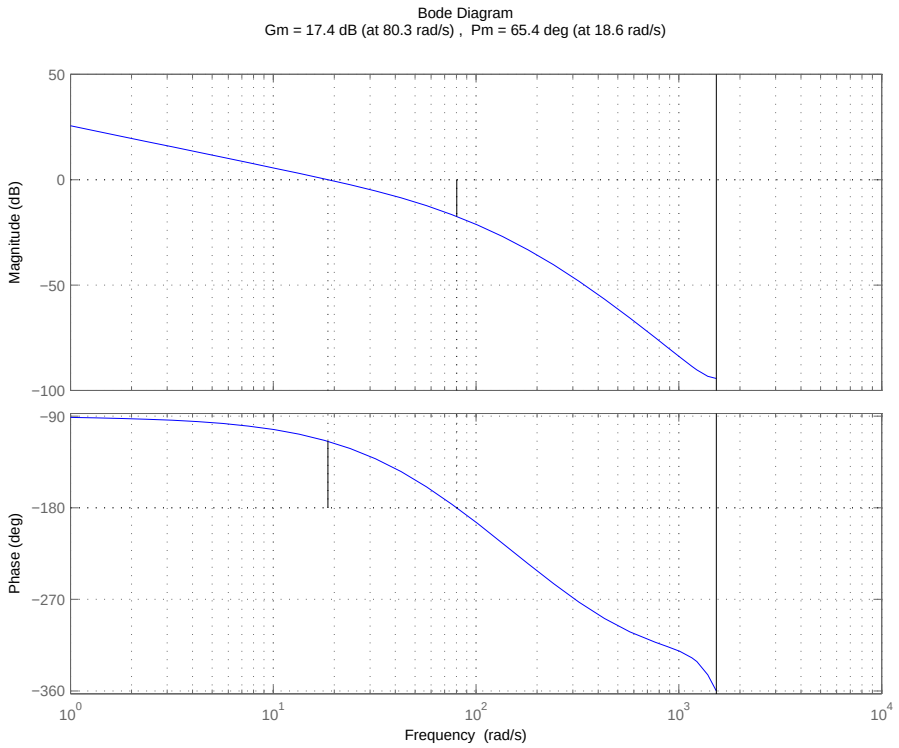

Figure G.4: *Bode plot of the open loop roll angular velocity PD-controller as shown in figure G.3*

The bandwidth of the closed loop PD-controller, shown in figure G.5, is 12.97 rad/s, which is an increase of 56% compared to the bandwidth of the P-controller. The step response of the controller can be seen in section 8.1.

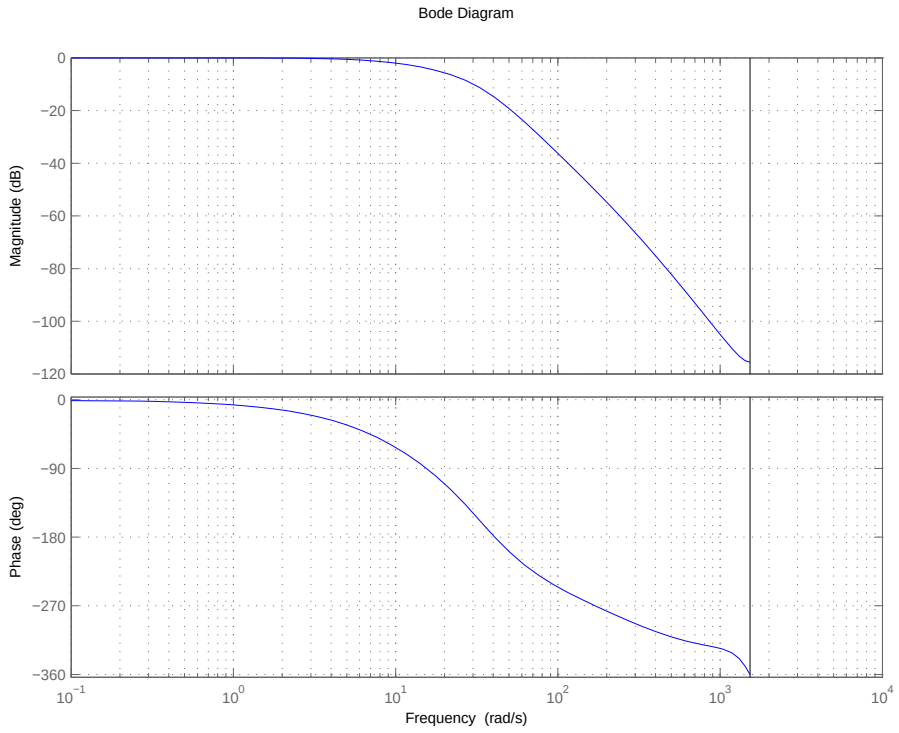

Figure G.5: *Bode plot of Roll angular velocity closed loop PD-controller*

G.1.2 Pitch PD control

The angular velocity controller on the pitch axis is a PD controller. The pitch angle velocity controller is setup the same way as the roll angle velocity controller. Figure G.1 from the previous section can therefore also be used to represent the pitch angle velocity P-controller. The bode plot of the open loop P-controller, with the proportional gain K_p^{vel} equal to $10^{-18/20}$=0.126, is shown in figure G.6. It can be seen from the figure that the phase margin is 65.3. The bandwidth of the closed loop P-controller is 8.32 rad/s, which is the same as the one found for the roll angle velocity control.

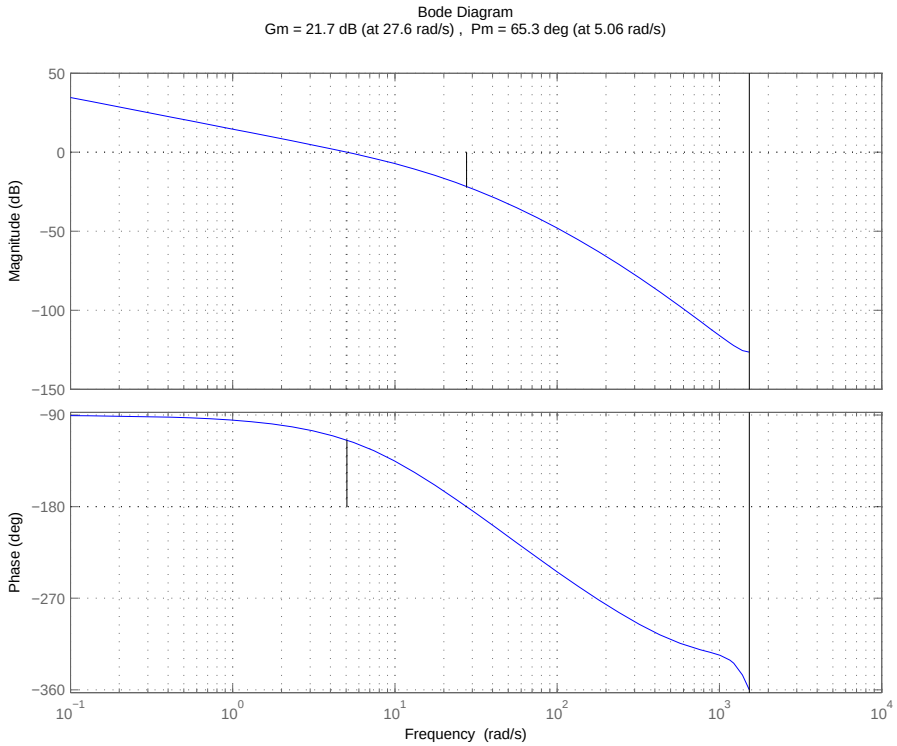

Figure G.6: *Bode plot of the open loop pitch angular velocity P-controller as shown in figure G.1*

To increase the the bandwidth of the close loop system a Derivative is designed, where the derivative is placed based on equation G.1, where τ_D is equal to 5.06 rad/s which is the frequency corresponding to the phase margin of 65.3 deg. The PD controller is setup with the D-part in the feedback to reduce the overshoot and is shown in figure G.3, with the new $K_p^{vel} = 10^{-7/20} = 0.45$. The bode plot of the open loop PD controller is shown in figure G.7.
The bandwidth of the closed loop PD-controller is 12.97 rad/s, which is the same as the roll angle velocity controller. The step response of the controller can be seen in section 8.1.
The bode plots from figure G.6 and G.7 looks very similar with the plots for the roll controller. The models are also very similar, and the only difference is the inertia of the x and y axis. In this project the inertia is practical the same on the axis and the difference is therefore not visible in the plots.

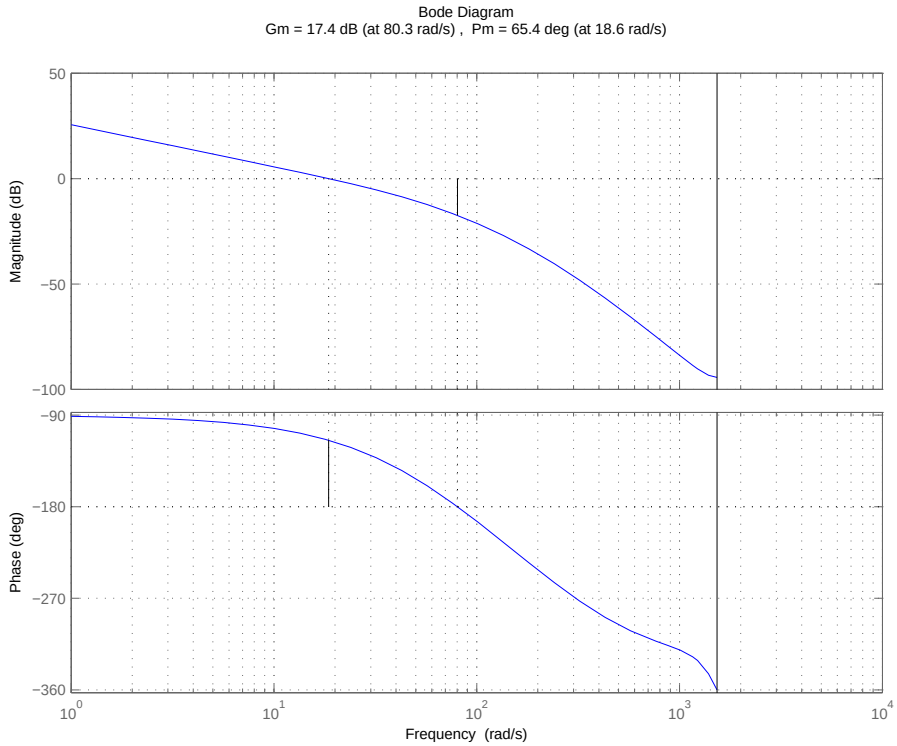

Figure G.7: *Bode plot of pitch angular velocity PD-controller as shown in figure G.3*

G.1.3 Yaw velocity PID control

The angular velocity controller on the yaw axis is a PID controller. The yaw angle velocity controller is designed using the same method as in the previous sections, but an integrator has been added to avoid steady state errors. The model is now just the model of the Yaw acceleration. Figure G.1 from the previous section can therefore also be used to represent the yaw angle velocity P-controller. The bode plot of the open loop P-controller, with the proportional gain K_p^{vel} equal to $10^{9/20}$=2.81, is shown in figure G.8. It can be seen from the figure that the phase margin is 21.3.

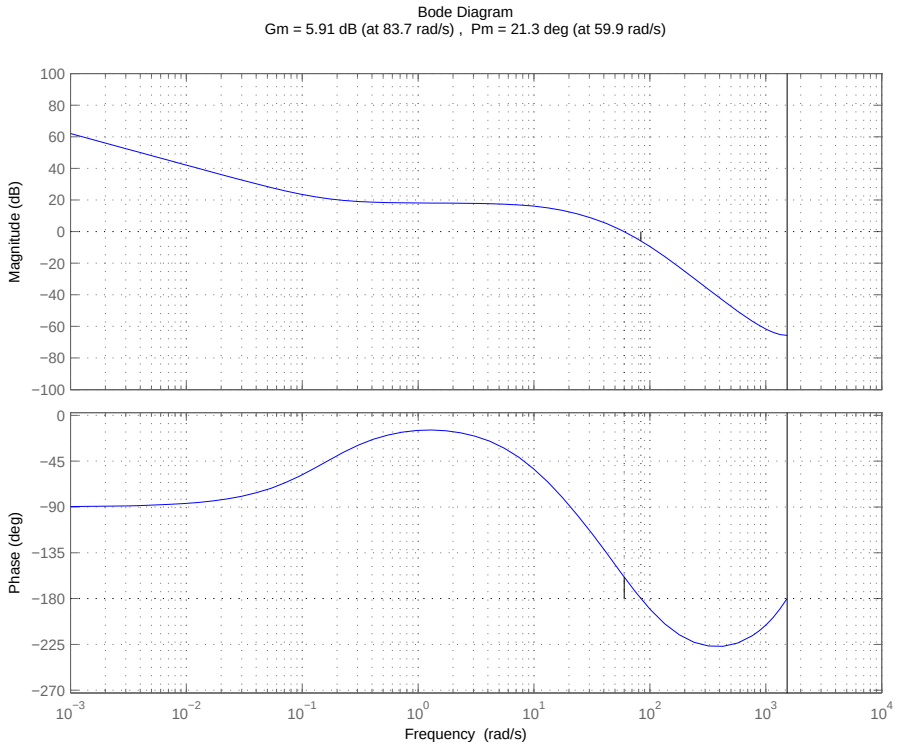

Figure G.8: *Bode plot of the open loop yaw angular velocity P-controller*

To increase the the bandwidth of the close loop system a Derivative is designed, where the derivative is placed based on equation G.1, where τ_D is set to 0.0053 rad/s. The PD controller is setup with the D-part in the feedback to reduce the overshoot. An integrator is added based on equation G.3 to avoid stationary errors. τ_i is set to 0.013 and the open loop bodeplot of the PID yaw controller is shown in figure G.9, where $K_p^{vel} = 10^{13/20} = 4.467$.

$$I_{vel/pos} = \frac{\tau_i s + 1}{\tau_i s} \tag{G.3}$$

The bandwidth of the closed loop Yaw PD-controller is 39.97 rad/s. The step response of the controller can be seen in section 8.1.

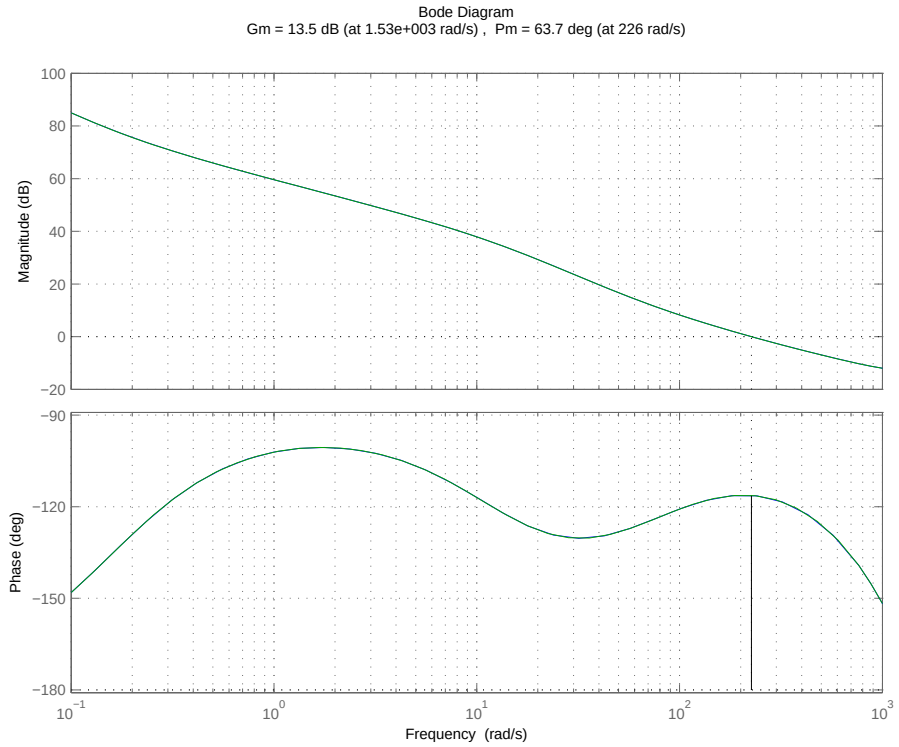

Figure G.9: *Bode plot of the open loop yaw angular velocity PID-controller.*

G.2 Roll & pitch Angle control

Since there was not any noticeable difference between the velocity controllers on the roll and pitch axis, the controller for the roll and pitch angle is designed based on the roll angle model. The same control parameters are therefore used for the roll and pitch angle controllers. They are designed based on equation 7.6 and by using the same method as the angle velocity controllers. The bode plot of the open loop P-controller is shown in figure G.10, with $K_p = 10^{1/20} = 1.12$.

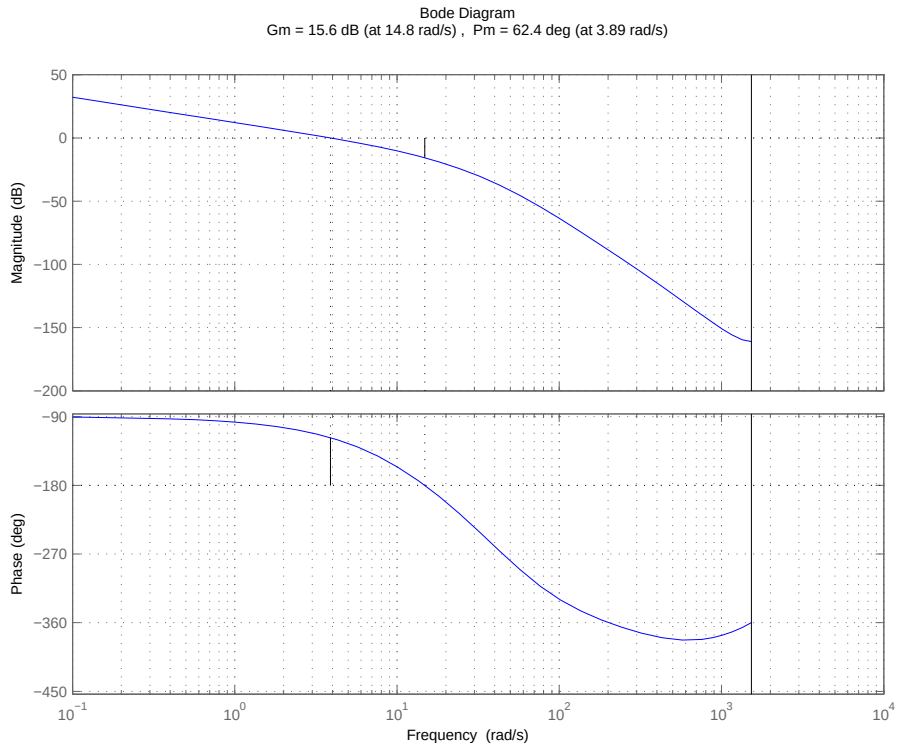

Figure G.10: *Bode plot of Roll angle P-controller as shown in figure G.1*

A derivative and an integrating part is added to the P-controller where the derivative is found by using equation G.1. τ_D is set to 3.89 rad/s. The integrating part of the controller is calculated as shown in equation G.3,

where τ_i is set to 1. The open loop bode plot of the angle controller is depicted in figure G.11. The bandwidth of the closed loop system is 5.42 rad/s and the bode plot of the system is shown in figure G.12.

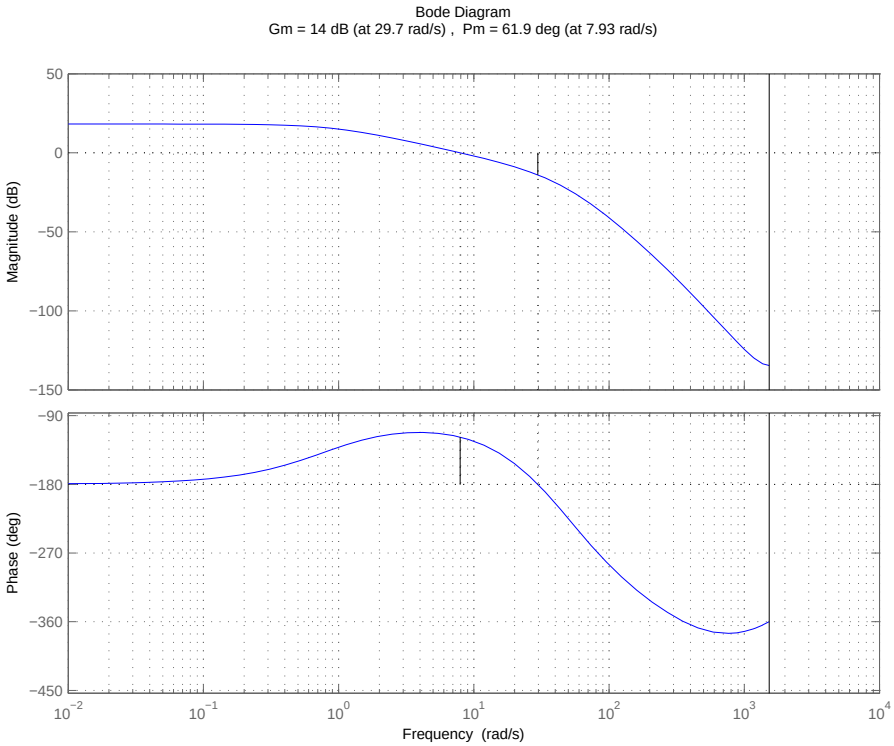

Figure G.11: *Bode plot of Roll angle PID-controller as shown in figure G.1*

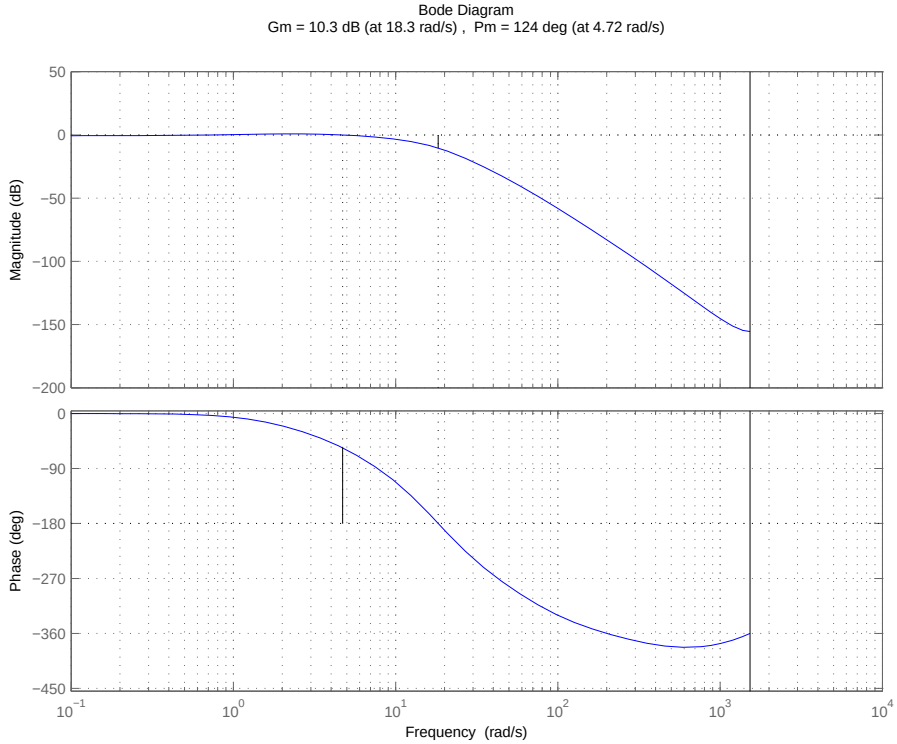

Figure G.12: *Bode plot of the closed loop angle PID-controller, as shown in figure 7.3*

G.3 Control parameters

Controller	P	I	D
Roll vel.	0.447	-	$\frac{0.06255s+1}{0.006255s+1}$
Pitch vel.	0.447	-	$\frac{0.06255s+1}{0.006255s+1}$
Yaw vel.	4.467	$\frac{0.013s+1}{0.013s}$	$\frac{0.005275s+1}{0.0005275s+1}$
Roll ang.	2.114	$\frac{s+1}{s}$	$\frac{0.08139s+1}{0.008319s+1}$
Pitch ang.	2.114	$\frac{s+1}{s}$	$\frac{0.08139s+1}{0.008319s+1}$

Table G.1: *Continues control transfer functions*

Controller	P	I	D
Roll vel.	0.447	-	$\frac{10-9.72z^{-1}}{1-0.72z^{-1}}$
Pitch vel.	0.447	-	$\frac{10-9.72z^{-1}}{1-0.72z^{-1}}$
Yaw vel.	4.467	$\frac{1-0.846z^{-1}}{1-z^{-1}}$	$\frac{10-9.02z^{-1}}{1-0.02z^{-1}}$
Roll ang.	2.114	$\frac{1-0.9979z^{-1}}{1-z^{-1}}$	$\frac{10-9.777z^{-1}}{1-0.777z^{-1}}$
Pitch ang.	2.114	$\frac{1-0.9979z^{-1}}{1-z^{-1}}$	$\frac{10-9.777z^{-1}}{1-0.777z^{-1}}$

Table G.2: *Discrete control transfer functions with sample time (1/487)s*

G.4 Control response time

The rise time for the controllers are defined as the time from 10% and 90% of the final value of the step.

Control	Model (ms)	Measurement (ms)	Mikrokopter (ms)
Roll angle	196.20	243.42	475.64
Pitch angle	196.20	260.92	416.98
Roll ang. vel.	259.95	210.46	N/A
Pitch ang. vel.	260.35	216.11	N/A

Table G.3: *Rise time of the SISO controllers*

Control	**Model (%)**	**Measurement (%)**	**Mikrokopter (%)**
ϕ (PID)	9.21	7.42	7.40
θ (PID)	9.21	7.18	11.39
$\dot{\phi}$ (PD)	0.0	0.0	N/A
$\dot{\theta}$ (PD)	0.0	0.0	N/A

Table G.4: *Overshoot of the SISO controllers*

Appendix H

Implementation

An overview of the implementation of the angle estimation algorithm and the controllers are presented in this appendix. The control transfer functions are calculated in appendix G.
The first sections present the arctangent and the cosine approximation.
The last section present the controller implementation on the flight control board.

H.1 Arctangent approximation

The roll and pitch angle is calculated using the arctangent function as shown in equation 6.19. It is however not possible for the microprocessor on *Flight Control Board* (FCB) to calculated the arctangent function of two vectors. An approximation is therefore created based on the work done by [Rajan(MAY 2006)] and [Shima(1999)]. The approximation is based on equation H.1.

$$arctan(x) \approx \frac{\pi}{4}x + 0.285x(1 - |x|) \tag{H.1}$$

The c-code for the resulting algorithm is shown in appendix H.3.3, and the error of the approximation is plotted in figure H.1.

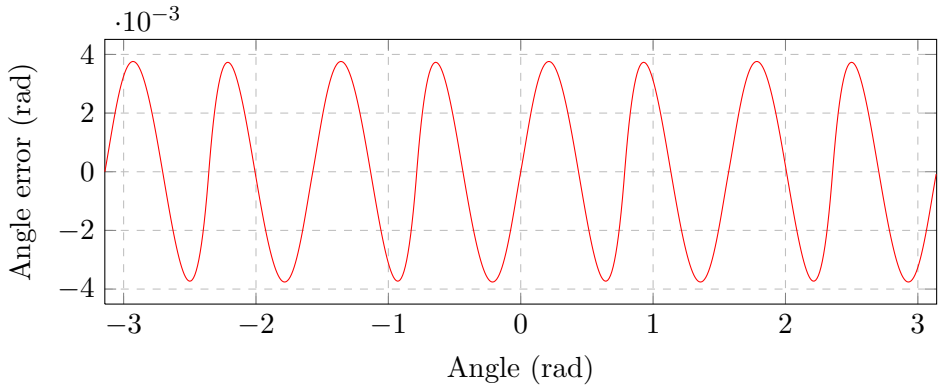

Figure H.1: *Error of applied arctan approximations*

The maximal error of the implemented arctangent approximation is 0.0038 rad or 0.21 degree.

H.2 Cosine approximation

The thrust compensation, described in section 7.3, is based on the cosine function. To make the quadrocopter able to use the thrust compensation a cosine approximation is used. The approximation is based on the Taylor polynomial expressed by equation H.2.

$$f(a) \approx \frac{f'(a)}{1!}(x-a) + \frac{f''(a)}{2!}(x-a)^2 + \frac{f^{(3)}(a)}{3!}(x-a)^3 + \dots \tag{H.2}$$

If the cosine function is inserted into a Taylor polynomimal of degree 4 the result can be expressed by equation H.3

$$cos\theta \approx 1 - \frac{1}{2}\theta^2 + \frac{1}{24}\theta^4 \tag{H.3}$$

The approximation and the error are shown in figure H.2, where it can be seen that

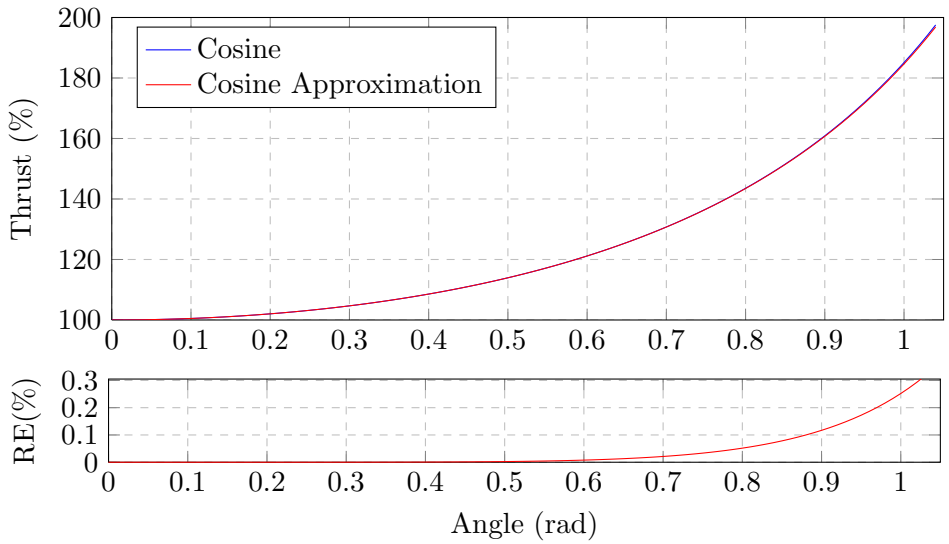

Figure H.2: *Cosine approximation, where RE is the Relative error in percent and Thrust describe the necessary thrust to maintain the given height acceleration.*

the relative error of the approximation is well below 0.3 percent at angles below 1 radian.

H.3 Controller implementation

The angle and angle velocity controllers are implemented in C on the flight control board. The angle velocities, $\dot{\phi}$, $\dot{\theta}$ and $\dot{\psi}$ is controlled using 16 bit fix point controllers. The roll and pitch angles are controlled using floating point.

Mikrokopters code is used as a template and the controllers made by Mikrokopter is disabled and the following code is added to the FC.c file.

H.3.1 Initialize control variables

The variables used to control the quadrocopter is initialized by applying the code below to the top of the FC.c file. The variables are arrays of size 3. All variables starting with "Angle_" are used by the angle controllers and the array is defined as:

$$\begin{pmatrix} \phi \\ \theta \\ \psi \end{pmatrix} \tag{H.4}$$

Likewise the array used by the angle velocity controllers ("AngVel_") are defined as:

$$\begin{pmatrix} \dot{\phi} \\ \dot{\theta} \\ \dot{\psi} \end{pmatrix} \tag{H.5}$$

The initializing code:

```
1  static float Angle_PI_b0[3]={2.1134890,2.1134890,0.0000000};
2  static float Angle_PI_b1[3]={-2.1091492,-2.1091492,0.0000000};
3  static float Angle_D_b0[3]={10.0000000,10.0000000,0.0000000};
4  static float Angle_D_b1[3]={-9.7770085,-9.7770085,0.0000000};
5  static float Angle_D_a1[3]={-0.7770085,-0.7770085,0.0000000};
6
7  unsigned char AngVel_Kp_exp[3]={1,1,7};
8  signed short AngVel_Kp[3]={7318,7318,1144};
9  unsigned char AngVel_b0_exp[3]={4,4,4};
10 unsigned char AngVel_b1_exp[3]={4,4,4};
11 unsigned char AngVel_a1_exp[3]={1,1,1};
12 signed short AngVel_b0_fix[3]={20480,20480,20480};
13 signed short AngVel_b1_fix[3]={-19906,-19906,-18473};
14 signed short AngVel_a1_fix[3]={-11798,-11798,-333};
15
16 signed short Yaw_I_Dummy=0;
17 signed short Yaw_I_b1_exp=1;
18 signed short Yaw_I_b1=-13860;
19
20 signed long Acc_Gyro_Ang_Rate=8;
21 float Acc_Gyro_Ang_Est_b1=0.0009329;
22 float Acc_Gyro_Ang_Est_a1=-0.9990671;
```

H.3.2 Angle estimation algorithm

The angle estimation algorithm from section 6.4.1 is implemented as the function "Get_Roll_Pitch_Angle", where the code is printed in the last part of this section. The first two parameters of the function is respectively the signals from the gyro and the angles created by the accelerometers. These two are combined as shown in section 6.4.1 and the result is inserted into the 3. parameter; Angle_Estimate. If an magnetometer is added to the helicopter the function can easily be expanded to return the Yaw angle which is equal to the heading of the helicopter. The code to generate the angles from the accelerometer is presented in appendix H.3.3.

```
1 void Get_Roll_Pitch_Angle(signed short AngleSpeed_Gyro[3], signed ...
    short Angle_Acc[3], signed short Angle_Estimate[3]){
2   static float dummy_input[3];
```

```
3   static float dummy_output[3];
4   static float f0[3];
5   static float f1[3];
6
7   unsigned char i;
8   for(i=0;i<2;i++){
9     f0[i] = (float)((signed long)(AngleSpeed_Gyro[i])*...
          Acc_Gyro_Ang_Rate+(signed long)Angle_Acc[i])-dummy_input[i];
10    Angle_Estimate[i] = (signed short)dummy_output[i];
11    f1[i] = f0[i];
12    dummy_input[i] = f1[i]*Acc_Gyro_Ang_Est_a1;
13    dummy_output[i] = f1[i]*Acc_Gyro_Ang_Est_b1;
14  }
15 }
```

H.3.3 Arctangent approximation algorithm

The the following code implements the approximation to equation 6.19, shown in section H.1.

```
1  signed short arctan2(float Z,float y)
2  {
3     const float coeff_1 = 0.785398163397448; //(pi/4);
4     const float coeff_2 = 2.356194490192345; //(pi/4)*3
5     static float coeff_3 = 0;
6     static float r = 0.0;
7     static float abs_r=0.0;
8     static float angle = 0.0;
9     float abs_y = y+0.0000001f;            // +1 to prevent 0/0 ...
          condition
10    if (y<0) abs_y = -y;
11
12    if (Z>=0)
13    {
14       r = (Z - abs_y)/(Z + abs_y);
15     if (r<0) abs_r=-r;
16     else abs_r = r;
17     coeff_3 = (0.273*r*(1-abs_r));
18       angle = coeff_1 - (coeff_1*r) - coeff_3;
19    }
20    else
21    {
22       r = (Z + abs_y)/(abs_y - Z);
23     if (r<0) abs_r=-r;
24     else abs_r = r;
25     coeff_3 = (0.273*r*(1-abs_r));
26       angle = coeff_2 - (coeff_1*r) -  coeff_3;
27    }
28    if (y < 0){
29     return (signed short)(-(angle*1024));      // negate if in quad ...
          III or IV
30    }
31    else
32    {
33     return (signed short)((angle*1024));
34    }
35 }
```

H.3.4 Angle compensated thrust

The angle compensated thrust described in section 7.3 is implemented as shown in the following code:

```
1  signed short Get_Angle_Compensated_Thrust(signed short FixPoint_Angle...
       [3], signed short Stick_Thrust){
2    float Angle[3] = {0,0,0};
3    float Angle2[3] = {0,0,0};
4    float ThrustRatio[3] = {0,0,0};
5    float Stick_T = 0;
6    unsigned char LoopCnt;
7
8    for(LoopCnt=0;LoopCnt<2;LoopCnt++){
9      LIMIT_MIN_MAX(FixPoint_Angle[LoopCnt],-1024,1024); //1024 = Angle...
           of 1 radian = 57,3 degreees
10     if (FixPoint_Angle[LoopCnt] < 0) Angle[LoopCnt] = -(float)...
           FixPoint_Angle[LoopCnt];
11     else Angle[LoopCnt] = (float)FixPoint_Angle[LoopCnt];
12     Angle[LoopCnt] = Angle[LoopCnt]/1024;
13     Angle2[LoopCnt] = Angle[LoopCnt]*Angle[LoopCnt];
14     ThrustRatio[LoopCnt] = (0.0416667*Angle2[LoopCnt]-0.5);
15     ThrustRatio[LoopCnt] = ThrustRatio[LoopCnt]*Angle2[LoopCnt]+1;
16   }
17
18   Stick_T = (float)Stick_Thrust;
19   Stick_T = Stick_T/(ThrustRatio[0]*ThrustRatio[1]);
20   return ((signed short)Stick_T);
21 }
```

H.3.5 Angle Control loop

The angle and angle velocity controllers are implemented as shown below. The code uses a few of Mikrokopters own functions and some of the authors sensor variables from the file analog.c on the attached CD. The code below is presented to give an general idea of the implementation. The sub16, add16 and mul16 is presneted in appendix H.4.

```
1    static unsigned char axis = 0;
2
3    //Calculate Roll and Pitch control signals:
4    for(axis=0;axis<3;axis++){
5
6      if (axis!=2){
7        //PID controller D-part (is placed in the feedback):
8        Angle_D_f0[axis] = (float)Ang_Corr[axis] - Angle_D_dummy1[axis...
             ];
9        Angle_D_Out[axis] = (Angle_D_b0[axis] * Angle_D_f0[axis])+...
             Angle_D_dummy2[axis];
10       Angle_D_f1[axis] = Angle_D_f0[axis];
11       Angle_D_dummy1[axis]= Angle_D_a1[axis]*Angle_D_f1[axis];
12       Angle_D_dummy2[axis]= Angle_D_b1[axis]*Angle_D_f1[axis];
13
14       Angle_Error[axis] = sub16(Angle_Ref[axis],(signed short)...
             Angle_D_Out[axis]); //Signed Short
15
16       Angle_PI_f0[axis] += (float)Angle_Error[axis];
17       //Integrator anti wind up:
18       if (Angle_PI_f0[axis]>100000) Angle_PI_f0[axis] = 100000;
```

```
19        if (Angle_PI_f0[axis]<-100000) Angle_PI_f0[axis] = -100000;
20
21        Angle_PI_Out[axis] = (Angle_PI_b0[axis]*Angle_PI_f0[axis]) + ...
              Angle_PI_dummy[axis];
22        Angle_PI_dummy[axis] = Angle_PI_b1[axis]*Angle_PI_f0[axis];
23
24        //Angular velocity-controller [Signed Short]:
25        AngVel_Ref[axis] = (signed short)Angle_PI_Out[axis];
26      }else{ // Yaw Controller:
27        //I-part:
28        AngVel_Error[axis] = sub16((stick_yaw*2),Gyro_Speed[axis]);
29        AngVel_Ref[axis] = add16(AngVel_Error[axis],Yaw_I_Dummy);
30        Yaw_I_Dummy = mul16(Yaw_I_b1,AngVel_Error[axis],Yaw_I_b1_exp);
31      }
32        //D-part:
33        AngVel_Out[axis]=add16(mul16(AngVel_b0_fix[axis],Gyro_Speed[...
              axis],AngVel_b0_exp[axis]),AngVel_dummy[axis]);
34        AngVel_Error[axis]=sub16(AngVel_Ref[axis],AngVel_Out[axis]);
35        AngVel_dummy[axis]=sub16(mul16(AngVel_b1_fix[axis],Gyro_Speed[...
              axis],AngVel_b1_exp[axis]),mul16(AngVel_a1_fix[axis],...
              AngVel_Out[axis],AngVel_a1_exp[axis]));
36        //P-part:
37        AngVel_Out[axis] = mul16(AngVel_Kp[axis],AngVel_Error[axis],...
              AngVel_Kp_exp[axis]);
38    }
```

H.4 Fix point algorithms

To avoid overflow and underflow of the fix point calculations the following functions are used to do additions, subtractions and multiplications of 16 bit integers. The functions are created by [Andersen(2009)], where further details can be found in the paper.

H.4.1 16 bit addition

Adds two 16 bit fixpoint integers:

```
1  signed short add16(signed short add1,signed short add2){
2    signed long t;
3    t=add1;
4    t+=add2;
5    if (t > 32767l)
6    t=32767l;
7    else
8    if(t < -32768l)
9    t=-32768l;
10   return(t);
11 }
```

H.4.2 16 bit substraction

Subtracts two 16 bit fixpoint integers:

```
1  signed short sub16(signed short min,signed short sub){
2    signed long t;
3    t=min;
4    t-=sub;
5    if (t > 32767l)
6    t=32767l;
7    else
8    if(t < -32768l)
9    t=-32768l;
10   return(t);
11 }
```

H.4.3 16 bit multiplication

Multiply two 16 bit fixpoint integers.

```
1  signed short mul16(signed short fac1,signed short fac2,signed short ...
       exp){
2    signed long f1;
3    f1=fac1;
4    f1*=fac2;
5    if (exp>15)
6    f1<<=1;
7    else
8    f1>>=(15-exp);
9    if (f1 > 32767l)
10   f1=32767l;
11   else
12   if (f1 < -32768l)
13   f1=-32768l;
14   return(f1);
15 }
```

Appendix I

CD content

The Flight Control Board source code, Matlab model files, demonstration videos are located on the CD attached to this report. An outline of the CD content is depicted below:

- **Articles**
  - *List of articles used in the thesis*
- **FCB Software**
  - **Source Code**
  - **Mikrokopter programming tool**
  - Compiled hex code for the Atmega 1284P
- **Rotor Dataset**
  - *Rotor measurement and calculations*
- **Simulink Model**
  - **Linear Models**
  - **Matlab model functions**
  - Nonlinear N rotor model
- **Vidoes**
  - *Video demonstrations*
- Report